

The Cold Debris Disk Surveys I. Host Star Properties

SCOTT J. KENYON,¹ BENJAMIN C. BROMLEY,² AND JOAN R. NAJITA³¹*Smithsonian Astrophysical Observatory, 60 Garden Street, Cambridge, MA 02138, USA*²*Department of Physics & Astronomy, University of Utah, 201 JFB, Salt Lake City, DC 20006, USA*³*NSF's NOIRLab, 950 N. Cherry Avenue, Tucson, AZ 85719, USA*

(Received 2025 Sep 25; Revised 2026 Feb 13; Accepted 2026 Feb 15; Published 2026 Mar 12: AJ, vol 171, 223)

ABSTRACT

We describe the dynamical, photometric, and spectroscopic data available for stars targeted by *Spitzer* and *Herschel* to search for cold circumstellar dust emission from debris disks, a collection that we name the Cold Debris Disk Surveys (CDDS). These data include *Hipparcos* and *Gaia* parallaxes, 0.4 μm to 1250 μm photometry, spectral types, effective temperatures, gravities, bolometric luminosities, visual extinctions, metallicities, lithium abundances, rotational periods, projected rotational velocities, the Ca II HK and IR triplet activity indicators, and X-ray luminosities for 3675 stars. Within this sample, we investigate the frequency of stellar and planetary companions (including potential new proper motion companions); use the data to assign CDDS stars to the field or one of many moving groups, open clusters, or stellar associations; and investigate correlations between stellar activity indicators. In future papers, we plan to explore the magnitude and frequency of infrared excess emission as a function of host star properties; to search for new companions with *Gaia*; and to examine the evolution of infrared excesses with the ages of stars in clusters and the field.

1. INTRODUCTION

In the core accretion picture of planet formation, planets grow from the accumulation of many planetesimals, small solid bodies a few to hundreds of kilometers in size. Planetesimals that survive the first few Myr of planet formation, avoiding incorporation into large bodies, should later collide and generate disks of collisional debris. First detected 40 years ago around the nearby A star Vega (H. H. Aumann et al. 1984), these debris disks have since been detected and studied around thousands of stars spanning a wide range of stellar ages and spectral types (A. M. Hughes et al. 2018).

Debris disks lend unique insights into the architectures of planetary systems and the planet formation process. Substructure in the debris (gaps, rings, and spiral arms) may reveal the presence of planets not seen directly; the detailed properties of the substructure can be used to infer planetary masses and orbits (e.g., P. Kalas et al. 2005; D. A. Golimowski et al. 2006; K. B. Follette et al. 2017; J. Olofsson et al. 2018; T. D. Pearce et al. 2022). Debris production has been proposed as a signpost of late-stage icy or rocky planet formation (e.g., S. J. Kenyon & B. C. Bromley 2002, 2004). More generally, as the product of collisions within the surviving solid mass reservoir of early planet formation, debris disks give us a handle on the efficiency of the planet for-

mation process, i.e., what the first few Myr of planet formation leaves behind.

Planetesimals (and their collisional debris) that survive beyond a star's main sequence lifetime may eventually fall onto the central white dwarf. The resulting chemical (metal) "pollution" of the white dwarf's atmosphere provides clues to the late-time evolution of planetary systems (e.g., J. Farihi 2016; D. Veras 2021). The properties of younger debris disks, the presumed evolutionary progenitors of such systems, provide context for understanding where the metals originate and how they are delivered to the star.

The debris disk population known today results from numerous studies designed to search for and characterize the properties of debris disks and their occurrence rates. Studies have targeted stars spanning wide ranges in stellar spectral type (B through M) and age (~ 10 Myr to ~ 10 Gyr), including stars located in both clusters and the field. Observations have been carried out at a wide range of wavelengths (optical through millimeter), notably in work with the *Hubble Space Telescope*, *Spitzer Space Telescope*, the *Herschel Space Telescope* and the *Atacama Large Millimeter Array* (e.g., B. C. Matthews et al. 2014; C. H. Chen et al. 2020; M. C. Wyatt 2021; C. F. Manara et al. 2023).

While many of these studies focus on the interpretation of individual samples, new insights can come from integrating the results of the ensemble. As one example from our own work, we recently illustrated how the debris disk properties studied by *Spitzer*/FEPS (e.g., M. R. Meyer et al. 2006) and *Herschel*/DEBRIS/DUNE (B. C. Matthews et al. 2010; C. Eiroa et al. 2013; B. Montesinos et al. 2016; B. Sibthorpe et al. 2018), when combined with evolutionary models of rings of solids, are consistent with a simple evolutionary picture in which the known population of cold debris disks surrounding FGK stars is a single evolutionary population, the descendants of protoplanetary disks with large, massive rings (J. R. Najita et al. 2022). That is, the $\sim 25\%$ of protoplanetary disks with large rings evolve to produce detectable debris throughout their lives, from ~ 10 Myr to ~ 10 Gyr, producing the known debris disk population.

With new datasets now in hand, the time appears ripe for a new synthesis of the available data on debris disk samples. In particular, *Gaia* data make it much easier to obtain stellar distances and ages and to identify cluster members (e.g., Gaia Collaboration et al. 2023a; E. L. Hunt & S. Reffert 2024, and references therein). Additional valuable photometric datasets include Pan-STARRS (K. C. Chambers et al. 2016), the Skymapper Southern Sky Survey (C. A. Onken et al. 2024), and WISE (E. L. Wright et al. 2010; R. M. Cutri et al. 2013). Along with many individual studies, the large optical spectroscopic surveys APOGEE (Abdurro'uf et al. 2022), Gaia-ESO (S. Randich et al. 2022), GALAH (S. Buder et al. 2021), LAMOST (M. Xiang et al. 2019; R. Wang et al. 2020), and RAVE (M. Steinmetz et al. 2020) yield complementary physical properties for debris disk host stars.

To build on these developments, here we combine the available data on existing debris disk samples to enable studies of integrated debris disk populations. In subsequent papers in this series, we use these data to derive the extent of IR excess among CDDS stars and examine how debris properties depend on host star properties (Paper II), search for dynamical companions to CDDS stars using *Gaia* data and a relation (if any) of companions to debris (Paper III), and estimate stellar ages and assess the evolution of debris with age (Paper IV). The present paper lays the foundation for these investigations by collecting the needed data.

To support the study of IR excesses in Papers II and III, here we compile optical and IR photometry for the sample and their parallaxes (§2). We also collect information on host star properties, including companions, stellar and planetary (§3), and stellar metallicity (§4).

To support the assessment of stellar ages needed for Paper IV, we collect information needed for estimates of isochronal ages (T_{eff} , $\log g$, M_{\star} , R_{\star}), as well as ages from gyrochronology ($v \sin i$, P_{rot}), activity (L_X/L_{\star} , $\log \log R'_{HK}$, $\log R'_{IRT}$), and Li (§4). We also update the membership of CDDS stars in stellar associations, clusters, and moving groups, relying on recent *Gaia*-based studies and supplementing these with isochronal constraints (section 6) and stellar activity measures (section 5).

We begin with an introduction to the sample of stars, a summary of available photometric data, and a description of parallaxes and proper motions (§2). We continue with an accounting of stellar and planetary companions (§3); physical properties of the host stars (§4); membership in stellar associations, clusters, and moving groups (§5); and a short discussion of HR diagrams for cluster and field stars (§6). We conclude with a discussion (§7) and summary (§8).

2. THE COLD DEBRIS DISK SURVEYS SAMPLE

2.1. Sample Selection

To compile a set of stars with strong constraints on cold dust emission, we select published data from *Spitzer* and *Herschel* photometric surveys of relatively nearby stars. For *Spitzer* programs, we require observations with the MIPS instrument (G. H. Rieke et al. 2004) at $24 \mu\text{m}$ (and preferably also at $70 \mu\text{m}$) to isolate cold dust emission from warm dust emission (e.g., S. J. Kenyon et al. 2016). We do not require robust detections at $24\text{--}70 \mu\text{m}$. Often, *Spitzer* studies report observations of some stars with the IRAC instrument at $3.6\text{--}8 \mu\text{m}$ (G. G. Fazio et al. 2004) along with upper limits at $24 \mu\text{m}$. We include these stars in the compilation. With observations at wavelengths $\gtrsim 70 \mu\text{m}$, *Herschel* programs with the PACS (A. Poglitsch et al. 2010) and SPIRE (M. J. Griffin et al. 2010) instruments automatically provide constraints on cold dust emission. With *Spitzer* and *Herschel* observations, we make no requirement on the level of IR excess emission above the stellar photosphere.

In collecting targets from *Spitzer* and *Herschel*, we include programs focused on stars with ages $\gtrsim 10$ Myr. This criterion eliminates *Spitzer* surveys of (i) very young, nearby star-forming regions such as Ophiuchus (e.g., D. L. Padgett et al. 2008), Perseus (e.g., J. K. Jørgensen et al. 2006), and Taurus-Auriga (e.g., E. Furlan et al. 2006), where the frequency of pre-main sequence stars with optically thick protoplanetary disks is much larger than the frequency of stars with debris disks; and (ii) more distant regions of ongoing star formation such as Orion B1 and σ Ori, which also have a

much larger frequency of protoplanetary disks than debris disks (e.g., J. Hernández et al. 2006, 2007). This approach allows us to focus on one of the main goals of this study: relating the stellar properties of *Spitzer* and *Herschel* targets at shorter wavelengths, $\lesssim 2\text{--}5\ \mu\text{m}$, to the properties of debris disk emission at longer wavelengths, $\gtrsim 10\text{--}20\ \mu\text{m}$. Among stars younger than 5–10 Myr, emission from optically thick protoplanetary disks veils optical emission from the central star and complicates estimates of stellar effective temperature T_{eff} , luminosity L_* , and surface gravity $\log g$ (e.g., P. Hartigan et al. 1989; L. Hartmann et al. 2016; G. J. Herczeg et al. 2023; A. P. Sousa et al. 2023). In these systems, it is also challenging to separate stellar chromospheric and coronal emission from accretion energy (e.g., N. Calvet & E. Gullbring 1998; C. F. Manara et al. 2013; C. V. Pittman et al. 2025). We prefer to avoid these extra issues.

Excluding targets younger than ~ 10 Myr also allows us to focus on relating the properties of stellar and planetary companions to the properties of debris disk emission. As discussed below, stellar and planetary companions are common among the *Spitzer* and *Herschel* targets, where the lack of protoplanetary disk emission eases detection of radial velocity variability and transits. Adding a set of much younger stars with less robust constraints on planetary and stellar companions would complicate the analysis planned in Paper III.

To avoid confusion, we include all of the stars in the *Spitzer* compilations listed below even when a few stars have ages $\lesssim 10$ Myr. These additional stars have negligible impact on the analysis described below. The youngest stars among the *Spitzer* and *Herschel* targets are within or in the vicinity of Taurus-Auriga (1–3 Myr; K. L. Luhman 2023a), CrA (4.5 Myr; M. Gennaro et al. 2012), ϵ Cha (~ 5 Myr; D. A. Dickson-Vandervelde et al. 2021), Orion (3–11 Myr; J. Hernández et al. 2023), Cha-Near (10 Myr; J. H. Rhee et al. 2007), TW Hya (~ 10 Myr; C. P. M. Bell et al. 2015), Sco-Cen (10–16 Myr; M. J. Pecaut & E. E. Mamajek 2016), and η Cha (11 Myr; C. P. M. Bell et al. 2015). Table 7 in §5 summarizes aspects of the moving groups, open clusters, and stellar associations included in the CDDS. In all, nineteen stars (0.5% of the CDDS sample) have nominal ages less than 10 Myr and would not be in the compilation without inclusion in one of the publications listed below.

Published *Spitzer* studies have various targeting strategies. Several programs focused on older, apparently single (C. A. Beichman et al. 2005; C. H. Chen et al. 2005b; C. A. Beichman et al. 2006; G. Bryden et al. 2006; B. Riaz et al. 2006; I. Gautier et al. 2007; D. E. Trilling et al. 2008; G. Bryden et al. 2009; P. Plavchan

et al. 2009; D. W. Koerner et al. 2010; A. Moór et al. 2011) or binary (D. E. Trilling et al. 2007) main sequence stars. Others concentrated on main sequence stars in nearby stellar associations, open clusters, and moving groups (e.g., N. Gorlova et al. 2004; E. T. Young et al. 2004; C. H. Chen et al. 2005a; F. J. Low et al. 2005; G. H. Rieke et al. 2005; J. R. Stauffer et al. 2005; N. Gorlova et al. 2006; K. Y. L. Su et al. 2006; N. Gorlova et al. 2007; J. R. Stauffer et al. 2007; N. Siegler et al. 2007; L. A. Cieza et al. 2008; T. Currie et al. 2008; I. Gautier et al. 2008; L. M. Rebull et al. 2008; Z. Balog et al. 2009; J. M. Carpenter et al. 2009; A. Gáspár et al. 2009; J. M. Sierchio et al. 2010; J. R. Stauffer et al. 2010; C. H. Chen et al. 2011; B. Zuckerman et al. 2011; C. H. Chen et al. 2012; L. E. Urban et al. 2012). The FEPS survey (J. S. Kim et al. 2005; M. R. Meyer et al. 2006; M. D. Silverstone et al. 2006; J. M. Carpenter et al. 2008; L. A. Hillenbrand et al. 2008) observed nearby stars from the field and somewhat more distant stars in clusters (e.g., α Per and the Pleiades).

Among these *Spitzer* programs, most centered on FGK stars (or a subset thereof; C. A. Beichman et al. 2005; C. H. Chen et al. 2005a; J. R. Stauffer et al. 2005; C. A. Beichman et al. 2006; G. Bryden et al. 2006; M. R. Meyer et al. 2006; D. E. Trilling et al. 2007; M. R. Meyer et al. 2008; D. W. Koerner et al. 2010; J. M. Sierchio et al. 2010; C. H. Chen et al. 2011; A. Moór et al. 2011). Bucking this trend, G. H. Rieke et al. (2005) concentrated on B-type and A-type stars (see also K. Y. L. Su et al. 2006; C. H. Chen et al. 2012); B. Riaz et al. (2006) and I. Gautier et al. (2007) selected M-type stars. Others cast a wider net for a broader range of spectral types that could be detected at 24–70 μm with reasonable signal-to-noise (C. H. Chen et al. 2005a; F. J. Low et al. 2005; N. Gorlova et al. 2006; N. Siegler et al. 2007; L. M. Rebull et al. 2008; D. E. Trilling et al. 2008; P. Plavchan et al. 2009; J. R. Stauffer et al. 2010; L. E. Urban et al. 2012). Surveys of associations and clusters probed as far down the main sequence as possible within a predefined area. For regions within 100–250 pc (250–500 pc), these observations yielded good samples of BAFG (BA) stars.

C. H. Chen et al. (2014) compiled spectroscopic observations of 571 debris disk candidates acquired with the *Spitzer* IRS instrument (J. R. Houck et al. 2004). Aside from a detailed analysis of spectral energy distributions, this study reports photometric measurements at 13, 24, 31, and 70 μm (for other IRS studies see M. Jura et al. 2004; C. H. Chen et al. 2006, 2009; F. Y. Morales et al. 2009). The host stars of these systems have spectral types of B9–K5 and ages of ~ 10 Myr to ~ 10 Gyr (for an analysis of IRS spectra of stars in the Sco-Cen asso-

ciation, see also H. Jang-Condell et al. 2015). Some are field stars; others are members of nearby associations, clusters, and moving groups.

Compared to *Spitzer* programs, *Herschel* surveys of main sequence stars are less extensive. The DEBRIS (B. C. Matthews et al. 2010; N. D. Thureau et al. 2014; G. M. Kennedy et al. 2018; B. Sibthorpe et al. 2018; J. F. Lestrade et al. 2025) and DUNES (C. Eiroa et al. 2013; B. Montesinos et al. 2016) surveys selected targets from the N. M. Phillips et al. (2010) list of ~ 250 main sequence stars roughly equally divided among AFGKM spectral types. The DUNES program included additional nearby FGK main sequence stars selected from *Hipparcos*. Several programs focused on smaller samples of nearby AFGK (e.g., S. E. Dodson-Robinson et al. 2016; F. Y. Morales et al. 2016; L. Vican et al. 2016; S. Hengst et al. 2017) and M-type (A. Tanner et al. 2020) main sequence stars. Others focused on the presence of debris disks in binary (B. Yelverton et al. 2019) and planetary (B. Yelverton et al. 2020) systems. Nearly all *Herschel* programs targeted field stars. J. K. Donaldson et al. (2012, Tuc-Hor), G. S. Mathews et al. (2013, Upper Sco), L. A. Cieza et al. (2013); P. Riviere-Marichalar et al. (2013, TW Hya), P. Riviere-Marichalar et al. (2014, β Pic), and P. Riviere-Marichalar et al. (2015, η Cha) surveyed stars in specific nearby clusters or moving groups; A. Bonsor et al. (2014) focused on planet-hosting subgiants with GK spectral types and masses $\sim 1.5 M_{\odot}$.

In the sections that follow, we discuss the observations included in the compilation and the conclusions we draw about the sample from these observations. In this section, we consider photometric data (infrared, submillimeter, and optical), the *Gaia* catalog, and astrometric data (distances, parallaxes, and proper motions). We then explore the frequency of stellar and binary companions. Stellar companions are common (43%); planetary companions are much less common (9%). In §4, we summarize the derived extinction A_V , physical properties of stellar photospheres (T_{eff} , L_{\star} , $\log g$, metallicity [Fe/H], lithium abundance $A(\text{Li})$, rotational period P_{rot} , and projected rotational velocity $v \sin i$), and observations of stellar activity (X-ray emission and Ca II H & K and IR triplet indices). Finally, we conduct a census of CDDS stars that are members of moving groups, open clusters, and stellar associations (§5).

Throughout this discussion, we demonstrate that CDDS stars span a broad range of spectral types (B5–M9), luminosity classes (main sequence stars to bright giants) and are typically younger and more active than stars in the vicinity of the Sun. This result is a feature of the *Spitzer* and *Herschel* targeting strategies for de-

bris disk stars. Approximately 44% of CDDS stars are members of a stellar association, open cluster, or moving group with an age $\lesssim 1$ Gyr (see below: Table 7, §6, and §7). The fraction of CDDS stars in a young stellar group is roughly 30 times larger than a random set of stars within 100–200 pc (§7; see also *Gaia* Collaboration et al. 2021a; E. L. Hunt & S. Reffert 2024). With a focus on groups with ages less than ~ 1 Gyr to maximize the probability of detecting cold dust emission, the *Spitzer* and *Herschel* surveys guaranteed that targeted stars would have ages considerably less than the age of a typical field star (e.g., ~ 4 –10 Gyr; R. Andrae et al. 2023b; M. Founesneau et al. 2023; A. Rathsam et al. 2023, and references therein).

2.2. Infrared and Submillimeter Data

To analyze *Spitzer* and *Herschel* data, we compile near-infrared (NIR) JHK data from the *Two Micron All Sky Survey* (2MASS; R. M. Cutri et al. 2003; M. F. Skrutskie et al. 2006), the COBE DIRBE Point Source Catalog (B. J. Smith et al. 2004), the DENIS catalogs (S. Kimeswenger et al. 2004; C. Denis 2005; J. Borsenberger et al. 2006), and the Catalog of Infrared Observations (CIO; D. Y. Gezari et al. 1993). We supplement and verify these data with results from other compilations (D. Engels et al. 1981; J. Koornneef 1983; C. Koen et al. 2010). Although the DIRBE and CIO catalogs are not as deep as 2MASS or DENIS, they provide more accurate photometry for JHK $\lesssim 4$ where 2MASS observations are saturated. The DENIS catalog of bright stars serves a similar purpose. In the mid-infrared (MIR), the AllWISE catalog (R. M. Cutri et al. 2013) from the Wide-field Infrared Survey Explorer (WISE; E. L. Wright et al. 2010) supplies all-sky photometry at 3.4 μm (W1), 4.6 μm (W2), 12 μm (W3), and 22 μm (W4). Saturation also plagues bright WISE sources with W1–W2 $\lesssim 6$ –7. IRAC measurements and photometry for bright sources at 3.5 μm and at 4.8 μm in the CIO provide good alternatives to W1 and W2 for bright stars.

At longer wavelengths, data from the *Infrared Astronomical Satellite* (IRAS; G. Neugebauer et al. 1984) supplement WISE, MIPS, and PACS photometry. We collect measurements from the Point Source (C. A. Beichmann 1985) and Faint Source (M. Moshir et al. 1992) catalogs. As part of the MSX Astrometric Catalog, M. P. Egan & S. D. Price (1996) match IRAS sources from both catalogs to high quality optical positions. For many of the brightest CDDS stars, good *IRAS* measurements at 12–100 μm constrain the spectral energy distributions (SED) for systems without complete *Spitzer* or *Herschel* data. Similarly, data from the *Infrared As-*

tronomical Mission (AKARI; H. Murakami et al. 2007) and the *Infrared Space Observatory* (ISO; M. F. Kessler et al. 1996) complement *Spitzer* and *Herschel* data. For CDDS stars, AKARI photometry in the 18 μm and 90 μm bands have much smaller uncertainties than in other AKARI bands.

The *Spitzer* IRS Enhanced Products provides calibrated synthetic photometry at 8, 12, 16, 22, 24, and 25 μm . The synthetic filters were designed to mimic the IRAC 8 μm , IRAS 12 and 25 μm , and the MIPS 24 μm filters. The 22 μm filter is similar to the WISE W4 filter.

Observations at 450–1250 μm generally trace the Rayleigh–Jeans tail of the spectral energy distribution of circumstellar dust (e.g., M. A. MacGregor et al. 2016, 2017; J. P. Marshall et al. 2017; W. S. Holland et al. 2017; D. J. Wilner et al. 2018; J. A. White et al. 2018; A. G. Sepulveda et al. 2019; M. Booth et al. 2021; V. Faramaz et al. 2021; D. Sullivan et al. 2022; L. Matrà et al. 2025, and references therein). Care is required to distinguish dust emission from a background galaxy. Measurements at multiple wavelengths may constrain the slopes of the opacity law and the grain size distribution. To complement the shorter wavelength *Spitzer* and *Herschel* observations, we collect data for 302 stars at wavelengths 450–9000 μm (J. S. Greaves et al. 1998, 2004; M. C. Liu et al. 2004; I. Sheret et al. 2004; J. P. Williams et al. 2004; J. Najita & J. P. Williams 2005; J. P. Williams & S. M. Andrews 2006; R. Liseau et al. 2008; V. Roccatagliata et al. 2009; R. Nilsson et al. 2010; G. S. Mathews et al. 2012; J. M. Carpenter et al. 2014; S. A. Barenfeld et al. 2016; J. Lieman-Sifry et al. 2016; A. Steele et al. 2016; W. S. Holland et al. 2017; S. Marino et al. 2017, 2018; V. Faramaz et al. 2019; S. Marino et al. 2019, 2020; L. Matrà et al. 2020; A. Nederlander et al. 2021; N. Pawellek et al. 2021; B. J. Norfolk et al. 2021; J. B. Lovell et al. 2021; A. S. Hales et al. 2022; M. A. MacGregor et al. 2022; D. Sullivan et al. 2022; J. P. Marshall et al. 2023; V. Roccatagliata et al. 2024; J. M. Carpenter et al. 2025; L. Matrà et al. 2025; S. Marino et al. 2026).

2.3. Optical Data

To enable construction of broadband spectral energy distributions (SEDs), we supplement IR data with ground-based optical photometry. For the brightest stars, we rely on BVI_C data in the Johnson–Cousins system. Starting with observations in the Gliese (W. Gliese 1969; M. S. Bessel 1990; W. Gliese & H. Jahreiß 1991) and *Hipparcos* (C. Turon et al. 1993; M. A. C. Perryman et al. 1997; F. van Leeuwen et al. 1997) catalogs, we compile data available in original articles, in

Vizier data sets, and in the *WEBDA* (J.-C. Mermilliod 1995) database (J. C. Mermilliod 1987a; M. A. Hamdy et al. 1993; E. W. Weis 1993; J. R. Ducati et al. 2001; T. Naylor et al. 2002; I. N. Reid et al. 2002; H. Sung et al. 2002; L. Prisinzano et al. 2003; E. Costa et al. 2006; W. Lyra et al. 2006; J. R. Stauffer et al. 2007; J. M. Carpenter et al. 2008; Z. Balog et al. 2009; S. Lépine et al. 2009; M. Kiraga 2012; M. Kiraga & K. Stepien 2013; B. L. Kamai et al. 2014; G. Kovács et al. 2014; J. C. Lurie et al. 2014; R. J. Oelkers et al. 2016; A. A. Henden et al. 2018; D. J. Fritzewski et al. 2020). As in J. C. Mermilliod (1987b), we carefully curate these data to avoid associating incorrect measurements with a specific star and to minimize measurement errors. When multiple accurate measurements for a star are available, we adopt the median. Of the 3496, 3551, and 2686 observations respectively available in the BVI_C filters, 3043, 3355, and 2686 have quoted photometric uncertainties $\lesssim 0.05$ mag in the original literature. The remainder have uncertainties as large as 0.25 mag.

For fainter CDDS stars without BVI_C data, we rely on Pan-STARRS (N. Kaiser et al. 2010; K. C. Chambers et al. 2016) and the SkyMapper Southern Sky Survey (S. C. Keller et al. 2007; C. A. Onken et al. 2024). We retrieve *grizY* ($g'r'i'z'$) photometry for 182 (764) CDDS stars with $\delta \geq -30^\circ$ ($\delta \leq +30^\circ$) in Pan-STARRS DR2 (SkyMapper DR4). For SkyMapper data, we verify targets with associated *Gaia*, *2MASS*, and *WISE* identifications. Stars with $g'r'i'z' \lesssim 9.5$ are often saturated (C. A. Onken et al. 2024). To allow for changing sensitivity across the survey, we check the individual measurements, errors, and colors of each star; observations that fall outside the well-defined main sequence locus of fainter stars are rejected. Pan-STARRS has a much fainter saturation limit, $grizY \lesssim 14$ (K. C. Chambers et al. 2016) and therefore yields fewer useful measurements of CDDS stars. As with SkyMapper, we verify saturation for each star using colors and measurement errors. To supplement Pan-STARRS and SkyMapper, we include $g'r'i'$ data from APASS for stars with $V \approx 10.5$ –15 (A. Henden & U. Munari 2014; A. A. Henden et al. 2018). Stars with $V < 10$ are often saturated; we use colors and measurement errors to eliminate saturated observations.

For bright CDDS stars, the first and second Tycho catalogs from the *Hipparcos* mission provide B_T , V_T , and their associated errors (E. Høg et al. 1997, 2000). Stars with $\text{V}_T \lesssim 9$ have typical uncertainties $\lesssim 0.02$ mag. Errors grow for fainter stars and are $\gtrsim 0.10$ mag for $\text{V}_T \gtrsim 11$. Nearly 68% (2292) of CDDS stars have a Tycho-2 measurement; 73% (1682) have a high quality measurement with $\text{V}_T \lesssim 9$.

2.4. The *Gaia* DR3 Catalog: Basic Data

Gaia DR3 is a treasure trove ([Gaia Collaboration et al. 2023a](#)). We compile *Gaia* identifications along with G, BP, and RP magnitudes for 3658 CDDS stars with $G \gtrsim 2$. The G-band data have exquisite precision, with uncertainties $\sigma_G \lesssim 0.01$ mag ([M. Riello et al. 2021](#)). Stars with $G < 8$ ($G \gtrsim 13$) require a saturation (color) correction that depends on G (BP–RP) as summarized in Appendix C (Fig. 28 and Table 5) of [M. Riello et al. \(2021\)](#). Both corrections are small, $\Delta G \approx -0.02$ to $+0.01$ for 1660 bright stars and $\Delta G \lesssim 0.025$ mag for 486 faint stars. Although BP and RP also have issues, most do not apply to CDDS stars. BP and to a lesser extent RP are too bright relative to expectations for $G \gtrsim 20$ [M. Riello et al. \(2021\)](#). All CDDS stars have $G \lesssim 18.4$. For $G \lesssim 4$, BP and RP must be adjusted for saturation: $\Delta BP \approx -0.6$ mag to zero for 149 stars with $G = 2-4$ and $\Delta RP \approx -0.8$ mag to zero for 68 stars with $G = 2-3.45$ ([M. Riello et al. 2021](#)). We apply these corrections as needed in the following analysis.

To measure the relative quality of the BP and RP fluxes for *Gaia* DR2, [D. W. Evans et al. \(2018\)](#) defined a dimensionless ratio $C(G) = (I_{BP} + I_{RP})/I_G$, where I_i is the flux in band $i = G, BP, \text{ or } RP$. High quality sources have $C(G) \simeq 1$; those with much larger $C(G)$ are often extended, variable, or near a much brighter star. For *Gaia* DR3, [M. Riello et al. \(2021\)](#) introduce a correction to $C(G)$ that allows a better measure of the relative quality of BP and RP. We compile $C(G) = \text{phot_bp_rp_excess_factor}$ from *Gaia* DR3 for each source and calculate $C^*(G) = C(G) - f(x)$, where $x = BP-RP$ and $f(x)$ is a polynomial with coefficients listed in Table 2 of [M. Riello et al. \(2021\)](#). With correction, high quality sources have $C^*(G) \simeq 0$; stars with $C^*(G) > 0$ ($C^*(G) < 0$) have more flux in BP and RP (G) than in G (BP and RP). From a set of ‘gold’ stars, [M. Riello et al. \(2021\)](#) also derive the dimensionless scatter in $C^*(G)$ about zero

$$\sigma(G) = 5.9898 \times 10^{-3} + 8.817481 \times 10^{-12} G^{7.618399} \quad (1)$$

High quality measurements typically have a dimensionless noise measure $S_C(G) = C^*(G)/\sigma(G) \lesssim 3-5$ ([M. Riello et al. 2021](#)).

Among the 3500 stars with $G \gtrsim 4$, 87% (91%) have $S_C(G) \lesssim 3$ (5). Another 2% (1.7%) have $S_C(G) \approx 5-10$ ($S_C(G) \gtrsim 100$). All stars with $S_C(G) \gtrsim 10$ are either variables (GJ 866, V1176 Tau, and V1299 Tau) or very close to a much brighter nearby star (e.g., α Cae B, ψ Vel B, and GJ 542.1B). Many of these do not have parallax, proper motion, or stellar photospheric properties within *Gaia* DR3.

As another check on G, BP, and RP photometry, we compare Johnson–Cousins and 2MASS photometry derived from G, BP, and RP (Tables C.1 and C.2 in [M. Riello et al. 2021](#)) with the data discussed above. When the difference between *Gaia*-synthesized data and published optical or near-IR data is smaller than or comparable to the σ in the [M. Riello et al. \(2021\)](#) relations, we accept *Gaia* photometry. Otherwise, we flag the observation as contaminated and do not use it in the analysis that follows. This test demonstrates that the conversion from BP and RP to V and I is (reasonably) robust when $S_C(G) \lesssim 3$ ($S_C(G) = 3-5$), with a typical uncertainty of 0.03 (0.06) in V and 0.05 (0.10) in I. However, for J and K, the conversion is less accurate. The typical uncertainty is 0.10 (0.14) for J (K) when $S_C(G) \lesssim 3$.

We also collect XP spectra for 2754 stars. Instead of converting these to standard spectra with flux as a function of wavelength, we compile the spectra in the *Gaia* natural system as coefficients of a set of basis vectors (e.g. [M. Weiler et al. 2023](#); [F. De Angeli et al. 2023](#)). As discussed in [Gaia Collaboration et al. \(2023b\)](#), the ‘generate’ routine enables calculation of broadband and narrowband photometry from XP spectra using project-supplied or user-supplied bandpasses. With fairly complete photometry from some combination of ground-based BVI_C, Pan-STARRS, Skymapper, and Tycho, we do not consider ‘generated’ photometry. [B. Huang et al. \(2024\)](#) discusses this aspect of *Gaia* data in detail.

2.5. Photometry Statistics

Fig. 1 and the upper half of Table 1 summarize the fraction of CDDS stars with reliable optical and near-IR photometry as a function of wavelength. Table 1 lists the fraction of all CDDS stars compiled for each entry. In parentheses, we include the fraction of stars where the photometric uncertainty is $\delta m \lesssim 0.05$ mag. For the ‘All Optical’ entry, we calculate the fraction of stars with at least one of (i) B or B_T, (ii) V, V_T, or g , and (iii) I_C or i . For ‘All JHK’, we select stars with the smallest errors among the CIO, COBE, and 2MASS measurements. The ‘All Optical’ and ‘All JHK’ entries illustrate how adding measurements with multiple origins enhances the compilation.

In Fig. 1, filled symbols illustrate the fraction of stars with high quality observations at a particular wavelength. Typically, the fraction of stars with high quality photometry ($\delta m \lesssim 0.05$ mag) is 5% to 20% smaller than the complete set of photometry at that wavelength (Table 1). For the ‘All Optical’ set, we plot symbols as plus signs. With this convention, *Gaia* G-band, all K-band data, and the ‘All Optical’ V-band data are nearly complete for the full sample of CDDS stars. The good

Table 1. Photometry Statistics

Passbands	f_{obs} ($f_{obs}, err < 0.05 \text{ mag}^1$)
B _T , V _T	0.768,0.781 (0.634,0.683)
BV _I C	0.951,0.966,0.731 (0.828,0.913,0.703)
<i>griz</i>	0.319,0.322,0.297,0.241 (0.23,0.23,0.23,0.23)
All Optical	0.958,0.995,0.917 (0.828,0.975,0.873)
BP, G, RP	0.995,0.995,0.995 (0.94,0.99,0.93)
2MASS JHK	0.998,0.998,0.998 (0.834,0.801,0.897)
All JHK	1.000,1.000,1.000 (0.913,0.865,0.951)
WISE W1–W4	0.978,0.980,0.979,0.980 (0.475,0.673,0.823,0.466)
IRAC B1–B4	0.245,0.275,0.162,0.245 (0.245,0.275,0.155,0.235)
All 3.4–4.6	0.985,0.981 (0.645,0.706)
IRS 8,12,16	0.185,0.316,0.316 (0.171,0.267,0.189)
IRS 22,24,25	0.320,0.320,0.320 (0.155,0.163,0.159)
IRAS 12,25,60,100	0.379,0.202,0.060,0.009 (0.356,0.123,0.032,0.003)
All 12,22,24	0.985,0.979,0.803 (0.764,0.461,0.751)
MIPS 24,70	0.772,0.335 (0.742,0.171)
PACS 70,100,160	0.077,0.191,0.098 (0.071,0.176,0.069)
All 24, 70	0.842,0.369 (0.745,0.203)
SPIRE 250,350,500	0.0207,0.0180,0.0103 (0.0074,0.0011,0.0000)
submm 450–1200	0.0035,0.0302,0.0199 (0.0035,0.0229,0.0169)

¹ At wavelengths $\gtrsim 20 \mu\text{m}$, numbers in parentheses correspond to the fraction of stars with $\delta m \leq 0.10 \text{ mag}$ (MIPS 24 μm), $\delta m \leq 0.15 \text{ mag}$ (MIPS 70 μm), SNR = 5 (PACS), and SNR = 3 (SPIRE and submm).

set of BP and RP data are almost as complete; more than 80% of CDDS stars have data at B, I_C or *i*, J, and H. Although we compile high quality *griz* data for less than 25% of the CDDS sample, these data help to make the V-band and I-band data more complete. The lower half of Table 1 and Fig. 2 summarize the fraction of CDDS stars with measurements at longer wavelengths. With observations for $\sim 98\%$ of the CDDS sample, WISE provides nearly a full set of mid-IR data at 3.4–22 μm . Most of the 12 μm data have uncertainties $\lesssim 0.05 \text{ mag}$; saturation of bright stars at W1 and W2 and low signal-to-noise for faint stars at W4 limits the fraction of high quality measurements. Ground-based L-band and *Spitzer* IRAC data nicely supplement the WISE data, increasing the fraction of sources with high quality measurements from 45% to 65%. At the other WISE bands, ground-based M-band data along with IRAC, IRS, and IRAS data add a small amount of high quality observations ($\lesssim 1\%$) to WISE data at 4.6, 12, and 22 μm . Moving to the far-IR, sub-mm, and mm, we collect photometry from the *Spitzer* MIPS instrument for 78% (34%) of the sample at 24 μm (70 μm). Most of the 24 μm data have errors $\lesssim 0.10 \text{ mag}$; roughly half of the 70 μm data have errors $\lesssim 0.15 \text{ mag}$. With much lower sensitivity, *IRAS* detected $\sim 6\%$ (1%) of the sample at 60 μm (100 μm). *Herschel* added observations at 70 μm (8% of the sample), 100 μm (19%), and 160 μm (10%) with PACS. Although *Herschel*’s SPIRE instrument added some high quality observations at longer

wavelengths, only $\sim 2\%$ (1%) of the sample has measurements at 250–350 μm (500 μm). Combining the set of 22–25 μm data yields data for more than 82% of the sample. Similarly, roughly 36% of the sources have at least one 60–70 μm measurement with IRAS, MIPS or PACS. Finally, $\sim 2\%$ to 3% of CDDS stars have at least one measurement at 450–9000 μm .

2.6. Parallaxes and Proper Motions

We compile parallaxes π and proper motions μ from *Gaia*, *Hipparcos*, and *Tycho-2* (E. Høg et al. 2000; F. van Leeuwen 2007; Gaia Collaboration et al. 2023a). Of the 3675 CDDS stars, 3478 (2219) have a *Gaia* (*Hipparcos*) parallax with $\pi > 0$. Defining the error in the parallax $\delta\pi$, we select observations with the largest signal to noise, $S_\pi = \pi/\delta\pi$. This choice yields 3461 (169) stars with a *Gaia* (*Hipparcos*) parallax. For the remaining stars, 25 have no parallax in *Gaia*, *Hipparcos*, or SIMBAD; others have measurements from the literature (W. F. van Altena et al. 1995; J. A. Dittmann et al. 2014; A. R. Riedel et al. 2014; T. J. Henry et al. 2018). Stars with $\pi \gtrsim 3 \text{ mas}$ ($\pi \gtrsim 10 \text{ mas}$) have a typical $S_\pi \gtrsim 50$ ($\gtrsim 200$). For the few CDDS stars with *Gaia* $\pi \lesssim 0.2 \text{ mas}$, the typical $S_\pi \lesssim 5$ –10.

Prioritizing *Gaia* parallaxes over *Hipparcos* parallaxes for any S_π yields 17 additional (fewer) parallaxes from *Gaia* (*Hipparcos*). For these 17 stars, the *Gaia* and *Hipparcos* π values are similar; however, the *Gaia* errors are larger. Thus, we favor parallax choices with S_π .

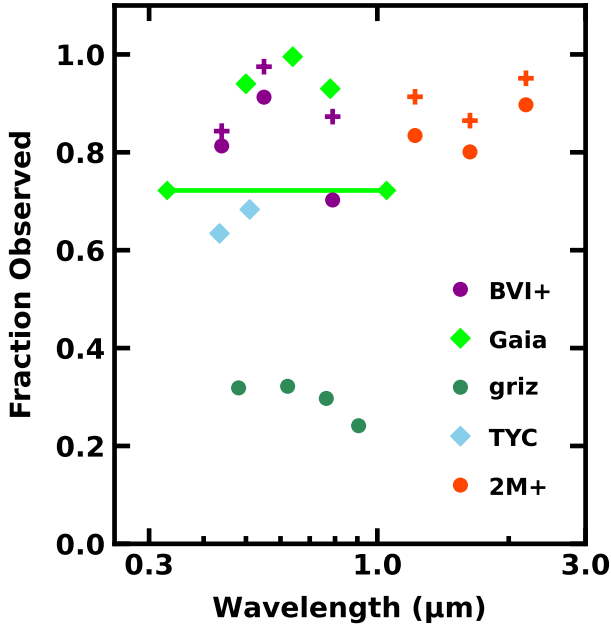


Figure 1. Fraction of CDDs targets with photometric uncertainty $\delta m \lesssim 0.05$ mag as a function of wavelength for BVI_C (purple), *Gaia* (light green), Pan-Starrs and SkyMapper *griz* (dark green), Tycho (light blue), and 2MASS (orange-red). The purple plus signs illustrate the fraction of stars with (i) B_T and B, (ii) *g*, V_T , and V, (iii) *i* and I, and (iv) 2MASS JHK plus other JHK data. The light green solid line indicates the fraction of CDDs stars with *Gaia* low resolution XP spectra. The fraction of targets with high quality optical and near-IR data ranges from $\sim 22\%$ (*griz*) to $\sim 70\%$ (Tycho) to $\sim 80\text{--}90\%$ (BVI_C and JHK) to close to 100% (*Gaia*).

Parallaxes from *Gaia* have a mean systematic offset of -0.021 mas (e.g., K. G. Stassun & G. Torres 2016, 2018; L. Lindegren et al. 2021; M. A. T. Groenewegen 2021). Among others, L. Lindegren et al. (2021) and M. A. T. Groenewegen (2021) offer methods to correct for the zero-point offset, which depends on brightness, color, sky position, and perhaps other variables. C. A. L. Bailer-Jones et al. (2021) discuss two Bayesian algorithms to treat the zero-point offset and the error distribution for observations with $S_\pi \sim 1$. For the ensemble of 3349 CDDs stars with geometric distances d_g and photogeometric distances d_p derived in C. A. L. Bailer-Jones et al. (2021), d_g and d_p are typically $\sim 0.2\%$ smaller at 100 pc than the simple estimate $d_s = 1000/\pi$ where d_s is in pc and π is in mas. For 99% of CDDs stars, the ratio of the geometric distance to the simple distance is 0.996–1.007 (0.989–1.013, 0.979–1.024) with median ratios of 0.999 (0.996, 0.992) for distances $d \leq 100$ pc ($d = 100\text{--}200$ pc, 200–400 pc). Beyond 400 pc, the ratio has a much larger range, 0.58–1.27, and a some-

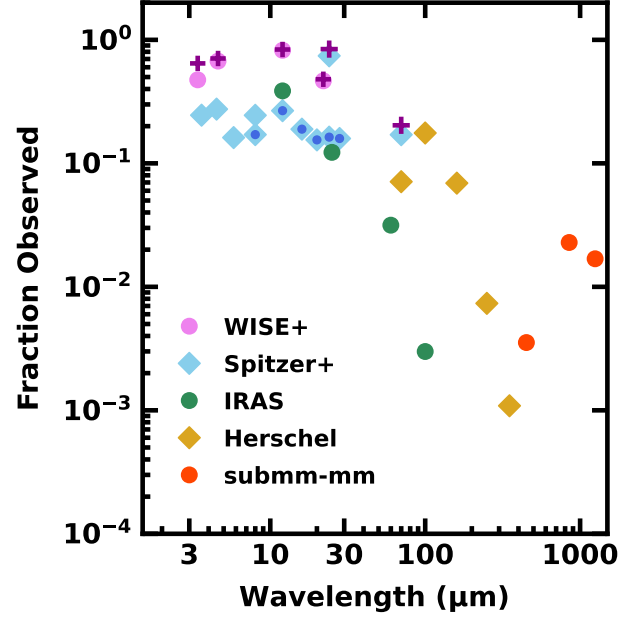


Figure 2. As in Fig. 1 for data from WISE (purple), *Spitzer* IRAC and MIPS (light blue), IRAS (dark green), *Herschel* PACS and SPIRE (gold), and submm–mm (red). The light blue symbols with a dark blue center indicate the fraction of CDDs stars with high quality synthetic photometry at 8–25 μm from *Spitzer* IRS. The fraction of observed sources ranges from $\sim 1\text{--}2\%$ at the longest wavelengths to $\sim 10\text{--}20\%$ for *Spitzer* IRAC, *Spitzer* IRS, and IRAS 25 μm to $\geq 50\%$ for W3, W4, and MIPS 24 μm measurements. With a fraction observed of zero for 500 μm SPIRE data with $\text{SNR} \geq 3$, this point is not shown.

what smaller median of 0.981. Approximately 90% of CDDs stars without d_g or d_p lie within 100 pc; none have $d_s \gtrsim 500$ pc.

For the applications discussed here, we generally adopt d_g to place stars on an HR diagram and as a check for astrometric companions and membership in moving groups, open clusters, and stellar associations. In the few cases of a distant star without d_g , we apply a correction factor derived from the median ratio d_g/d_s for stars with a range of parallaxes that bracket the parallax of the star without d_g . For nearly all stars, the difference in stellar luminosity between estimates based on d_g or d_s is less than 1%, which is smaller than the overall uncertainty in luminosity. Similarly, the impact of distance uncertainties on astrometric companions and cluster membership is negligible.

Due to uncertain parallaxes, several stars in the CDDs have d_g significantly *larger* than d_s . In five cases, δ Cru, ν Phe, λ UMa, Cl* NGC 2632 S 169, and HD 110698, we adopt d_s . The smaller distances result in more appropriate kinematics for stars clearly in associations or

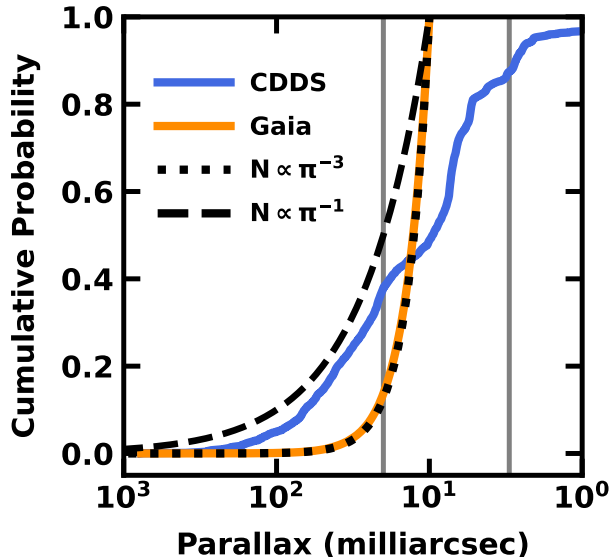


Figure 3. Cumulative probability distribution of parallaxes for CDDS stars (blue curve) and stars in the *Gaia* 100 pc sample (*Gaia* Collaboration et al. 2021a) that lie close to the M. J. Picaud & E. E. Mamajek (2013) main sequence (orange curve). The set of CDDS (*Gaia*) stars follows an $n \propto \pi^0$ ($n \propto \pi^{-2}$) volume density distribution, as indicated by the dashed (dotted) black curves.

clusters based on their lithium abundances or stellar activity measures and luminosities for pre-main sequence or main sequence stars. Other stars with $d_g \gg d_s$ are giant stars with $d \gtrsim 500$ pc and have no spectroscopic features that allow favoring one distance over another. Thus, we adopt d_g for these stars. Hereafter, we use d for the adopted distance.

Fig. 3 illustrates the cumulative probability distribution of the 3652 CDDS stars with measured parallaxes. The distribution follows a trend $N \propto \pi^{-1}$ for $\pi \gtrsim 20$ mas ($d \lesssim 50$ pc), rises more slowly to $\pi \sim 10$ mas ($d \lesssim 100$ pc), follows the linear trend again to 5 mas, and then levels off. Approximately 40% of the sample has $\pi \gtrsim 20$ mas ($d \lesssim 50$ pc); another 45% has $\pi \approx 5$ –20 mas. Fewer than 3% of the sample has $\pi \lesssim 1$ mas ($d \gtrsim 1$ kpc).

To compare CDDS stars with a complete sample, we select stars from the *Gaia* catalog of nearby stars (GCNS; *Gaia* Collaboration et al. 2021a) that lie within a band 0.25 mag below and 0.75 mag above the M. J. Picaud & E. E. Mamajek (2013) main sequence locus. The 187749 stars in this sample closely follow the $N \propto \pi^{-3}$ curve expected for an ensemble of stars with $\pi \gtrsim 10$ mas ($d \lesssim 100$ pc) (Fig. 3, orange and dot-dashed curves). Relative to the GCNS, the shape of the distribution for CDDS stars is a result of the *Spitzer* and *Herschel* selection strategies, which favor nearby, appar-

ently older field stars and stars in younger and somewhat more distant open clusters.

To select proper motions for analysis, we follow procedures outlined above for parallaxes. Choosing by signal-to-noise yields 3456 *Gaia* (187 *Hipparcos* and *Tycho-2*, 29 SIMBAD) proper motions. Prioritizing *Gaia* data over *Hipparcos* and *Tycho-2* data yields twenty-six additional stars with *Gaia* proper motion. As with parallax, *Gaia* data for the extra twenty-six *Gaia* stars in the second example have similar proper motions and lower signal-to-noise than *Tycho-2* data. Thus, the *Tycho-2* data provide a better measure of the proper motions for these stars. Although the proper motions of bright stars with $G \lesssim 13$ show a residual spin relative to fainter stars by $\lesssim 0.080$ mas yr $^{-1}$ (T. Cantat-Gaudin & T. D. Brandt 2021), this difference has a negligible impact on our analysis. In §5, we discuss proper motion data in the context of membership in stellar associations, clusters, and moving groups.

2.7. Source Identifications

To facilitate cross-matching of CDDS sources with other catalogs, we compile a limited set of source identifications. The main source identifier always succeeds in returning information on a particular star from a SIMBAD query. We select other SIMBAD-compatible source identifiers from the BD, CD, CPD, *Gaia*, Gliese, HD, *Hipparcos*, 2MASS, *ROSAT*, TESS Input Catalog, Tycho, UCAC4, and WISE catalogs (e.g., W. Gliese & H. Jahreiß 1991; M. A. C. Perryman et al. 1997; W. Voges et al. 1999, 2000; E. Høg et al. 2000; R. M. Cutri et al. 2003, 2013; N. Zacharias et al. 2013; T. Boller et al. 2016; K. G. Stassun et al. 2019; *Gaia* Collaboration et al. 2023a). We prioritize HD, *Hipparcos*, and 2MASS source identifiers when available. Aside from Bayer/Flamsteed designations and variable star names from the *General Catalog of Variable Stars* (e.g., N. N. Samus’ et al. 2017), we include specific cluster names such as ‘Cl* Blanco 1 ZS 165’ which serve to distinguish stars in various compilations for individual star clusters.

2.8. First Look

To characterize the host stars in the CDDS sample, we compile data on the photospheric and chromospheric properties, stellar and planetary companions, and membership in associations, clusters, and moving groups. We target the spectral type SpT, effective temperature T_{eff} , luminosity L_* , visual extinction A_V , surface gravity $\log g$, metallicity [Fe/H], projected rotational velocity $v \sin i$, rotational period P_{rot} , the Ca II H and K emission index R_{HK} , the Ca II infrared triplet emission index R_{IRT} , and the X-ray flux F_X . Although we do

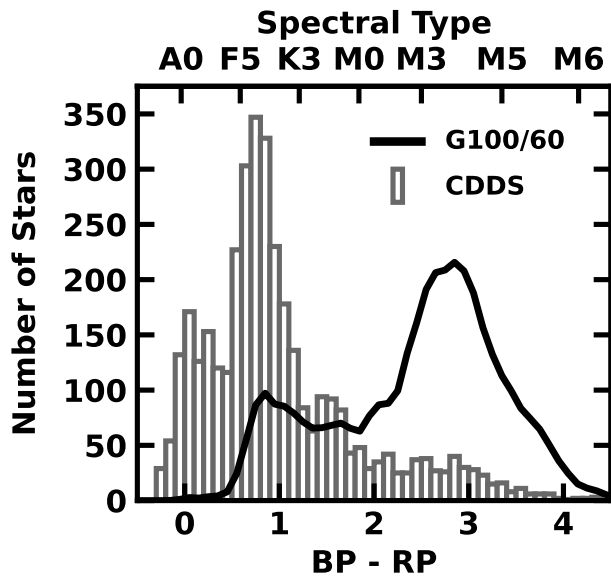


Figure 4. Frequency of BP–RP colors (lower x-axis labels) and main sequence spectral types (upper x-axis labels; M. J. Pecaut & E. E. Mamajek 2013) of stars in the CDDS sample (histogram) and main sequence stars in the Gaia 100 pc sample (solid line; Gaia Collaboration et al. 2021a). The frequency of Gaia stars has been normalized by a factor of 1/60. Relative to the Gaia sample of MS stars within 100 pc, the CDDS sample has many more AFGK stars and many fewer M-type and later stars.

not consider stellar ages, we illustrate the breadth of the compilation with HR diagrams of cluster and field stars.

To set the stage for the rest of the discussion, Fig. 4 summarizes the frequency of the observed *Gaia* BP–RP color for the 3642 CDDS stars with BP and RP magnitudes. There is a modest peak at BP–RP ~ -0.1 to 0.25 (A-type stars), a large peak at BP–RP ~ 0.8 (late F-type and G-type stars), and a long tail with larger BP–RP. Middle K-type stars produce the small rise at BP–RP ~ 1.3 –1.6. The roughly linear decline in the number of stars for BP–RP ~ 2 –4.5 results from cool stars with spectral types M1–M9. The solid line in Fig. 4 represents the scaled frequency of main sequence stars within 100 pc (Gaia Collaboration et al. 2021a). This ensemble has a small G star peak at BP–RP ~ 0.8 and a large peak at BP–RP ≈ 2.75 (M3–M6 stars).

Stars in the CDDS are not a fair sample of stars within 100 pc. Within the CDDS sample, 21% are B-type and A-type stars, 67% are FGK stars, and 12% are M-type stars. Among the *Gaia* nearby stars, only 0.3% have BP–RP colors earlier than an F0 star. There are more FGK stars in the 100 pc sample, 27%, but this fraction is ~ 2.5 times smaller than the frequency of FGK stars

in the CDDS. Finally, slightly more than 72% of all stars within 100 pc have *Gaia* colors that correspond to M0 stars and later. Only 12% of CDDS stars have *Gaia* colors as cool as M-type stars; thus the CDDS has a factor of six fewer M-type stars than the nearby star sample.

With the basic character of the CDDS set, we now delve deeper into the properties of the ensemble. We begin with the frequency of companion stars and planets.

3. COMPANIONS

3.1. Non-Single Stars in the CDDS Sample

The interpretation of observations of a star often depends on whether it is a single star or a member of a binary or multiple system. Depending on the separation of companion stars relative to disk dimensions, debris disk emission may also be sensitive to stellar multiplicity. Although it is not possible to have complete knowledge of binaries and multiples within the CDDS, we can compile a set of known binary and multiple systems from published catalogs to quantify stellar properties and the connection between debris disks and their stellar hosts in more detail. As a starting point, we query the SIMBAD database, which lists object types for each star (the `otype` field). Object types **, EB*, and SB* denote double or multiple stars, eclipsing binaries, and spectroscopic binaries. Of our 3675 samples, SIMBAD flags 1334 sources — close to a third of the total sample — with one of these object types.

Individual star catalogs referenced by SIMBAD provide more detail. The Washington Double Star Catalog (WDS), maintained at the U.S. Naval Observatory (C. E. Worley & G. G. Douglass 1997), offers data from visual binaries with separations of a fraction of an arc-second and larger. We accessed the WDS 2020 version through the *Vizier* service. The Sixth Catalog of Orbits of Visual Binary Stars (ORB6; W. I. Hartkopf et al. 2001; B. D. Mason et al. 2001) offers orbital elements of a subset of WDS stars. The *Gaia* DR3 `non_single_star` (NSS) field for each source in the main catalog references the `nss_two_body_orbit` table with stellar binary orbit solutions from astrometry, spectroscopy and photometry (Gaia Collaboration et al. 2023c; J.-L. Halbwachs et al. 2023). We leave consideration of other *Gaia* non-single-star tables, which do not provide complete orbit solutions and which may include stars with substellar companions, for a separate work. We also consider the Spectroscopic Binary Orbits Ninth Catalog (SB9, 2013 version from *Vizier*; D. Pourbaix et al. 2004) that includes orbital periods, as well as the General Catalog of

Table 2. Stellar Companions¹

Catalog	**	WDS	ORB6	SB9	Gaia	GCVS	not **
SIMBAD **	1385	713	338	270	121	75	0
WDS (field)	–	726	264	104	29	18	13
ORB6	–	–	342	96	20	17	4
SB9	–	–	–	270	46	52	0
Gaia NSS	–	–	–	–	144	15	23
GCVS	–	–	–	–	–	90	15
not **	–	–	–	–	–	–	2290

¹ SIMBAD ** sources refer to objects listed as belonging to a binary or multiple star systems. The WDS stars include only those that are not part of a star cluster (see §5 below). The Gaia sources are those with the `non_single_star` flag set to a non-zero value.

Variable Stars (GCVS, 2020 version (5.1); N. N. Samus’ et al. 2017) with the periods of eclipsing binaries.

Table 2 gives a summary of CDDS sources that are cross-listed in these catalogs, a total of 1398 objects. We also provide additional, candidate binary and triple stars that we identified in searches of stars with common proper motion (Appendix, Table 8). In both tables, we consider whether a star is in the field or identified as a member of a star cluster where confusion between bound stellar pairs and plentiful interlopers is high. If a CDDS star is in a cluster, then we ignore its membership in the WDS catalog, and do not consider it when searching for common-proper-motion companions.

Figure 5 illustrates the orbital separation between companions of non-single CDDS sources. For sources with reported orbital periods (ORB6, SBC, the *Gaia* `two_body_orbit` table, and eclipsing binaries in the GCVS), we estimate orbital distance with Kepler’s Third Law assuming that the total stellar mass is that of the Sun. With the range of masses in our catalog spanning $\sim 0.3 M_{\odot}$ to $\sim 5 M_{\odot}$, the true semimajor axis of these sources is within a factor of three of the values in the plot, a small shift compared with the seven orders of magnitude covered by the plot’s horizontal axis. The WDS sources, the gray points in the figure, have orbital distance estimated from observed angular separation and parallax. When WDS data provide multiple separations, we use the largest value, ignoring complications from detailed orbital configurations and projection effects. For stars on circular orbits, the points shown are lower limits to the orbital semimajor axis.

As a proxy for more meaningful stellar properties, Figure 5 plots absolute magnitude on the vertical axis. For most sources (1380 of 1398), the *Gaia* G band magnitude is shown, while for the few remaining objects we use the V band magnitude as listed in SIMBAD. Absolute magnitudes here may be either that of individual

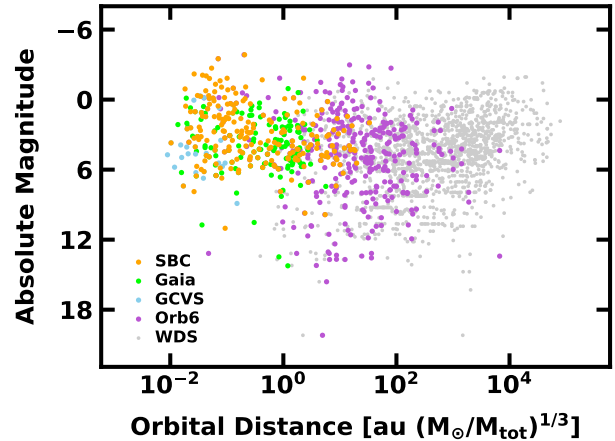


Figure 5. Summary of CDDS stars with companions. Each data point has some uncertainty or ambiguity, as described in the text, but is anticipated to be within a factor of a few of a true or well-determined value. Since each coordinate axis spans orders of magnitude, the broad characteristics of known non-single stars in the CDDS are well represented here.

stars, or, if unresolved, are from the combined starlight of system components.

Overall Figure 5 shows no particular trends other than the sensitivity of various observational techniques to orbital distance. For example, many visual binaries in WDS data have orbital separations well above 1 au, while eclipsing binaries from the GCVS have orbital separations below 1 au. We have not eliminated or otherwise connected sources that are repeated in individual surveys, leading to some horizontally aligned points in the plot that correspond to the same source. In some cases, individual WDS sources have a half dozen or more “components,” leading to the horizontal groups in Figure 5. These groups emerge from crowded regions of the sky, and do not signify multiple stars that are in isolated, bound systems.

3.2. Planets

A principal goal of this work is to understand the connection between debris disks — signposts of planet formation (S. J. Kenyon & B. C. Bromley 2002) — and planets. To identify known planet hosts in the CDDS sample, we use the NASA *Exoplanet Archive* (NXA). From a query to this database (15-Dec 2025), we find that 302 CDDS sources host a total of 471 planets. The planetary system around Trappist 1, with seven confirmed planets, is the most populated (M. Gillon et al. 2016). Four binary stars – HD 202206 (A. C. M. Correia et al. 2005), SCR J0103-5515 (2MASS J01033563-5515561; P. Delorme et al. 2013), HIP 71865 (b Cen; M.

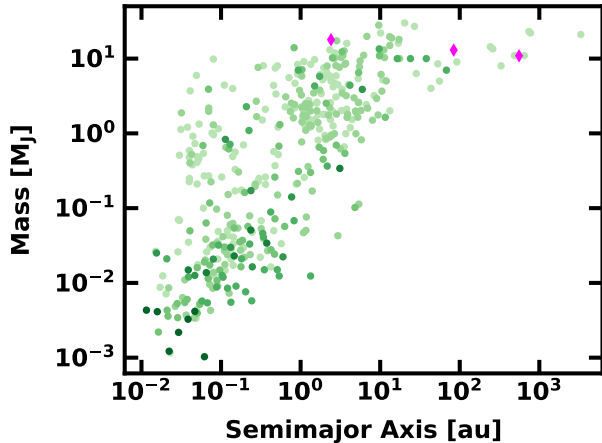


Figure 6. The semimajor axis and mass of exoplanets around stars in the CDDS from the NASA *Exoplanet Archive* database. Here we adopt the database’s best estimate for planetary mass (bmass_j). The shade of the green circles in the plot correlates with the number of planets around a stellar host. The lightest shade is a single planet around a single host and the shade darkens with increasing number of planets around a single host. The darkest green points (lower left) correspond to the seven planets around Trappist 1. The three magenta diamonds (upper center-right) represent single planets orbiting binary stars.

Janson et al. 2021), and HD 143811 (N. K. Jones et al. 2025) – host a large circumbinary planet.

Figure 6 reveals broad trends for planet mass and semimajor axis in the CDDS. A wide range of planetary masses, from less than one Earth mass to greater than a Jupiter mass, is found at semimajor axes well inside of 1 au. As the semimajor axis increases, lower mass planets become increasingly scarce. By 10 au, all known CDDS planets are more massive than Jupiter. This trend, seen also in the census of all known exoplanets (W. Zhu & S. Dong 2021, figure 1 therein), is consistent with the limitations of exoplanet discovery methods. Transits are less sensitive to smaller planets, radial velocity surveys are less sensitive to lower-mass planets, and the two survey types lose sensitivity with increasing orbital distance from the host star. Direct imaging favors larger planets at greater distances. The empty region at small planetary mass and large semimajor axis in the figure (lower right region of the plot) is expected to fill in with space-based gravitational lensing measurements (W. Zhu & S. Dong 2021, and references therein).

Table 3 summarizes the statistics of stellar and planetary companions as a function of spectral type. Anticipating the results of §4 where we derive effective temperatures T_{eff} for all CDDS stars, we use the M. J. Pecaut &

E. E. Mamajek (2013) relation between T_{eff} and spectral type to bin CDDS stars in spectral type. In this tabulation, B-type stars have $T_{\text{eff}} = 9700\text{--}31400$. The T_{eff} ranges for other spectral types are 7220–9700 K (A stars), 5930–7220 K (F stars), 5270–5930 K (G stars), 3850–5270 K (K stars), and 2270–3850 K (M stars).

Among B and A stars, the binary frequency for CDDS stars, 53% and 41%, is somewhat smaller than observed in the LAMOST survey (60% and 48%; Y. Guo et al. 2022). The fraction of binaries for CDDS FGK stars, 41% to 44%, is similar to the 43% fraction in SDSS SEGUE and somewhat larger than the $\sim 30\%$ from LAMOST (S. Gao et al. 2014). A later analysis derives a 42% binary fraction for GK dwarfs in LAMOST and *Gaia* data (Z. Niu et al. 2021). Approximately 46% of all M dwarfs are in binaries (N. Susemihl & M. R. Meyer 2022), which is only slightly larger than the fraction among CDDS M dwarfs. Overall, the binary fraction of CDDS stars is similar to the fractions derived as a function of spectral type among larger samples of stars, with perhaps a deficit of binaries among the B and A stars.

At present, the complete census of exoplanets in the *Exoplanet Archive* consists of approximately 10% hot Jupiters (mass m_p greater than $100 M_{\oplus}$ and semimajor axis a_p less than 0.1 au), 17% cool Jupiters ($m_p > 100$, $a_p \geq 0.1$ au), and 73% Earths and super-Earths at any orbital distance. In contrast, the CDDS planets consist of 6% hot Jupiters, 52% cool Jupiters, and 42% Earths and super-Earths. The differences may reflect multiple factors associated with the selection of stellar hosts. For example, the CDDS sample contains a significant number of young stars whose atmospheric activity may make Earths and super-Earths harder to detect than Jupiters. These demographics are reflected in Table 3, which highlights that the frequency of exoplanets among CDDS stars depends on spectral type as observed in larger samples of main sequence stars (e.g., L. Ghezzi et al. 2018). We will consider these differences in more detail in Papers II and III.

4. HOST STARS: DATA AND ANALYSIS

To characterize the host stars, we collect data from large wide-field surveys and more focused studies of individual stars or clusters. The large surveys usually provide T_{eff} , $\log g$, $[\text{Fe}/\text{H}]$, and radial velocity v_{rad} . Some approaches include A_V along with M_{\star} , R_{\star} , and ages derived from isochrone fitting. More focused efforts add some combination of SpT, $A(\text{Li})$, P_{rot} , $v \sin i$, L_X/L_{\star} , $\log R'_{\text{HK}}$ and $\log R'_{\text{IRT}}$. We start with pertinent details for the sources of T_{eff} , $\log g$, and $[\text{Fe}/\text{H}]$ and then discuss observations of these parameters, extinction, and

Table 3. Companion Statistics¹

type	N_{total}	N_{bin}	f_{bin}	N_{hosts}	f_{hosts}	f_{J}
B	359	171	0.476	5	0.014	1.000
A	516	207	0.401	6	0.012	1.000
F	860	375	0.436	52	0.060	0.750
G	675	297	0.440	110	0.163	0.618
K	771	262	0.340	75	0.097	0.613
M	492	163	0.331	54	0.110	0.148

¹The first column lists the spectral type derived from T_{eff} . The next two columns are the total number of stars in each temperature range and the number with binary partners (Table 2). The planet host information follows, indicating the number of hosts (N_{hosts}), the fraction of the total of each type known to host planets (f_{hosts}), and the fraction of hosts with at least one planet that is Jupiter-mass or greater (f_{J}). A value of $f_{\text{J}} = 1$ indicates that all stars with planets host at least one giant planet.

spectral type for CDDS stars. Later, we describe observations of P_{rot} , $v \sin i$, and measures of chromospheric and coronal activity.

The *Gaia* astrophysical parameters inference system (Apsis) derives stellar parameters from the *Gaia* low resolution XP spectra and the high resolution radial velocity spectrometer (RVS) data (C. A. L. Bailer-Jones et al. 2013; O. L. Creevey et al. 2023; R. Andrae et al. 2023b; M. Foesneau et al. 2023). Within the Apsis framework, the General Stellar Parameterizer from Photometry (GSP-Phot) uses an MCMC approach to derive atmospheric parameters – T_{eff} , $\log g$, $[\text{Fe}/\text{H}]$, R_{\star} , M_G , distance, and extinction in the *Gaia* bands (A_G , A_{BP} , and A_{RP}) – from XP spectra. For an adopted extinction curve, the module constructs a large set of reddened model atmospheres with known T_{eff} , $\log g$, and a_g , and finds the set of parameters (and their uncertainties) that yields the best match to an individual XP spectrum. The Final Luminosity and Age Estimator (FLAME) derives L_{\star} from T_{eff} and distance and then infers the age from fitting model isochrones to T_{eff} , L_{\star} , and $[\text{Fe}/\text{H}]$. This analysis yields results for 2754 stars.

The APOGEE (Abdurro’uf et al. 2022), *Gaia*-ESO (S. Randich et al. 2022), GALAH (S. Buder et al. 2021), and RAVE (M. Steinmetz et al. 2020) programs are high resolution spectroscopic surveys with a variety of goals. Although APOGEE mainly acquired H-band spectra of red giant stars in the northern hemisphere, many programs surveyed main sequence stars of all spectral types. *Gaia*-ESO, GALAH, and RAVE collected optical spectra of main sequence and giant stars in the southern hemisphere. *Gaia*-ESO made a special effort to target stars in young clusters. All of these programs employed a variety of analysis tools to derive stellar parameters

from high signal-to-noise spectra. Our reconnaissance yields T_{eff} , $\log g$, $[\text{Fe}/\text{H}]$, $v \sin i$, and v_{rad} for 791 stars in APOGEE, 185 in *Gaia*-ESO, 345 in GALAH, and 262 in RAVE.

The optical surveys with the Large sky Area Multi-Object Spectroscopy Telescope (LAMOST) consist of low resolution (e.g., M. Xiang et al. 2019) and medium resolution (e.g., R. Wang et al. 2020) modes in the northern hemisphere. As with the various high resolution surveys, several approaches to analyzing LAMOST data provide estimates of stellar parameters with uncertainties that are a function of the signal-to-noise of the spectra. The low and medium resolution catalogs from LAMOST DR7 yields 391 measurements from 878 spectra.

A. B. A. Queiroz et al. (2023) derive a set of stellar parameters – M_{\star} , T_{eff} , $\log g$, distance, A_V , and age – with StarHorse, a Bayesian isochrone fitting tool that analyzes results from stellar spectroscopic surveys. With astrometric data from *Gaia* eDR3 and photometric data from 2MASS, WISE, Pan-STARRS, and SkyMapper, they analyze curated data from APOGEE, *Gaia* RVS, *Gaia*-ESO, GALAH, LAMOST DR7 low and medium resolution data, RAVE, and SDSS DR12/SEGUE (B. Yanny et al. 2009). Among more than 10^7 stars, this study includes 1025 estimates of M_{\star} , T_{eff} , $\log g$, A_V , and distance for 630 CDDS stars. Results for T_{eff} and $\log g$ agree with those from the original surveys to better than $\sim 3\%$. The CDDS contains no stars within SDSS DR12/SEGUE.

More focused efforts collect or derive some combination of T_{eff} , $\log g$, $[\text{Fe}/\text{H}]$, $v \sin i$, and v_{rad} , sometimes for BA stars (E. J. de Geus et al. 1989; F. Royer et al. 2007; J. Zorec & F. Royer 2012; T. J. David & L. A. Hillenbrand 2015; Z. H. Draper et al. 2018) and more often for FGKM stars (T. Preibisch et al. 2002; B. Nordström et al. 2004; J. Holmberg et al. 2009; C. Schröder et al. 2009a; R. Martínez-Arnáiz et al. 2010; I. Ramírez et al. 2012; B. Rojas-Ayala et al. 2012; E. Gaidos et al. 2014; J. Gomes da Silva et al. 2014; E. R. Newton et al. 2014; I. Ramírez et al. 2014; N. Astudillo-Defru et al. 2017; J. D. Cummings et al. 2017; N. R. Hinkel et al. 2017; J. I. Bailey et al. 2018; S. Boro Saikia et al. 2018; A. Reiners et al. 2018; É. R. Houdebine et al. 2019; J. Gomes da Silva et al. 2021; F. Llorente de Andrés et al. 2021; E. L. Brown et al. 2022; N. Meunier et al. 2022; A. M. Boesgaard et al. 2022; A. Reiners et al. 2022; C. J. Marvin et al. 2023; L. Mignon et al. 2023; A. Rathsam et al. 2023; F. Zuo et al. 2024; C. Cifuentes et al. 2025). Several include all spectral types (K. G. Stassun et al. 2019). These approaches use a variety of photometric and spectroscopic methods to derive basic stellar pa-

rameters. In general, the most accurate results perform detailed model atmosphere fits to high signal-to-noise high resolution spectra. All told, we collect more than 100,000 measurements for more than 2000 CDDS stars.

Operations. For stars with multiple measurements of the same parameter, we construct the average (for two measurements) or the median (for three or more measurements). Typically, the differences between multiple measurements are similar to the quoted uncertainties. For the uncertainty in the average or median, we adopt the standard deviation of the average or the interquartile range of the median and add measurement uncertainties in quadrature. Where needed, we discuss the impact of combining different studies into a single average or median.

Many figures below illustrate the dependence of one stellar parameter with respect to another *and* the density of stars across the figure. To encode density, we generally adopt the Python ‘copper’ sequence of black (low density), gold (intermediate), and yellow (high density). In some figures, we use the ‘Blues’, ‘Greens’, or ‘Reds’ sequences where darker (lighter) colors indicate higher (lower) density. In all of these plots, we use density to indicate the relative concentrations; however, the density values themselves have no significance.

In the discussion that follows, we derive A_V , T_{eff} , and L_\star with optical and infrared photometry. From *Gaia* (the literature), we compile 2664 (2890) measurements of T_{eff} derived from model atmosphere fits. Combined, these data yield T_{eff} ’s for 3391 stars, $\sim 92\%$ of the sample. Using tables for main sequence (M. J. Pecaut & E. E. Mamajek 2013) or giant (A. Alonso et al. 1999; G. T. van Belle et al. 2021) stars, optical spectral types provide T_{eff} ’s for 3443 stars, $\sim 94\%$ of the sample.

With so many T_{eff} measurements from model atmosphere fits, we adopt another approach to derive A_V , T_{eff} , and L_\star from optical and infrared photometry. For each star, we compile a set of colors, B_T-V_T , $B-V$, $V-I$, $V-K$, $J-K$, $G-K$, and $BP-RP$, that minimizes contamination from dusty debris at longer wavelengths. For an adopted A_V and extinction curve (see below), matching the observed colors to a set of colors tabulated as a function of T_{eff} yields an estimate of T_{eff} for each observed color. To enable the best match between observed and tabulated colors, we interpolate in $(\log T_{\text{eff}}, \text{color})$ space. We then iterate on A_V to minimize the differences in T_{eff} among the available colors and adopt the median T_{eff} as the color T_{eff} . The interquartile range in the set of T_{eff} ’s establishes the uncertainty in the color T_{eff} .

Once A_V and T_{eff} are set, we use bolometric corrections at G, K, and V to derive L_\star . As discussed below,

the typical ratio between the T_{eff} ’s and L_\star ’s derived from this method and those from *Gaia*, the literature, and spectral types for the same star is almost identical to one with an interquartile range similar to the respective errors of the measurements. Thus, we consider this approach successful.

For most stars, the full set of colors yields the color T_{eff} . The full range in T_{eff} estimates is usually less than 5% of the median T_{eff} ; the interquartile range is roughly half that value. Sometimes B_T-V_T or $V-I$ are not available; $BP-RP$ may be compromised by light from a nearby brighter star. Still, the remaining colors are sufficient to derive a color T_{eff} with an uncertainty of a few per cent. Luminosity estimates follow a similar pattern. The typical uncertainty for L_\star derived from G, K, and V is $\lesssim 2\%$. If one or two measures are unavailable, we sometimes substitute J or make do with one or two measures. Typical uncertainties remain the same.

An advantage of this approach is the ability to consider various tables of stellar properties commonly used in the literature. As the basis for the algorithm, we adopt (i) the M. J. Pecaut & E. E. Mamajek (2013) tables to relate SpT, T_{eff} , and $\log g$ to broadband colors, radii, and masses for main sequence stars, (ii) the G. Worthey & H.-c. Lee (2011) tables to relate T_{eff} , $\log g$, and V-band bolometric corrections to optical-IR colors for giant stars with $\log g \lesssim 3.5-4$ (see also A. Alonso et al. 1999), and the A. Mucciarelli et al. (2021) expressions to derive T_{eff} from $BP-RP$ and $G-K$ for main sequence stars and giants. To compare the first two tables, we derive $\log g$ for stars in M. J. Pecaut & E. E. Mamajek (2013) from the listed M_\star and R_\star . We interpolate in the G. Worthey & H.-c. Lee (2011) tables to match $\log g$ and $B-V$ to M. J. Pecaut & E. E. Mamajek (2013) and then calculate the differences in $U-B$, $V-I$, $J-K$, and $V-K$ as a function of $B-V$. The typical color difference is $\lesssim 0.01$ mag for all $B-V$. These differences grow with decreasing $\log g$; although the differences remain small ($\lesssim 0.02$ mag) for $U-B$ and $V-I$, they reach ~ 0.05 mag for $J-K$ and $V-K$ when $\log g = 3$.

We repeat this exercise comparing M. J. Pecaut & E. E. Mamajek (2013) T_{eff} as a function $BP-RP$ and $G-K$ with T_{eff} derived from the polynomial relations in A. Mucciarelli et al. (2021). For the A. Mucciarelli et al. (2021) main sequence star relations, the median of the ratio $T_{\text{eff,m}}/T_{\text{eff,p}}$ is 0.99 for $BP-RP$ and 1.00 for $G-K$ with inter-quartile ranges of 0.01. Results with the giant relations are identical for $BP-RP$ and somewhat smaller, 0.98, for $G-K$. We conclude that the combination of the G. Worthey & H.-c. Lee (2011) and A. Mucciarelli et al. (2021) relations accurately relate the set of CDDS colors to T_{eff} for giant stars.

As an additional check, we calculate color differences between the *S. J. Kenyon & L. Hartmann (1995)* colors for main sequence stars and the adopted color tables. Although the differences for the *S. J. Kenyon & L. Hartmann (1995)* table are somewhat larger, ~ 0.01 – 0.02 mag for each B–V, the tabulated values for colors involving broadband LMNQ and IRAS fluxes complement the *Gaia* and WISE colors in *M. J. Pecaut & E. E. Mamajek (2013)*. These comparisons suggest that the choice of table has a small impact on the derived A_V , T_{eff} , and L_* .

Interstellar Extinction. Modern observations now provide detailed maps of interstellar extinction within a few kpc of the Sun (e.g., *G. M. Green et al. 2019*; *R. Lallement et al. 2019*; *G. Edenhofer et al. 2024*; *C. Zucker et al. 2025*, and references therein). In addition to revealing the structure of nearby interstellar clouds, these data demonstrate that the Sun lies within a ‘Local Bubble’ having negligible visual extinction within ~ 100 – 200 pc (see also *P. C. Frisch & D. G. York 1983*; *D. M. Sfeir et al. 1999*; *B. Y. Welsh & R. L. Shelton 2009*; *J. L. Linsky & S. Redfield 2021*; *T. J. O’Neill et al. 2024, 2025*). At larger distances, the optical extinction is patchy, $A_V \lesssim 2$ – 3 mag. The densest parts of local star-forming regions have much larger extinctions (e.g., *N. L. Chapman et al. 2009*; *Z. Cao et al. 2023*).

We adopt a simple approach to derive A_V . For ground-based optical and near-IR data, the *E. L. Fitzpatrick (1999)* relation is a popular choice for extinction in the standard Johnson BVRIJHKLM filters (see also *J. A. Cardelli et al. 1989*; *K. D. Gordon et al. 2021*; *M. Declair et al. 2022*). Recent updates analyze a broad collection of survey data and demonstrate that the extinction law in broadband filters depends on the stellar effective temperature (e.g., *S. Wang & X. Chen 2019*; *L. Li et al. 2023*; *R. Zhang & H. Yuan 2023*; *Z. Cao et al. 2024*). Nearly all CDDS stars have modest reddening, $A_V \lesssim 1$ mag, where the corrections due to stellar effective temperature are small. We adopt $A_V = 0.76 A_G = 3.1 E(\text{B-V}) = 2.67 E(\text{V-I}_C) = 2.46 E(\text{BP-RP}) = 1.37 E(\text{V-J}) = 1.12 E(\text{V-K}) = 1.98 E(\text{G-J}) = 1.51 E(\text{G-K})$. When we need a reddening for Tycho photometry, we convert B_T – V_T to B–V (*M. Bessell & S. Murphy 2012*, and references therein) and then correct B–V for reddening.

In addition to deriving A_V from the algorithm for T_{eff} and L_* , we estimate A_V from comparisons with the full set of color indices – B_T – V_T , B–V, BP–RP, V– I_C , V–J, V–K, and G–K – appropriate for the *Gaia*, literature, and spectral type T_{eff} ’s from *M. J. Pecaut & E. E. Mamajek (2013)* or *G. Worthey & H.-c. Lee (2011)*. This exercise yields up to seven independent measures of A_V

for each T_{eff} measure. The median of these results are indistinguishable for the results with the iterative algorithm described above.

In addition to deriving A_V , we include results from the literature quoted above, including *Gaia* and various *Spitzer* and *Herschel* studies. For stars inside the Local Bubble, we adopt $A_V = 0$ and confirm that the median extinction for stars with $d \leq 80$ pc is zero with an interquartile range of 0.05 mag. For stars beyond 80 pc, detailed analyses of open cluster color-magnitude diagrams yield estimates and uncertainties for the visual extinction. Some results quote A_V ; others quote the color excess $E(\text{B-V})$. We include the following estimates with those derived from optical and infrared colors, A_V (mag) = 0.18 (α Per; *A. W. Boyle & L. G. Bouma 2023*, see also *Pinsonneault et al 1998*), 0.03 (Blanco-1; *R. J. Jackson et al. 2020*), 0.005 (Coma; *D. Souto et al. 2021*), 0.0 (η Cha; *M. Rugel et al. 2018*), 0.003 (Hyades; *W. Brandner et al. 2023a*, see also *Taylor 2006*), 0.06 (IC 2391; *R. J. Jackson et al. 2020*), 0.03 (IC 2602; *R. J. Jackson et al. 2020*), 0.19 (NGC 2232; *R. J. Jackson et al. 2020*), 0.22 (NGC 2422 (M47); *N. V. Kharchenko et al. 2005*), 0.06 (NGC 2451a; *R. J. Jackson et al. 2020*), 0.22 (NGC2451 b; *R. J. Jackson et al. 2020*), 0.40 (NGC 2516; *R. J. Jackson et al. 2020*), 0.25 (NGC 2547; *R. J. Jackson et al. 2020*), 0.30 (Ori OB1a and Ori OB1b; *C. Briceño et al. 2019*), 0.12 (Pleiades; *W. Brandner et al. 2023b*, see also *Taylor 2008*), 0.08 (Praesepe; *B. J. Taylor 2006*), and 0.20 (σ Ori; *W. H. Sherry et al. 2008*).

Some young stars have K-band excesses, as measured by the ground-based K–L and K–M colors or the K–W1 and K–W2 colors. We derive A_V from observations at I_C or J, which minimizes the contribution from circumstellar disk emission (e.g., *S. J. Kenyon & L. W. Hartmann 1990*; *L. A. Cieza et al. 2005*). The results agree with extinction measurements from B–V and BP–RP. Thus, these stars appear to have little optical emission from accretion.

Collectively, we have at least 3 A_V measurements for each CDDS star. Typically, the range in A_V estimates is 0.1–0.2 mag. Estimates from color excesses usually agree well with the *Gaia* and cluster results. To derive a single estimate and an associated uncertainty, we calculate the median and the interquartile range. Using the average and standard deviation produces identical results. Sometimes, multiple A_V estimates have a spread of more than 0.5 mag. Using the T_{eff} , $\log g$, and [Fe/H] measurements as a guide, we analyze the outliers and choose the A_V estimate where the derived T_{eff} and L_* are most consistent with the atmospheric parameters.

Effective Temperature. The set of literature studies quoted above includes T_{eff} measurements for 2890 CDDS stars. To consolidate these data among the various ground-based surveys, we compare the ratio of each pair of T_{eff} estimates as a function of T_{eff} . For stars common to any of two surveys, the maximum ratio of 1.02 corresponds to a temperature difference of ~ 100 K for solar-type stars. Among CDDS stars, the temperature differences and ratios show no trend with T_{eff} . These results are similar to those derived for APOGEE, LAMOST and RAVE (G. Nandakumar et al. 2017) or for APOGEE, *Gaia*-ESO, and GALAH (V. Hegedűs et al. 2023). By deriving the average or median of multiple measurements, we minimize differences in T_{eff} scales across the compilation.

In addition to T_{eff} from *Gaia* and the literature, we convert dereddened broadband colors and adopted SpTs into T_{eff} estimates as discussed above. Error estimates assume uncertainties of ± 1 spectral subclass for SpT (see below) and the measured uncertainties for colors and extinction estimates. Including the *Gaia* and literature estimates, each CDDS star has at least two T_{eff} estimates.

To evaluate the four sets of T_{eff} estimates, we calculate the temperature ratio, $r_{T,il} = T_{\text{eff},i}/T_{\text{eff},l}$, where i represents the color, *Gaia*, or SpT T_{eff} estimate and l represents the adopted value from the ground-based literature. With 3675 (color), 2664 (*Gaia*), 2890 (ground-based literature), and 3443 (spectral types) estimates for T_{eff} , we use the average (or median) ratio and the variance (inter-quartile range) to assess the accuracy of the estimates.

Figure 7 shows temperature ratios for common stars in the *Gaia*-literature (upper panel) and the color-literature (lower panel) samples. As described in the caption, light (dark) colors indicate results for all CDDS stars (stars within 80 pc). The ratios for the full and 80 pc samples cluster around unity. For the full sample, the median ratios are 0.986 (upper panel) and 1.003 (lower panel) with inter-quartile ranges of 0.031. The spread about unity for the 80 pc samples is smaller: median ratios of 0.983 (upper panel) and 0.998 (lower panel) with interquartile ranges of 0.017 and 0.021. As in G. Nandakumar et al. (2017) and V. Hegedűs et al. (2023), we look for trends in the ratio with T_{eff} ; there are none.

Extinction causes many of the outliers in Figure 7. Sometimes, the *Gaia* analysis appears to overestimate the extinction, which results in higher T_{eff} and $r_{T,gl} \approx 1.1$ –1.5 for AF and KM stars. With no extinction correction, the larger B–V and other colors of reddened stars systematically reduce T_{eff} 's and generate a set of

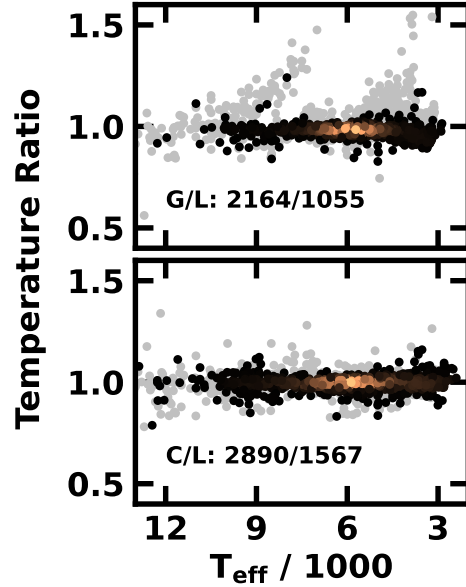


Figure 7. Ratio of T_{eff} estimates from *Gaia* and the literature (upper panel) and from B–V and the literature (lower panel). In each panel, light grey points plot results for the complete set of common stars. The ‘copper’ sequence of black, gold, and yellow points indicates ratios for stars within 80 pc of the Sun; yellow (black) regions have the highest (lowest) density of points. The numbers in each panel indicate the number of common stars in the full sample and the 80 pc sample. In the upper (lower) panel, the median ratio for all stars is 0.986 (0.998) with an interquartile range of 0.032 (0.027). For the 80 pc sample, the median ratio is 0.983 (upper panel) and 0.999 (lower panel) with an interquartile ranges of 0.018 and 0.021. There is no correlation between the ratios and T_{eff} .

stars with $r_{T,cl} \approx 0.5$ –0.9. As shown in the lower panel of Figure 7, using reddening-corrected colors eliminates nearly all outliers.

The set of T_{eff} 's derived from SpT provide a good substitute for other options. The median T_{eff} ratio is 1.000 (1.001) for the full (80 pc) sample. The interquartile ranges of 0.024 (all stars) and 0.021 (stars within 80 pc) are nearly identical to those for the *Gaia* and color samples. The spectral types derived from *Gaia* XP spectra are responsible for the excellent agreement between the literature and spectral type T_{eff} measures. Using spectral types from the literature, the median temperature ratios are still very close to unity, but the interquartile ranges are a factor of two larger. Thus, the spectral types discussed below from *Gaia* spectra are somewhat more robust than those from the literature.

Finally, we compare color T_{eff} 's with those derived from *Gaia* and spectral types. For the full sample, color T_{eff} 's are typically 1% (0.5%) smaller (larger) than *Gaia*

(spectral type) T_{eff} 's. The differences between color T_{eff} 's and spectral type T_{eff} 's are independent of distance. At large distances, $\gtrsim 80$ pc, the color and *Gaia* T_{eff} 's are typically identical. The inter-quartile ranges of these comparisons are similar, 0.01–0.02.

Spectral Types. Most of the *Spitzer* and *Herschel* studies quoted above draw spectral types from the literature (e.g., A. J. Cannon & E. C. Pickering 1924; N. Houk 1978; D. Hoffleit & C. Jaschek 1991; M. A. Hamdy et al. 1993; R. O. Gray et al. 2003; C. O. Wright et al. 2003; H. A. Abt 2004; R. O. Gray et al. 2006). To construct a more uniform set of types, we compile types from more recent analyses (J. Zorec & F. Royer 2012; T. J. David & L. A. Hillenbrand 2015; A. Reiners et al. 2018; J. Gomes da Silva et al. 2021; F. Llorente de Andrés et al. 2021; E. L. Brown et al. 2022; N. Meunier et al. 2022). Most classifications date from the HD catalog and tend to emphasize subclasses 0, 2, 5, and 8. Many are more recent. When a star has more than one classification, we adopt the average or median of multiple measurements. This exercise yields spectral types for 3334 CDDS stars.

To modernize the older classifications, we analyze 2754 *Gaia* XP spectra. These spectra come in two forms: a set of 55 coefficients for each XP spectrum or a more traditional set of fluxes as a function of wavelength. Converting the natural system of 55 coefficients to a fluxed spectrum introduces features that compromise analysis (e.g., F. De Angeli et al. 2023; P. Montegriffo et al. 2023; R. Andrae et al. 2023b; B. Huang et al. 2024). Thus, we analyze the coefficients.

As outlined in F. De Angeli et al. (2023), the first few coefficients of the BP and RP spectra contain sufficient information to classify most stellar types. We first normalize the XP spectra. Defining $S_i = \sum_{n=0}^{54} c_i$, the normalized coefficients for the blue (b_i) and red (r_i) spectra are

$$b_i, r_i = c_i/S_i \quad (2)$$

where c_i is the set of coefficients for the BP or RP spectra supplied by the *Gaia* project. We then define a *Gaia* spectral index from the first six normalized coefficients for the blue spectra:

$$I_B = b_0 - b_1 + b_2 - b_3 + b_4 - b_5. \quad (3)$$

Even-numbered (odd-numbered) coefficients of the XP spectra are usually positive (negative). To add the information contained in these coefficients, the signs in the expression for I_B alternate.

Figure 8 illustrates the relation between the *Gaia* spectral index and the B–V color for the complete set of CDDS stars (light grey symbols) and the 80 pc sample (black, gold, and yellow points). This relation excludes

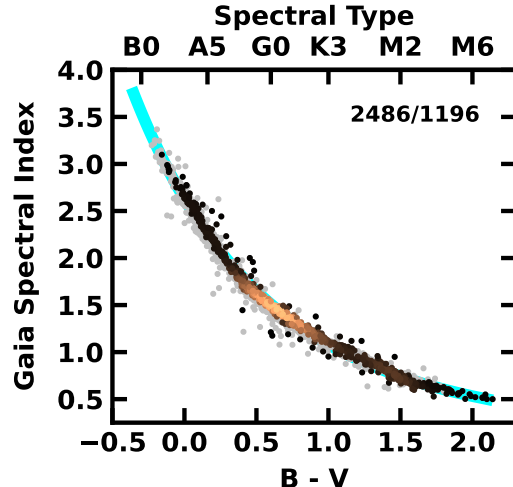


Figure 8. Relation between the *Gaia* spectral index I_B and the B–V color. The upper x-axis relates spectral types of main sequence stars to B–V (M. J. Pecaut & E. E. Mamajek 2013). Grey points: all 2527 stars with *Gaia* spectra, B–V colors, and no saturation issues; black, yellow, and gold points: 1195 stars with $d \leq 80$ pc. The cyan curve is the best-fitting polynomial to the 80 pc data (eqs. 4–5). The clear correlation between I_B and B–V enables spectral classification with an accuracy of ± 0.5 – 0.75 subclass.

stars with $S_C(G) \gtrsim 10$, large differences between observed and predicted V and I ($\delta V, I \gtrsim 0.1$), and large RUWE $\gtrsim 3$. Aside from a few outliers, there is a clear correlation, where stars with larger I_B have bluer colors. The full sample and the 80 pc sample follow the same relation.

Although there is also a strong correlation between I_B and the spectral type, the scatter about the relation is much larger than the scatter about the relation between I_B and B–V. Similarly, we consider relations between (i) B–V and an index derived from the red spectra I_R , (ii) the *Gaia* BP–RP color and either I_B and I_R , and (iii) the V–K and J–K colors and either I_B or I_R . In all cases, there is a clear correlation between color or spectral type and *Gaia* spectral index. However, none are as clean as the relation shown in Figure 8. There is more scatter about the relation and the relation breaks down for spectral types \gtrsim M5–M6 (B–V $\gtrsim 2$; BP–RP $\gtrsim 4.5$).

To make a useful relation between I_B and B–V, we take the logarithm of I_B and derive a simple quadratic:

$$\log I_B = 0.41958 - 0.42413 (B - V) + 0.03866 (B - V)^2 \quad (4)$$

The small quadratic term allows a better fit for small and large B–V where the correlation displays some curvature. Constructing samples of stars with $d \leq 20$ pc,

40 pc, and 60 pc yields nearly identical results. Solving this equation for B–V yields

$$B - V = 5.48544 - \sqrt{19.23779 + 26.85997 \log(I_B)}. \quad (5)$$

Adopting an expression between B–V and spectral type (e.g., [M. J. Pecaut & E. E. Mamajek 2013](#)) provides a method to infer spectral types from I_B . The upper x-axis of Fig. 8 illustrates this relation.

To test eq. 5, we explore results for ~ 1200 stars with $d \leq 80$ pc. For each star with a known spectral type, B–V, and I_B , we derive B–V from eq. 5. We then (i) interpolate in the [M. J. Pecaut & E. E. Mamajek \(2013\)](#) table for main sequence stars to infer a spectral type from the measured B–V and the B–V estimated from I_B and (ii) compute the difference in spectral types, d_i , where i represents the known spectral type, the type from B–V only, and the type from I_B . The median offset (interquartile range) between the *Gaia* and B–V types is 0.05 (0.9) subclass independent of B–V. Compared to literature spectral classifications, the *Gaia* and B–V types are 0.25 subclass later, with interquartile ranges of ~ 0.75 subclass. This comparison demonstrates that the *Gaia* I_B index and the B–V color yield accurate spectral types with an uncertainty of somewhat less than one subclass.

The BP spectra and BP–RP color yield a relation similar to eq. 5:

$$BP - RP = 3.13678 - \sqrt{2.94796 + 15.49763 \log(I_B)}. \quad (6)$$

As with eq. 5, this relation and [M. J. Pecaut & E. E. Mamajek \(2013\)](#) yield spectral types with a median offset (inter-quartile range) of 0.25 (0.85) of a subclass.

Both approaches to derive spectral types from I_B fail for types \gtrsim M5–M6. For these late-type stars, I_B changes little with B–V or BP–RP. Small fluctuations in I_B also produce much larger variations in the derived B–V and BP–RP, which creates large uncertainties in the derived spectral type. This behavior also occurs in red *Gaia* spectra and with additional coefficients in the expressions for I_B and I_R . We therefore recommend using eqs. 5–6 only for stars earlier than \sim M5.

For stars with $d > 80$ pc, the *Gaia* or B–V spectral types are generally later than the literature spectral types. Stars with negligible (measurable) reddening, $A_V \lesssim 0.01$ mag ($A_V \gtrsim 0.1$ – 0.2 mag) are typically $\lesssim 0.25$ subclass ($\gtrsim 1$ subclass) later than the literature spectral types. Correcting for extinction is straightforward. The dereddened B–V or BP–RP color yields a corrected I_B and SpT through eq. 4 or the equivalent result for BP–RP. As with the 80 pc sample, the corrected spectral types are nearly indistinguishable from the known

SpTs or SpTs derived from measured T_{eff} 's. Thus, the *Gaia* spectra yield accurate spectral types for stars with a measured B–V or BP–RP.

Stellar Luminosity. With T_{eff} estimates for all CDDS stars, combining a bolometric correction appropriate for the measured T_{eff} ([M. J. Pecaut & E. E. Mamajek 2013](#)); a G, K, or V magnitude; A_V ; and d yields the bolometric luminosity L_\star . For the brightest stars ($V \lesssim 5$), we prefer G or V to derive L_\star due to saturation issues with 2MASS K. Smaller uncertainties in the extinction favor K over G and V for fainter stars. In all cases, we adopt a T_{eff} from those available and derive L_\star from the average of the G, K, and V luminosity estimates and the uncertainty in L_\star from the dispersion in the average. For nine stars, we derive L_\star from a single measurement, either G, K, or V.

Formally, the lack of parallaxes prevent L_\star estimates for 32 stars. However, many stars without distances have positions, proper motions, and radial velocities that strongly imply cluster membership (see §5 below). Adopting the nominal distance of the cluster for these stars yields luminosities within a few percent of cluster stars with identical T_{eff} . Thus, we adopt the association or cluster distance for these stars. In other cases, the $\log g$ and T_{eff} measures together with data for the stellar activity measures discussed below place stars robustly on the [M. J. Pecaut & E. E. Mamajek \(2013\)](#) main sequence. Using a stellar mass from [M. J. Pecaut & E. E. Mamajek \(2013\)](#) that corresponds to the measured T_{eff} and the measured $\log g$ yields a luminosity and distance. With these approaches, we derive L_\star for 3675 CDDS stars.

Figure 9 summarizes aspects of the L_\star estimates. The lower panel shows the dispersion in the logarithm of L_\star , $\sigma_{\log L}$, as a function of L_\star . For the full (80 pc) sample, the median uncertainty in $\log L_\star$ is 0.004 (0.005); the interquartile range of the uncertainty is 0.009 (0.010) for the 80 pc (full) sample. Among the main sequence stars, the set of L_\star estimates ranges from 15% below to a factor of 2–3 above the [M. J. Pecaut & E. E. Mamajek \(2013\)](#) main sequence locus. As expected, K-type and M-type stars in the Sco–Cen association typically lie a factor of 5–10 above the main sequence. A small group of GKM giant stars are 10–1000 times more luminous than their main sequence counterparts.

The upper panel of Fig. 9 compares L_\star estimates with results from *Gaia* APSIS. We define $\Delta L_{CG} = \log L_\star - \log L_G$, where L_G is the APSIS estimate. For stars within 80 pc, the APSIS luminosity estimates are less than 2% larger than L_\star : the median $\Delta L_{CG} = -0.018$ with an interquartile range of 0.020. The median dif-

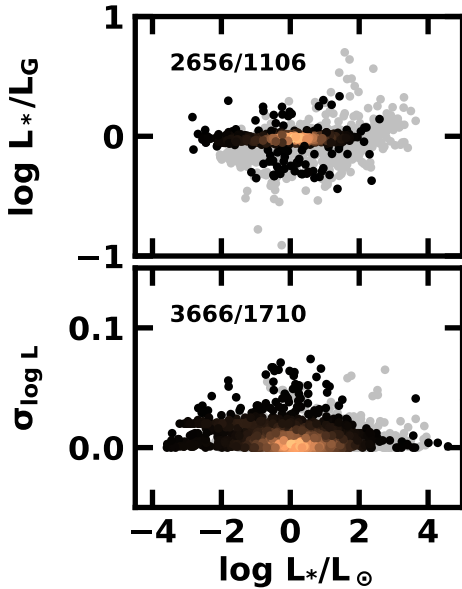


Figure 9. Properties of derived L_* for the full sample (light points) and the 80 pc sample (dark points). *Upper panel:* logarithms of the ratio of L_* to the *Gaia* luminosity L_G as a function of L_* . *Lower panel:* uncertainty in the logarithm of L_* derived from the G, K, and V luminosities.

ference grows to 3% among more distant stars, with an interquartile range of 9%.

There are two main sources of large outliers in the upper panel of Fig. 9. Within the 80 pc sample, unresolved binaries with approximately equal masses distort the APSIS luminosity estimate. We usually correct luminosities based on the measured magnitude difference (e.g., C. A. Hummel et al. 1995; C. E. Worley & G. G. Douglass 1997) or the measured masses (e.g., W. I. Hartkopf et al. 2001; B. D. Mason et al. 2001; D. Pourbaix et al. 2004; A. Tokovinin 2018; G. Torres et al. 2021; E. Gosset et al. 2024) and a mass–luminosity relation (M. J. Pecaut & E. E. Mamajek 2013). Sometimes, we add constraints derived from analyses of specific spectroscopic binaries (e.g., A. C. Cameron et al. 1981; F. C. Fekel et al. 1988; D. M. Popper 1990; F. C. Fekel et al. 1994; F. C. Fekel 1996, 1997; S. V. Berdyugina et al. 1998; G. Torres & I. Ribas 2002; O. Cakirli et al. 2003; F. C. Fekel et al. 2004; A. Tokovinin et al. 2006; K. Fuhrmann 2008; E. R. Houdebine 2009; D. Raghavan et al. 2009; K. Fuhrmann et al. 2011; R. E. M. Griffin & R. F. Griffin 2011; F. Baron et al. 2012; K. G. Hełminiak et al. 2012; I. Ramírez et al. 2012; Z. Eker et al. 2014; F. Anthonioz et al. 2015; K. Fuhrmann & R. Chini 2015; C. A. Hummel et al. 2017; F. Kiefer et al. 2018; I. Czekala et al. 2019; O. Kochukhov & D. Shulyak 2019; L. Piccotti et al. 2020; R. Akeson et al. 2021; A.

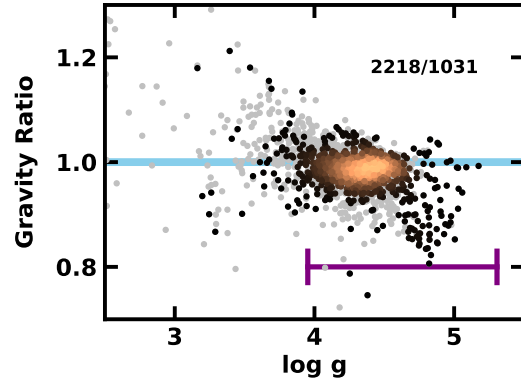


Figure 10. Ratio of gravity estimates from *Gaia* and the literature. Light (dark) points show results for stars with $d > 80$ pc ($d \leq 80$ pc). The light blue bar indicates a ratio of one. The bar in the lower right indicates the range of gravities for stars on the main sequence, from early OB stars with $\log g \sim 4$ to late M stars with $\log g \sim 5.3$ (M. J. Pecaut & E. E. Mamajek 2013).

Hahlin et al. 2021; N. Meunier & A.-M. Lagrange 2022; P. S. Muirhead et al. 2022; T. Ryabchikova et al. 2022; G. Torres et al. 2022; A. Gallenne et al. 2023; G. Torres et al. 2024). For more distant stars, differences in the adopted extinction estimate lead to differences in the derived luminosities. Typically, *Gaia* derives larger A_V and a larger luminosity. For distant stars, optical G and V along with 2MASS K yield a good estimate for the reddening; G, K, and V then enable a more accurate estimate for L_* than APSIS. Often, the measured $\log g$ helps to choose between possible options for T_{eff} , A_V , and L_* .

Surface Gravity. After discarding ~ 15 measurements where the surface gravity is a factor of more than two smaller or larger than the expected surface gravity for the measured SpT, T_{eff} , and L_* and deriving the average or median of multiple measurements, the compilation of stellar atmospheric parameters from the literature yields surface gravity measurements for 2955 stars. The *Gaia* DR3 catalog provides another 2664 estimates. Together, the full set of literature and *Gaia* data provides at least one measurement of $\log g$ for 3401 stars, $\sim 93\%$ of the full sample.

Figure 10 compares the ratio r_{grav} of $\log g$ values for the *Gaia* estimates relative to the literature estimates ($r_{\text{grav}} = \log g_{\text{Gaia}} / \log g_{\text{lit}}$). For most stars, the ratios are very close to unity. For the 80 pc (full) sample, the median ratio is 0.986 (0.989) with an inter-quartile range of 0.032 (0.036). Thus the *Gaia* $\log g$ values are typically 1% smaller than the literature estimates. The derived inter-quartile ranges are similar to the typical differences in $\log g$ among a set of multiple measurements, $\Delta \log g$

~ 0.05 – 0.06 . Thus, the difference between the *Gaia* and literature $\log g$ values is smaller than the typical differences among multiple ground-based literature estimates.

There are two sets of outliers in Fig. 10. For high gravity M dwarfs, the *Gaia* $\log g$ estimates are systematically lower than the literature estimates by 10% to 20%. Comparison with the expected $\log g$ for M dwarfs on the main sequence indicates that the *Gaia* estimates are smaller than the true gravity. Among some lower gravity stars, *Gaia* $\log g$ estimates are up to 20% larger than the ground-based literature estimates. This group mostly includes pre-main sequence stars and red giant stars, where the literature gravity appears more appropriate given results for T_{eff} , L_* , and the activity indicators discussed below. Based on this analysis, we prefer the literature gravity estimates when available.

Metallicity. As with T_{eff} and $\log g$, we extract $[\text{Fe}/\text{H}]$ data for CDDS stars from *Gaia*, large ground-based surveys, compilations of published results (A. Gáspár et al. 2016; X. Zhang et al. 2023), and recent, more focused studies on specific types of main sequence stars not included in the A. Gáspár et al. (2016) compilation. We construct two sets of $[\text{Fe}/\text{H}]$ measurements: a) 1400 stars from A. Gáspár et al. (2016) and b) 1792 stars with multiple measurements from more recent ground-based studies. For the second set, we set $[\text{Fe}/\text{H}]$ equal to the average (median) for stars with two (three or more) measurements; we adopt the standard deviation or the inter-quartile range as the uncertainty in $[\text{Fe}/\text{H}]$.

We verify the lack of a large systematic offset between these two sets. For the ~ 1000 stars with two or more measurements, the average adopted uncertainty in $[\text{Fe}/\text{H}]$ is 0.07 ± 0.06 , which is similar to the quoted uncertainty of a typical measurement. Nearly 97% of the stars with two or more measurements have an uncertainty $\lesssim 0.20$. As a function of $[\text{Fe}/\text{H}]$, there is no trend in the measured uncertainty. The lack of a trend suggests there is a negligible offset among the multiple sets of metallicity measurements.

As another test, we consider the 833 common sources between the A. Gáspár et al. (2016) compilation and subsequent non-*Gaia* studies. The median offset (inter-quartile range) is $\Delta[\text{Fe}/\text{H}] = 0.00$ (0.070). Following G. Nandakumar et al. (2017), we derive the median offset in bins from $[\text{Fe}/\text{H}] = -0.5$ to 0.5 in steps of 0.1 and look for trends in the median with $[\text{Fe}/\text{H}]$. The minimum (maximum) offset in this range is $\Delta[\text{Fe}/\text{H}] = -0.01$ for $[\text{Fe}/\text{H}] = -0.5$ to -0.4 (0.02 for $[\text{Fe}/\text{H}] = 0.2$ – 0.3). These offsets are less than the typical errors in $[\text{Fe}/\text{H}]$.

The combined studies of G. Nandakumar et al. (2017) and V. Hegedűs et al. (2023) demonstrate relationships between $[\text{Fe}/\text{H}]$ measures among the APOGEE,

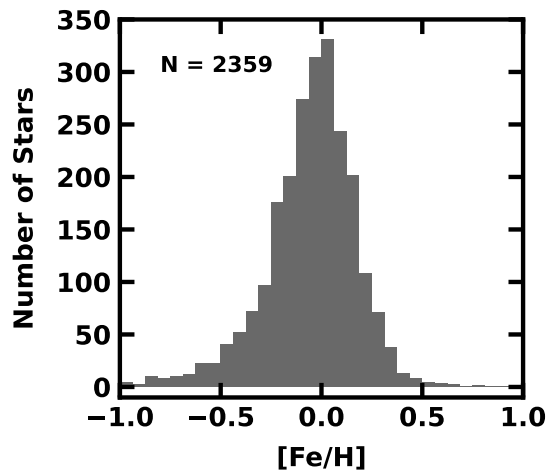


Figure 11. Frequency distribution of $[\text{Fe}/\text{H}]$ for the full sample of 2359 CDDS stars with metallicity estimates. The sample has a median $[\text{Fe}/\text{H}]$ of -0.03 and a full-width at half maximum ~ 0.13 .

GALAH, Gaia-ESO, LAMOST, and RAVE surveys. For the $[\text{Fe}/\text{H}]$ range among CDDS stars, the metallicity differences among these surveys is small compared to the uncertainties in $[\text{Fe}/\text{H}]$. We also consider offsets between common sources in the A. Gáspár et al. (2016) compilation and these recent, much larger surveys. Although we identify variations in $\Delta[\text{Fe}/\text{H}]$ with $[\text{Fe}/\text{H}]$, for the full A. Gáspár et al. (2016) sample with respect to the APOGEE, GALAH, and RAVE samples, the offsets for the subset of CDDS stars in the A. Gáspár et al. (2016) compilation are small, ~ 0.02 – 0.04 per dex, and less than the typical uncertainty in $[\text{Fe}/\text{H}]$. We conclude that the full set of 2359 $[\text{Fe}/\text{H}]$ measurements for CDDS stars are on a roughly similar scale.

To try to supplement these data, we consider several compilations of $[\text{Fe}/\text{H}]$ derived from *Gaia* XP spectra (R. Andrae et al. 2023b,a; X. Zhang et al. 2023). The median offsets are $+0.31$ for *Gaia* DR3 metallicities (R. Andrae et al. 2023b) and $+0.23$ for the machine-learning metallicities from X. Zhang et al. (2023). Eliminating the OBA stars where analyses of XP spectra have issues reduces the offsets to $+0.23$ for *Gaia* DR3 and $+0.20$ for X. Zhang et al. (2023). There is no obvious trend of the offset with $[\text{Fe}/\text{H}]$ for the *Gaia* metallicities. However, the offsets with the X. Zhang et al. (2023) metallicities show a clear trend with $[\text{Fe}/\text{H}]$. Rather than try to place these data on the same scale as the ground-based data, we discard them for this analysis.

The distribution of $[\text{Fe}/\text{H}]$ among CDDS stars resembles a Gaussian with a longer tail to smaller $[\text{Fe}/\text{H}]$ than to larger $[\text{Fe}/\text{H}]$ (Fig. 11). Although there are a few very low (high) metallicity stars with $[\text{Fe}/\text{H}] = -2.30$

(0.97), the distribution is highly concentrated about the median $[\text{Fe}/\text{H}] = -0.03$. Half (90%, 98%) of the sample has $[\text{Fe}/\text{H}] = -0.17$ to 0.09 (-0.48 to 0.26 , -0.93 to 0.40). This distribution is similar to that in other collections of nearby stars (e.g., N. R. Hinkel et al. 2014).

Lithium. With applications in big bang nucleosynthesis and galactic chemical evolution, lithium plays a big role in stellar astrophysics (e.g., T. Bensby & K. Lind 2018; X. Gao et al. 2020; D. Romano et al. 2021; S. Buder et al. 2022). On the main sequence, the convective atmospheres of late-F and GKM stars draw lithium into the hydrogen-burning core, where it is destroyed (e.g., M. Pinsonneault 1997). Hence the Li abundances of lower main sequence stars decline with time and may serve as a useful age indicator for CDDS and other main sequence stars (e.g., P. Sestito & S. Randich 2005; R. D. Jeffries et al. 2023; A. Rathsam et al. 2023; M. L. Gutiérrez Albarrán et al. 2024).

Published data for the Li abundance generally fall into three categories: the absolute lithium abundance on a log scale where the hydrogen abundance is 12 ($A(\text{Li})$; e.g., R. D. Jeffries 1999; A. Ford et al. 2001; A. M. Boesgaard et al. 2003; D. L. Lambert & B. E. Reddy 2004; L. da Silva et al. 2009; L. Ghezzi et al. 2010; G. Pace et al. 2012; I. Ramírez et al. 2012; E. Delgado Mena et al. 2014, 2015; R. López-Valdivia et al. 2015; G. Guiglion et al. 2016; J. D. Cummings et al. 2017; J. Bouvier et al. 2018; C. Aguilera-Gómez et al. 2018; M. Carlos et al. 2019; C. Chavero et al. 2019; F. Llorente de Andrés et al. 2021; A. M. Boesgaard et al. 2022; A. Hourihane et al. 2023; A. Rathsam et al. 2023; M. L. Gutiérrez Albarrán et al. 2024; D. Lubin et al. 2024), the lithium abundance relative to the solar abundance $[\text{Li}/\text{H}]$ (e.g., S. Buder et al. 2021), and the equivalent width of the Li I 670.8 nm absorption line (T. Preibisch et al. 2002; M. J. Pecaut & E. E. Mamajek 2016; M. Zerjal et al. 2019, 2021; K. L. Luhman & T. L. Esplin 2022; R. D. Jeffries et al. 2023; M. Zerjal et al. 2023). We derive the absolute abundance from the relative abundance: $A(\text{Li}) = [\text{Li}/\text{H}] + A(\text{Li})_{\odot}$, where $A(\text{Li})_{\odot} = 1.05$ is the solar Li abundance (M. Asplund et al. 2009).

Converting Li I equivalent widths $\text{EW}(\text{Li})$ to absolute or relative abundances requires a detailed model atmosphere calculation. Here, we adopt the grid of model atmospheres in E. Franciosini et al. (2022), which compiles Li I curves of growth as a function of T_{eff} , $\log g$, and $[\text{Fe}/\text{H}]$. For CDDS stars with measured T_{eff} , $\log g$, $[\text{Fe}/\text{H}]$, and Li I equivalent widths, we interpolate in their Table A.1 (for FGK stars) and Table A.3 (for M stars) to derive $A(\text{Li})$. For stars with literature estimates of $A(\text{Li})$ and quoted $\text{EW}(\text{Li})$ which we convert to $A(\text{Li})$, we derive a median offset from the model conver-

sion of $\Delta A(\text{Li}) = A(\text{Li})_{\text{lit}} - A(\text{Li})_{\text{EW}} = -0.04$ with an interquartile range of 0.09. Thus, the model-conversion of $\text{EW}(\text{Li})$ to $A(\text{Li})$ results in a slightly larger Li abundance than published abundances. However, this difference is smaller than the typical uncertainty, ~ 0.1 – 0.2 dex, of a single $A(\text{Li})$ estimate.

Some studies report T_{eff} and Li I equivalent widths without $\log g$ or $[\text{Fe}/\text{H}]$ data. As a test for stars in the Hyades and Praesepe (J. D. Cummings et al. 2017), we match a solar metallicity PARSEC isochrone (Y. Chen et al. 2014; J. Tang et al. 2014; Y. Chen et al. 2015) with age = 800 Myr to the measured T_{eff} , adopt the corresponding $\log g$, and estimate $A(\text{Li})$ for ~ 100 stars from observed equivalent widths. For Hyades stars and Praesepe stars, the results are indistinguishable: a median offset of -0.04 in $A(\text{Li})$ relative to the values in J. D. Cummings et al. (2017) and an interquartile range of 0.08. For an ensemble of Pleiades stars from diverse sources, we achieve similar uncertainties using a 100 Myr solar metallicity PARSEC isochrone to set $\log g$. Finally, a set of 150 stars with membership probability greater than 0.5 in the young cluster 25 Ori from the Gaia-ESO survey (A. Hourihane et al. 2023) also yields good agreement between the $A(\text{Li})$ derived in A. Hourihane et al. (2023) and $A(\text{Li})$ derived using a 10 Myr isochrone for $\log g$: a median offset of $+0.00$ and an interquartile range of 0.12. Thus, this approach provides reasonably accurate Li abundance estimates from a set of measured equivalent widths for ages 10 Myr to 1 Gyr.

For each CDDS star with two (or more) measurements of $A(\text{Li})$, we compute the average (median) value. The range of multiple published measurements for a single CDDS star, $\Delta A(\text{Li}) \approx 0.1$ – 0.2 , is generally comparable to the typical error of a single measurement. For stars with upper limits, we adopt the most recent measurement or the measurement from the highest signal-to-noise spectrum (when available).

Fig. 12 shows the variation of $A(\text{Li})$ with T_{eff} for 1301 CDDS stars. The overall morphology is similar to that in larger compilations of low mass MS stars (e.g., F. Llorente de Andrés et al. 2021; A. Rathsam et al. 2023; M. L. Gutiérrez Albarrán et al. 2024, and references therein). The upper envelope of the distribution peaks at $A(\text{Li}) \approx 3.5$ for mid F-type stars with $T_{\text{eff}} \sim 6500$ K and falls to $A(\text{Li}) \approx 3$ towards hotter and cooler T_{eff} . Stars in the densest part of the ensemble have $T_{\text{eff}} \approx 5000$ – 6500 K and $A(\text{Li}) \approx 2$ – 3 . These stars have abundances 10–100 times larger than the solar abundance. For $T_{\text{eff}} \approx 3500$ – 6000 K, there is a set of stars with $A(\text{Li}) \approx 0$ – 2 and a few stars with $A(\text{Li}) \approx -1$ to 0 . Within this T_{eff} range, many stars only have upper limits for $A(\text{Li})$.

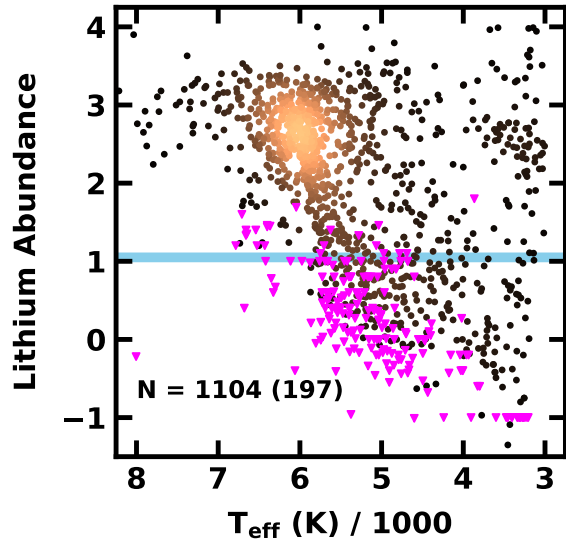


Figure 12. Lithium abundance $A(\text{Li})$ as a function of effective temperature for CDDS stars. Colors of filled circles (1104 points) indicate the relative density, ranging from low (black) to moderate (dark gold) to high (bright yellow). Filled fuchsia triangles indicate upper limits for 197 stars. The solid horizontal blue line indicates the solar lithium abundance (M. Asplund et al. 2009). CDDS stars follow the general trend of decreasing $A(\text{Li})$ with decreasing T_{eff} , but they display a clear gap at $1.0 \lesssim A(\text{Li}) \lesssim 2.0$ not observed in much larger samples.

Compared to the general population of FGKM stars, CDDS stars have larger lithium abundances (e.g., I. Ramírez et al. 2012; F. Llorente de Andrés et al. 2021; A. Rathsam et al. 2023; M. L. Gutiérrez Albarrán et al. 2024). In a population of cool stars with $T_{\text{eff}} \lesssim 4500\text{--}5000$ K, $A(\text{Li})$ declines to values comparable to or less than the solar Li abundance on time scales $\lesssim 100\text{--}200$ Myr (e.g., R. D. Jeffries et al. 2023). The CDDS K–M dwarfs with $A(\text{Li}) \gtrsim 1$ are likely much younger than typical nearby M dwarfs with ages $\gtrsim 1$ Gyr and negligible Li abundances. Among a sample of ‘solar-twin’ stars with ages $\tau \approx 0.5\text{--}11$ Gyr (M. Carlos et al. 2019; A. Rathsam et al. 2023), few (many) have $A(\text{Li}) \gtrsim 2$ ($A(\text{Li}) \lesssim 1.5$). In the Hyades and Praesepe ($\tau \approx 750\text{--}800$ Myr; W. Brandner et al. 2023a), solar-type stars with $T_{\text{eff}} \gtrsim 5600$ K ($T_{\text{eff}} \lesssim 5600$ K) have $A(\text{Li}) \gtrsim 2.0$ ($A(\text{Li}) \lesssim 2$; J. D. Cummings et al. 2017). Many solar-type stars in the CDDS have $A(\text{Li}) \gtrsim 2$ and are thus probably younger than stars in the Hyades. This group includes field stars *not* in an association, cluster, or moving group.

Stellar Rotation. Measurements of stellar rotation periods P_{rot} require a dedicated facility to cover time scales ranging from a few to a few hundred days. Along

with several studies based on *Gaia*, *Kepler*, and *TESS* data, programs with small ground-based telescopes provide P_{rot} for 1383 stars (L. M. Rebull et al. 2004; W. A. Lawson & L. A. Crause 2005; J. D. Hartman et al. 2010; P. Delorme et al. 2011; P. A. Cargile et al. 2014; G. Kovács et al. 2014; E. R. Newton et al. 2016; L. M. Rebull et al. 2016; N. Astudillo-Defru et al. 2017; S. T. Douglas et al. 2017; S. N. Mellon et al. 2017; S. Messina et al. 2017; E. R. Newton et al. 2017; L. M. Rebull et al. 2017; E. R. Newton et al. 2018; L. M. Rebull et al. 2018; E. Díez Alonso et al. 2019; S. T. Douglas et al. 2019; M. Küker et al. 2019; P. Schöfer et al. 2019; K. Bouchaud et al. 2020; B. L. Canto Martins et al. 2020; E. Gillen et al. 2020; E. Magaudda et al. 2020; L. M. Rebull et al. 2020; R. Rampalli et al. 2021; E. Magaudda et al. 2022; A. Núñez et al. 2022; P. Petit et al. 2022; A. Reiners et al. 2022; L. M. Rebull et al. 2022; E. Distefano et al. 2023; M. Popinchalk et al. 2023; A. Núñez et al. 2024; S. T. Douglas et al. 2024; I. L. Colman et al. 2024; J. P. S. Campelo et al. 2025). For some stars, we calculate the average (median) of two (three or more) measurements.

Sources for $v \sin i$ measurements cover a broad range. In addition to *Gaia*, we collect data from the APOGEE (Abdurro’uf et al. 2022), GALAH (S. Buder et al. 2021), and RAVE (M. Steinmetz et al. 2020) surveys. D. Hoffleit & C. Jaschek (1991) has a good compilation for the brightest stars. Other studies report data for B-type and A-type stars (H. A. Abt & N. I. Morrell 1995; H. A. Abt et al. 2002; F. Royer et al. 2002a,b, 2007; J. Zorec & F. Royer 2012; T. J. David & L. A. Hillenbrand 2015), FGK stars (R. J. White et al. 2007; C. Schröder et al. 2009a; M. Rainer et al. 2023), M-type stars (G. Torres & I. Ribas 2002; J. S. Jenkins et al. 2009; L. Malo et al. 2014; E. R. Houdebine 2011; A. Reiners et al. 2012; E. R. Houdebine & D. J. Mullan 2015; E. R. Houdebine et al. 2016; A. Reiners et al. 2018; P. Schöfer et al. 2019; A. Reiners et al. 2022), and stars in open clusters (R. Glebocki et al. 2000; J. I. Bailey et al. 2018; D. J. Fritzewski et al. 2020; L. G. Bouma et al. 2021). For all of the $v \sin i$ data, we eliminate duplicate measurements from multiple compilations and adopt the average (median) of two (three or more) measurements. Often, studies report upper limits for stars with small $v \sin i$. For these stars, we compute the average (or median) for all measurements without an upper limit and adopt the smaller of the average (or median) and the upper limit. Several studies using cross-correlation techniques report $v \sin i = 0$ for a dozen stars when the width of the cross-correlation peak is indistinguishable from that of a non-rotating star. We adopt an upper limit of 3 km s^{-1} , which is roughly half the median of all $v \sin i$ upper limits in the CDDS and corresponds to the peak

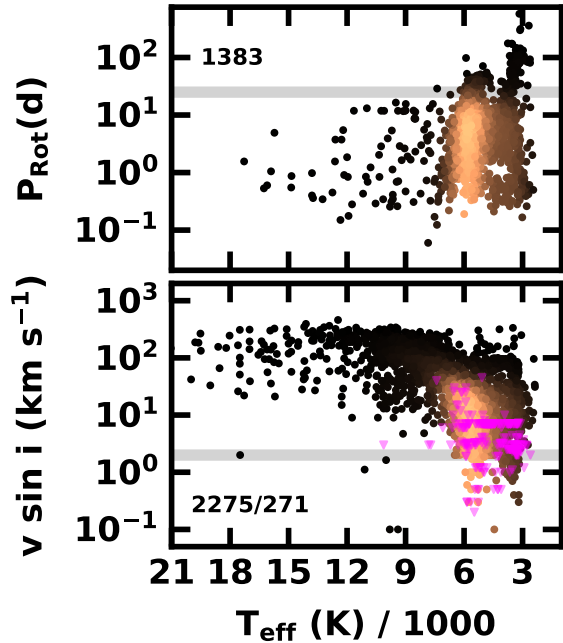


Figure 13. Rotation as a function of T_{eff} . *Upper panel:* rotational periods in days for 1383 stars. *Lower panel:* projected rotational velocities in km s^{-1} for 2275 stars (black, yellow, gold points) and upper limits for 271 stars (fuchsia triangles). In both panels, the horizontal grey band indicates solar values.

of the $v \sin i$ distribution in the extensive compilation of B. Nordström et al. (2004). Often these stars have measurements from other sources. We then adopt the smaller of the average of other measurements and the adopted upper limit.

Fig. 13 plots P_{rot} (upper panel) and $v \sin i$ (lower panel) as a function of T_{eff} . Among B-, A-, and early F-type stars, the lack of photospheric features prevents robust measurements for all but a handful of rapidly rotating stars with $P_{\text{rot}} \lesssim 10$ days. Late F-type and GK stars have a broad range of rotational periods, $P_{\text{rot}} \approx 0.1\text{--}100$ days, and a median $P_{\text{rot}} \approx 8$ days that is somewhat shorter than the typical $P_{\text{rot}} \sim 10$ days observed in recent large-scale surveys (e.g., A. McQuillan et al. 2014; C. P. Johnstone et al. 2021; D. Gruner et al. 2023; L. Ye et al. 2024). Nearly 90% of these stars rotate more rapidly than the Sun. M-type stars display the largest range in periods, with $P_{\text{rot}} \sim 100\text{--}300$ days for older M stars and $P_{\text{rot}} \sim 0.1\text{--}3$ days for the youngest M stars. The median rotational period of 5 days for M stars reflects the large frequency of younger stars in the CDDS sample (e.g., E. R. Newton et al. 2016, 2017; Y. Shan et al. 2024).

Among early-type stars with $T_{\text{eff}} \gtrsim 7500\text{--}8000$ K, the projected rotational velocity ranges from ~ 30 km s^{-1}

to ~ 300 km s^{-1} , with a median value of ~ 100 km s^{-1} . Although the sample of B-type stars is small, the lower envelope of $v \sin i$ appears to fall from ~ 30 km s^{-1} for the hottest stars with $T_{\text{eff}} \sim 20,000$ K to ~ 10 km s^{-1} for A-type stars with $T_{\text{eff}} \approx 9000$ K. Stars with $T_{\text{eff}} \sim 9000$ K have a bimodal distribution. A group of older stars has $v \sin i \sim 10\text{--}40$ km s^{-1} while the younger stars have $v \sin i \sim 50\text{--}300$ km s^{-1} .

The ensemble of FGK stars has a very broad $v \sin i$ distribution, with values ranging from ~ 1 km s^{-1} to ~ 300 km s^{-1} . Although there are many FG stars with $v \sin i \approx 100\text{--}300$ km s^{-1} , most have $v \sin i \sim 3\text{--}30$ km s^{-1} . Throughout this temperature range, the lower envelope of $v \sin i$ continues to fall with decreasing T_{eff} . Cooler G-type stars have lower values of $v \sin i$ than warmer F-type stars. Among the G stars, ~ 10 stars have $v \sin i \lesssim 1$ km s^{-1} (or upper limits below 1 km s^{-1}); only $\sim 4\%$ have $v \sin i$ values or upper limits below the Sun’s rotational velocity of 2 km s^{-1} . There are no F stars with such low $v \sin i$.

K-type and M-type stars generally follow the $v \sin i$ distribution of G-type stars. The lack of K and M stars in young clusters surveyed by *Spitzer* severely limits the population of rapidly-rotating KM stars with $v \sin i \gtrsim 100$ km s^{-1} . There is also a dearth of K-type stars at ~ 30 km s^{-1} . Despite these differences, the KM stars in the CDDS sample have a similar lower limit, ~ 1 km s^{-1} , and otherwise fill the space between 1 km s^{-1} and 100 km s^{-1} fairly uniformly.

Chromospheric and Coronal Emission. All late-type stars with convective envelopes have hotter material above the photosphere that generates continuum and line emission from X-ray to radio wavelengths (e.g., J. C. Hall 2008; P. Testa et al. 2015; I. De Moortel & P. Browning 2015; R. de Grijs & D. Kamath 2021). The European missions *ROSAT* and *SRG/eROSITA* conducted all-sky surveys that provide X-ray luminosities or upper limits for the corona of each CDDS star (B. Aschenbach et al. 1981; P. Predehl et al. 2006). Probing chromospheric emission requires ground-based observations, which are not available for every star. Here we focus on emission from the Ca H & K and IR triplet lines as robust chromospheric activity indicators (e.g., I. Busà et al. 2007; S. Boro Saikia et al. 2018). Although $H\alpha$ emission is a common activity indicator for M-type stars (e.g., P. V. Souza dos Santos et al. 2024), it is often omitted in studies of Ca II emission in FGK stars. Thus, we do not include it in this compilation.

Calcium emission. Emission in the cores of the Ca II H & K absorption lines is a hallmark of chromospheric activity in late F and GKM main sequence stars (e.g., O. C. Wilson 1963; A. H. Vaughan & G. W.

Preston 1980; T. J. Henry et al. 1996; S. Boro Saikia et al. 2018). The S index – defined as the ratio of the total flux in narrow filters centered on H & K to the continuum flux outside H & K – is ~ 0.1 (10) for stars with weak (strong) chromospheric emission (A. H. Vaughan & G. W. Preston 1980; R. W. Noyes et al. 1984). To correct for the dependence of S on spectral type, F. Middelkoop (1982) derived a color-dependent factor $\mathcal{C}(B - V) = R_{HK}/S$, where $R'_{HK} = F_{HK}/\sigma T_{\text{eff}}^4$ is the ratio of the stellar flux in the H & K passbands to the total stellar flux. R. W. Noyes et al. (1984) outline a procedure to eliminate the photospheric contribution to R_{HK} , yielding R'_{HK} as the ratio of the chromospheric flux in H & K to the total energy output. Most studies follow a variant of the R. W. Noyes et al. (1984) procedure (e.g., T. J. Henry et al. 1996; S. Boro Saikia et al. 2018); however, some measure the total equivalent width W_{HK} of the H & K emission features from high resolution spectra. As outlined in A. C. Lanzafame et al. (2023), $R'_{HK} = F_{HK}W_{HK}/\sigma T_{\text{eff}}^4$. The two approaches – $S_{HK} \rightarrow R'_{HK}$ and $W_{HK} \rightarrow R'_{HK}$ – are equivalent.

The success of S_{HK} and R'_{HK} as activity indicators led to similar measurements for the Ca II IR triplet lines at 849.8 nm, 854.2 nm, and 866.2 nm (e.g., J. L. Linsky et al. 1979; R. Cayrel et al. 1983; B. H. Foing et al. 1989; D. R. Soderblom et al. 1993b; I. Busà et al. 2007). Along with theoretical studies (e.g., Y. Chmielewski 2000; V. Andretta et al. 2005), these analyses demonstrate that the analogous indices S_{IRT} and R'_{IRT} yield similarly good measurements of activity as S_{HK} and R'_{HK} (see also D. Lorenzo-Oliveira et al. 2016; J. Martin et al. 2017). These efforts culminated in the release of IR triplet activity indices for two million stars in *Gaia* DR3 (A. C. Lanzafame et al. 2023).

We compile R'_{HK} from the literature (D. K. Duncan et al. 1991; T. J. Henry et al. 1996; K. Strassmeier et al. 2000; J. T. Wright et al. 2004; R. J. White et al. 2007; C. Schröder et al. 2009b; J. Gomes da Silva et al. 2014; N. Astudillo-Defru et al. 2017; E. R. Houdebine et al. 2017; S. Boro Saikia et al. 2018; D. Lorenzo-Oliveira et al. 2018; P. Gondoin 2020; J. Gomes da Silva et al. 2021; V. Perdelwitz et al. 2021; E. L. Brown et al. 2022; C. J. Marvin et al. 2023; L. Mignon et al. 2023). For each CDDS star, we adopt the average (median) of two (three or more) measurements. Many publications include summaries of previous R'_{HK} measurements. Before performing the median, we remove repeat measurements collected from several sources. Typically, the range in R'_{HK} for a single star is ~ 0.1 – 0.2 , which is similar to the amplitude of the variation in R'_{HK} over a complete stellar cycle (e.g., S. Boro Saikia et al. 2018).

Studies that quote some variant of the S index instead of R'_{HK} generally place their results on the original Mt. Wilson scale (e.g., W. Zhang et al. 2022). We convert these S values to R'_{HK} following the procedures described in R. W. Noyes et al. (1984) and T. J. Henry et al. (1996). For stars in common, the derived R'_{HK} values are within 10% of published results. Overall, we compile R'_{HK} for 1132 stars.

From the *Gaia* data set, we collect the activity index α for 1501 stars. The α index measures the strength of the Ca II IR triplet lines relative to a theoretical photospheric spectrum and is related to the emission line equivalent width W_{IRT} . For each measured α , the photospheric spectrum is matched to the values for T_{eff} , $\log g$, and metallicity [M/H] derived from analysis of the *Gaia* RVS spectrum. As with the H & K lines, deriving the IR triplet index R'_{IRT} requires a measurement of the stellar flux across the IR triplet lines: $R'_{IRT} = \mathcal{F}\alpha$. A. C. Lanzafame et al. (2023) adopt the theoretical spectrum and derive a function $\mathcal{F}([M/H], T_{\text{eff}})$ that depends on the [M/H] and T_{eff} derived from *Gaia* spectra. In their analysis, this function is nearly independent of $\log g$. For each CDDS star with a measured α , [M/H], and T_{eff} from *Gaia* measurements, we linearly interpolate \mathcal{F} in Table 1 of A. C. Lanzafame et al. (2023) to generate R'_{IRT} .

Among the set of 1501 stars, 1187 have a positive emission line equivalent width ($\alpha > 0$). The rest have extra absorption relative to the matching photospheric spectrum ($\alpha < 0$). Stars with weak chromospheres often produce extra absorption in the Ca II H & K and the IR triplet lines (e.g., V. Andretta et al. 2005; J. L. Linsky 2017, and references therein). Among the stars with extra absorption, those with the largest $|\alpha|$ are probably the most chromospherically active.

Fig. 14 shows the distribution of R'_{HK} (lower panel) and R'_{IRT} (upper panel) as a function of T_{eff} . Only 74 (222) of the 1235 (737) stars with $T_{\text{eff}} > 6500$ K ($T_{\text{eff}} < 4500$ K) have measured R'_{HK} . Most of the F stars are very active ($\log R'_{HK} \gtrsim -4.5$). Although a few KM stars are among the most active stars, most have low activity levels ($\log R'_{HK} \lesssim -5$). More than half (1132 out of 1703) of the stars with $T_{\text{eff}} = 4500$ – 6500 K have measured Ca II H&K emission, at levels ranging from minimal activity similar to the Sun ($\log R'_{HK} \sim -5$, as illustrated by the thin grey band in the figure; R. Egeland et al. 2017; S. Boro Saikia et al. 2018; E. Dineva et al. 2022; G. Zills et al. 2024) to maximal activity with $\log R'_{HK} \sim -4$. Roughly 32% (53%) of the stars lie below (above) the Vaughan–Preston gap, a region with very few stars in the first large-scale surveys of stellar activity among solar-type main sequence stars (A. H.

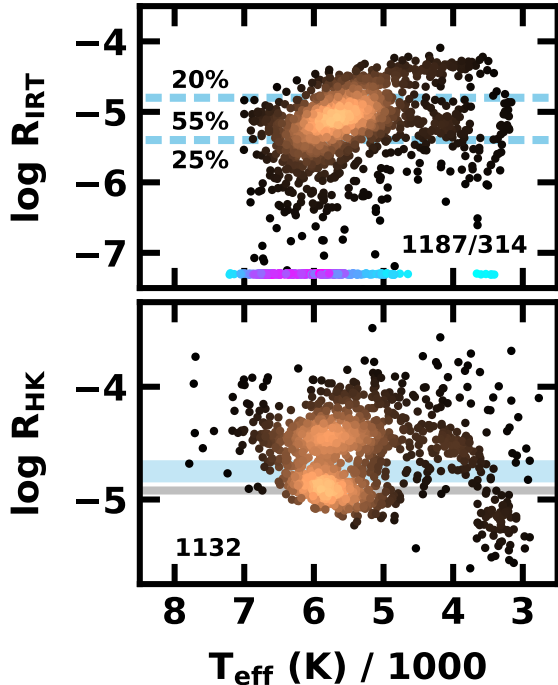


Figure 14. Activity indices for Ca II H & K (R'_{HK} ; lower panel, 1132 stars) and the Ca II infrared triplet (R'_{IRT} ; upper panel, 1501 stars including 314 upper limits) as a function of T_{eff} . *Lower panel:* The thin grey bar (thick blue bar) indicates the range of activity for the Sun (the Vaughan–Preston gap). *Upper panel:* Points with cyan (low density) to pink (high density) colors at the bottom of the plot show the 314 stars with $\alpha < 0$. Three points with $\alpha > 0$ have $\log R'_{IRT} \approx -7.5$ to -8.3 and lie below the extent of the plot. Dashed blue lines indicate the boundaries of the high, moderate, and low activity regimes of A. C. Lanzafame et al. (2023); the percentage of stars with $\alpha > 0$ in each regime appears at the left edge of the plot.

Vaughan & G. W. Preston 1980; R. W. Noyes et al. 1984).

To put these R'_{HK} measurements in context, we compare with the S. Boro Saikia et al. (2018) analysis of 4454 late-type stars. In their Figure 3, H & K emission is rare among middle F-type and earlier stars with $T_{\text{eff}} \gtrsim 6500$ K. A few M stars have high activity levels; most have low R'_{HK} . Compared to the S. Boro Saikia et al. (2018) sample, the CDDS has a much larger fraction of GK stars with high activity levels (above the Vaughan–Preston gap) and a much smaller fraction with low activity levels (below the gap). The CDDS GK stars have a somewhat stronger gap, but the sample is much smaller than the S. Boro Saikia et al. (2018) sample, where the gap is nearly absent.

As in the full sample of *Gaia* stars, stars with $T_{\text{eff}} = 3000$ – 7000 K have Ca II IR triplet indices ranging from a

maximum $\log R'_{IRT} \approx -4$ to a minimum $\log R'_{IRT} \approx -8$ (Fig. 14, upper panel). In the middle of the diagram, $\log R'_{IRT} \approx -5.4$ to -4.8 , FG stars produce a dense concentration with two tails: a group of KM stars with similar $\log R'_{IRT}$ and a group of mostly FG stars with weaker emission ($R'_{IRT} \lesssim -5.4$). Above the main body, there is a group of FGK stars with strong IR triplet emission ($\log R'_{IRT} \approx -4.8$ to -4.2).

In addition to the low activity stars with $\log R'_{IRT} \gtrsim -8.5$, another set of stars has extra Ca II absorption compared to the *Gaia* photospheric comparison spectrum (A. C. Lanzafame et al. 2023). Based on the photospheric models, these stars have extra chromospheric absorption (see the discussion in J. L. Linsky 2017; M. Carlsson et al. 2019). Following A. C. Lanzafame et al. (2023), we interpret this extra absorption as an indicator of a weak chromosphere. Most of the stars in this group are F-type stars, where chromospheric emission is generally weaker than for GK stars.

To compare with the full *Gaia* sample, we follow A. C. Lanzafame et al. (2023) and define stars with low ($-8.5 \lesssim \log R'_{IRT} \lesssim -5.4$), moderate ($\log R'_{IRT} = -5.4$ to -4.7), and high ($\log R'_{IRT} \geq -4.7$) activity levels. Most CDDS stars (55%) have moderate activity. This group contains the full range of spectral types with Ca II triplet emission, FGKM. Roughly 25% have low activity. Only a few KM stars have low activity levels. The rest of the sample (20%) have high activity levels. Most of these are G stars; some are K stars; very few are F or M stars.

Overall, CDDS stars for any T_{eff} have much larger activity levels than those in the ground-based (e.g., S. Boro Saikia et al. 2018) and the full *Gaia* sample (A. C. Lanzafame et al. 2023). In the CDDS (full sample), moderate (low) activity stars dominate; high activity stars are common (rare). Although the lowest activity stars in the CDDS and full samples have similar activity levels, CDDS stars with these levels are relatively rare. Similarly, CDDS stars with the highest activity levels are rare in the full ground-based and *Gaia* samples. As discussed above, the *Spitzer* and *Herschel* surveys favored younger stars with ages much smaller than the Sun, $\lesssim 1$ Gyr. Thus, CDDS stars have higher activity levels than stars with ages similar to the Sun’s.

Stellar X-rays For this study, we focus on data acquired with *ROSAT* (B. Aschenbach et al. 1981), *Chandra* (M. C. Weisskopf et al. 2002), *XMM-Newton* (F. Jansen et al. 2001), and *SRG/eROSITA* (P. Predehl et al. 2006). In addition to the *ROSAT* all sky survey (RASS; W. Voges et al. 1999; T. Boller et al. 2016; S. Freund et al. 2022), *ROSAT* acquired more sensitive measurements with pointed observations of selected

open clusters (e.g., G. Micela et al. 1999, and references therein). W. Voges et al. (2001) describe all of the ROSAT data catalogs; T. Boller et al. (2016) include a link to the catalog of pointed observations accessible in *Vizier*. S. Freund et al. (2022) associate RASS stellar sources with optical counterparts from *Gaia* eDR3 (C. Fabricius et al. 2021; Gaia Collaboration et al. 2021b). Explicit matches of an eDR3 identifier (or a Tycho-2 identifier) with each RASS source enables a robust association between a stellar X-ray source and its optical counterpart. S. Freund et al. (2022) also use the known maximum in the fractional X-ray luminosity L_X/L_\star to avoid spurious matches. We identify 1226 sources in these ROSAT databases.

Several *Chandra* and *XMM-Newton* programs conducted deep pointed observations of nearby open clusters. We collect *Chandra* data for the Pleiades (K. J. Daniel et al. 2002) and NGC 2516 (F. Damiani et al. 2003). Several other CDDS stars appear in various *Chandra Source Catalogs* (original versions: I. N. Evans et al. 2010; S. Wang et al. 2016). These compilations yield 225 X-ray sources.

The *XMM-Newton* coverage of nearby open clusters is more extensive, with data from the Pleiades (K. R. Briggs & J. P. Pye 2003), Praesepe (E. Franciosini et al. 2003), Blanco 1 (I. Pillitteri et al. 2004), NGC 2516 (I. Pillitteri et al. 2006), NGC 2547 (R. D. Jeffries et al. 2006), and Upper Sco (C. Argiroffi et al. 2006). As *XMM-Newton* moves from one pointed observation to the next, it identifies X-ray sources along its path. We select 716 CDDS stars from the S. Freund et al. (2018) catalog of stellar counterparts to these sources.

The first data release of the *SRG/eROSITA* all-sky survey covers the western galactic hemisphere, $l = 180^\circ - 360^\circ$ (A. Merloni et al. 2024). This region includes 2562 out of 3675 CDDS sources. In addition to η Cha (16 sources; J. Robrade et al. 2022) and the Sco-Cen association (106 sources; J. H. M. M. Schmitt et al. 2022), this release includes roughly half of the CDDS stars in the Hyades along with CDDS stars in Coma, IC 2391, NGC 2232, NGC 2422, NGC 2451, NGC 2516, NGC 2547, Praesepe, and the TW Hya association. However, it does not include α Per, Blanco 1, the Pleiades, and the other half of the CDDS stars in the Hyades, which are in the eastern galactic hemisphere and remain unpublished. Among the 2562 possibilities, the *SRG/eROSITA* catalogs list absolute flux measurements for 1153 stars and upper limits for the rest.

From *ROSAT*, *Chandra*, *XMM-Newton*, and *SRG/eROSITA*, the CDDS has X-ray fluxes F_X for 1996 stars. All fluxes lie within a similar bandpass of $\sim 0.1-2$ keV. To put the X-ray luminosities of these

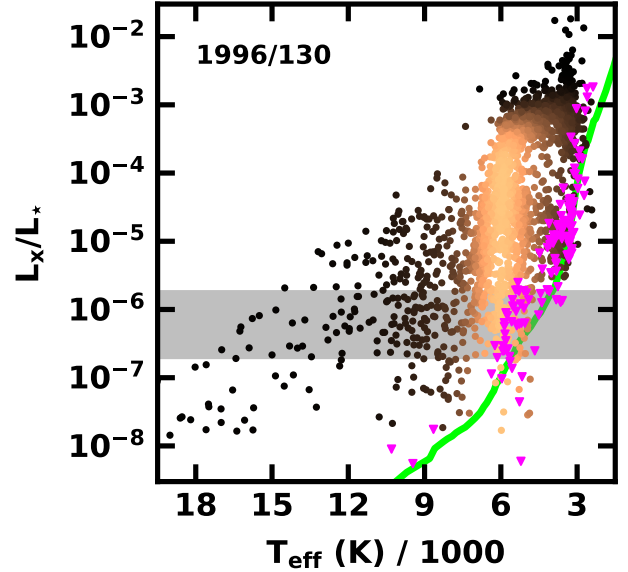


Figure 15. Fractional X-ray luminosity (L_X/L_\star) as a function of the effective temperature for 1996 stars with measured T_{eff} , L_\star , L_X . Filled fuchsia triangles indicate upper limits for 130 stars with $d \leq 17$ pc. The horizontal grey band shows the range of the fractional X-ray luminosity for the Sun (P. G. Judge et al. 2003). Adopting the M. J. Pecaut & E. E. Mamajek (2013) $T_{\text{eff}}-L_\star$ relation for main sequence stars, the green line indicates approximate *SRG/eROSITA* and ROSAT detection limits at distances of 10–20 pc.

stars in context, we derive the fractional X-ray luminosity L_X/L_\star . For each star with an accurate distance d , we calculate the average X-ray flux $\langle F_X \rangle$ of the individual measurements from each satellite; we then set $L_X = 4\pi d^2 \langle F_X \rangle$. Among stars with robust X-ray fluxes from several satellites, the brightest sources vary by a factor of $\sim 2-3$. For stars with accurate parallaxes and L_\star , the fractional X-ray luminosity, L_X/L_\star , follows.

Fig. 15 shows how L_X/L_\star depends on T_{eff} . The distribution follows that of all coronal X-ray sources in *SRG/eROSITA*: (i) an upper envelope with $L_X/L_\star \lesssim 10^{-5}$ for B-type stars with $T_{\text{eff}} \approx 12,000-20,000$ K that gradually rises to $L_X/L_\star \lesssim 10^{-2}$ for KM stars with $T_{\text{eff}} \approx 3000-4000$ K and (ii) a lower envelope with $L_X/L_\star \gtrsim 10^{-8}$ to 10^{-7} for early-type stars and $L_X/L_\star \gtrsim 10^{-6}$ for late-type stars (see Fig. 11 of S. Freund et al. 2024). Main sequence stars detected in the ROSAT all sky survey show a similar pattern (S. Freund et al. 2022). Once again, the concentration of stars with $T_{\text{eff}} \approx 4500-7500$ K is a feature of the *Spitzer* and *Herschel* programs that focus on FGK stars in their searches for debris disks.

As summarized in S. Freund et al. (2022, 2024), the maximum in L_X/L_\star reflects ‘saturation’ of the mechanism that generates coronal X-ray emission in the

youngest and most rapidly rotating solar-type stars (e.g., J. R. Stauffer et al. 1994; S. Randich et al. 1996; M. Güdel 2004; P. A. Cargile et al. 2009; C. Argiroffi et al. 2016; X.-S. Fang et al. 2018). Currently, there is no consensus on the origin of this maximum (e.g., P. Testa et al. 2015; I. De Moortel & P. Browning 2015). For FG stars, the lower limit of $L_X/L_\star \sim 10^{-8}$ is characteristic of old, slowly rotating stars (e.g., M. Güdel 2004), including the Sun (P. G. Judge et al. 2003).

The fuchsia triangles in Fig. 15 show upper limits for 130 stars with $d \lesssim 17$ pc. Most stars in this group hug the lower envelope of fractional X-ray luminosities for stars with $T_{\text{eff}} \approx 3000\text{--}9000$ K. Stars with X-ray upper limits and $d \gtrsim 17$ pc have similar T_{eff} as those with $d \lesssim 17$ pc and lie at larger L_X/L_\star . Two stars with measured T_{eff} and $L_X/L_\star = 5.1 \times 10^{-10}$ and 2.8×10^{-9} are not shown.

To demonstrate that the lower envelope of X-ray detections for GKM stars is a sensitivity limit, we derive L_X/L_\star using the approximate *ROSAT* (*SRG/eROSITA*) sensitivity limit, $F_X = 1.5 \times 10^{-13}$ erg cm $^{-2}$ s $^{-1}$ ($F_X = 5 \times 10^{-14}$ erg cm $^{-2}$ s $^{-1}$), from S. Freund et al. (2022) (A. Merloni et al. 2024). For the M. J. Pecaut & E. E. Mamajek (2013) locus of main sequence stars in the $T_{\text{eff}}\text{--}L_\star$ plane, the green line in Fig. 15 shows the expected $T_{\text{eff}}\text{--}L_X/L_\star$ relation for main sequence stars with $d = 17$ pc (10 pc) and an X-ray flux at the *SRG/eROSITA* (*ROSAT*) sensitivity limit. This estimate matches the lower limit of L_X/L_\star for late G and KM stars rather well.

Host Star Properties Summary. Table 4 summarizes basic statistics for the properties of CDDS stars as a function of spectral type. As in §3, we adopt the M. J. Pecaut & E. E. Mamajek (2013) relation between spectral type and effective temperature. Nearly all stars, $\sim 94\%$ have an accurate spectral type published in the literature or derived from *Gaia* low resolution spectroscopy. Together with published effective temperatures in the literature, from *Gaia*, and from color indices, the full set of spectral types yields stellar effective temperatures for 100% of the sample. All of the stars have an accurate K-band magnitude and most have an accurate optical magnitude (either G, V, or g), which yields a luminosity derived from G, K, V, or g ; the optical extinction; and a *Gaia* or *Hipparcos* parallax (or distance estimate based on cluster membership or location on the main sequence). Approximately 80% (64%) have a measured $\log g$ (metallicity). Among the other stellar properties, 30% to 38% of the sample has a measured Li abundance, rotational period, and the two Ca II chromospheric activity indicators. More than half

Table 4. Stellar Data Summary

Measure	All	B	A	F	G	K	M
SpT	0.937	1.000	1.000	0.972	0.960	0.859	0.855
T_{eff}	1.000	1.000	1.000	1.000	1.000	1.000	1.000
L_\star	1.000	1.000	1.000	1.000	1.000	1.000	1.000
$\log g$	0.804	0.709	0.907	0.937	0.919	0.645	0.627
[Fe/H]	0.642	0.179	0.461	0.829	0.865	0.700	0.446
[Li/H]	0.301	0.006	0.052	0.367	0.504	0.363	0.282
P_{rot}	0.376	0.109	0.098	0.336	0.626	0.407	0.538
$v \sin i$	0.586	0.641	0.620	0.627	0.683	0.505	0.433
L_X/L_\star	0.543	0.406	0.376	0.609	0.599	0.542	0.627
Ca II HK	0.312	0.000	0.015	0.358	0.630	0.354	0.268
Ca II IRT	0.303	0.000	0.000	0.351	0.604	0.432	0.141

(59%) have measurements for $v \sin i$; nearly 55% have $L_X/L_\star > 0$.

All of these measures have an uneven distribution with respect to SpT, T_{eff} , or L_\star . FG stars have an almost complete set of $\log g$ data; A stars lag; KM stars lag more; and B stars lag the most. BM stars have relatively less [Fe/H] data than AK stars and much less than FG stars. With little or no stellar activity, BA stars have few measurements of P_{rot} , A(Li), $\log R'_{\text{HK}}$, or $\log R'_{\text{IRT}}$. For these measures, G stars have a larger fraction of data than FKM stars. The $v \sin i$ and L_X/L_\star measurements are rather evenly distributed among all spectral types; A stars have the smallest fraction of L_X/L_\star measurements, but are well-represented in the set of $v \sin i$ measurements.

Table 5 addresses the frequency of activity indicators – [Li/H], P_{rot} , $v \sin i$, L_X/L_\star , $\log R'_{\text{HK}}$, and $\log R'_{\text{IRT}}$ – as a function of spectral type. BA stars have more than two measures less than 5% of the time, but they usually have at least one (71% for B stars and 72% for A stars). F-type stars are the most common stars in the CDDS; they often have two or three activity measures (44%); another 35% have one or four measures. F stars more often have five or six measures (13%) than none (8%).

G-type stars dominate the activity measure statistics. Only 2% have no measure of activity within the set of six. Among the six measures for G stars, 25% have four, 22% have five, 20% have three, 12% have two, 11% have six, and 7% have one. K-type stars have somewhat worse statistics than F-type stars. More than 90% of the K stars have at least one measure; two to four measures are most common, followed in frequency by one, five, and six. Although M-type stars rarely have none of the activity indicators, they never have all six. More than 55% of M stars have two or three indicators; another 35% have one or four.

Table 5. Stellar Activity Statistics

SpT	All	0	1	2	3	4	5	6
B	357	0.232	0.409	0.322	0.036	0.000	0.000	0.000
A	518	0.230	0.434	0.286	0.044	0.006	0.000	0.000
F	852	0.093	0.177	0.208	0.218	0.158	0.107	0.039
G	681	0.063	0.057	0.106	0.186	0.247	0.214	0.126
K	771	0.188	0.130	0.145	0.170	0.204	0.122	0.042
M	496	0.109	0.200	0.230	0.264	0.149	0.048	0.000

In the current paradigm, these activity indicators change as the interior structure of a star evolves (e.g., C. P. Johnstone et al. 2021; T. Dumont et al. 2021a). For example, the observed [Li/H] in low mass stars depends on metallicity and complex interactions between convection, rotation, and various transport processes, including diffusion, meridional circulation, magnetic torque, turbulence, and viscosity (e.g., C. P. Deliyannis et al. 2000; S. Talon & C. Charbonnel 2005; E. Semanova et al. 2020; T. Dumont et al. 2021b; T. Dumont 2023). The chromospheric properties of FGKM stars, including $\log R'_{HK}$, $\log R'_{IRT}$, and L_X/L_\star , depend on the evolution of the magnetic field and the Rossby number, Ro , which is the ratio of the rotational period to the convective turnover time, τ_c : $Ro = P_{rot} / \tau_c$ (e.g., E. E. Mamajek & L. A. Hillenbrand 2008; F. Gallet & J. Bouvier 2015; L. Tu et al. 2015; C. P. Johnstone et al. 2021). As P_{rot} , B , and Ro decline with time, [Li/H], $\log R'_{HK}$, $\log R'_{IRT}$, and L_X/L_\star should follow.

To make an initial analysis of activity indicators among CDDS stars, we consider correlations between each pair of measures. In a future paper, we explore ways to combine these into stellar age estimates. Here, we simply note which measures are more correlated with other measures. For this task, we employ the Pearson, Spearman, and Kendall methods to search for correlations. The number of (x, y) pairs for the correlations ranges from 467 for R'_{HK} -[Li/H] to 859 for R'_{HK} - $v \sin i$. We quote results for the Pearson and Spearman tests; the Kendall τ method yields results indistinguishable from the Spearman test. Table 6 summarizes the correlation coefficients and the p -values for each pair of variables. Small p -values indicate a small probability that the variables are uncorrelated. Fig. 16 shows the nearly complete set of measurements for CDDS stars. With the largest likelihood of no correlation, we do not plot results for $\log R'_{IRT}$ versus A(Li).

Aside from the R'_{IRT} -[Li/H] pair, all pairs of activity measures show obvious correlations. Among these, the p -values do not obviously depend on the number of stars with both activity measures. Two of the three

Table 6. Correlation Coefficients¹

Pair	N	r_p	p_p	r_S	p_S
R_{HK} - R_{IRT}	501	0.58	1×10^{-46}	0.63	9×10^{-58}
R_{HK} - L_X/L_\star	589	0.74	7×10^{-104}	0.84	2×10^{-158}
R_{HK} -[Li/H]	467	0.37	8×10^{-17}	0.49	3×10^{-29}
R_{HK} - P_{rot}	534	-0.75	1×10^{-98}	-0.84	5×10^{-142}
R_{HK} - $v \sin i$	859	0.58	6×10^{-80}	0.60	4×10^{-86}
R_{IRT} - L_X/L_\star	559	0.68	8×10^{-77}	0.74	8×10^{-99}
R_{IRT} -[Li/H]	469	0.14	2×10^{-3}	0.20	1×10^{-05}
R_{IRT} - P_{rot}	564	-0.53	7×10^{-43}	-0.54	3×10^{-44}
R_{IRT} - $v \sin i$	656	0.38	5×10^{-24}	0.40	3×10^{-26}
[Li/H]- L_X/L_\star	471	0.41	1×10^{-20}	0.51	3×10^{-32}
[Li/H]- P_{rot}	530	-0.61	3×10^{-54}	-0.70	5×10^{-78}
[Li/H]- $v \sin i$	627	0.43	3×10^{-30}	0.55	1×10^{-50}
P_{rot} - L_X/L_\star	586	-0.77	3×10^{117}	-0.81	6×10^{-137}
P_{rot} - $v \sin i$	671	-0.78	3×10^{-141}	-0.79	9×10^{-144}
$v \sin i$ - L_X/L_\star	682	0.63	1×10^{-77}	0.65	5×10^{-83}

¹These results measure correlations between logarithms of each quantity.

strongest correlations, R'_{HK} - P_{rot} (534) and P_{rot} - L_X/L_\star (586), have rather few data points compared to R_{HK} - $v \sin i$ (846), which has the most data points and one of the smaller p -values.

The three strongest correlations involve R'_{HK} , P_{rot} , and L_X/L_\star . Among others, C. P. Johnstone et al. (2021) demonstrates clear correlations between P_{rot} and L_X/L_\star with the evolution of the Rossby number, Ro . As stars age, P_{rot} grows while τ_c reaches an equilibrium. Thus, Ro steadily increases as P_{rot} increases. Increasing Ro leads to a decrease in L_X/L_\star , far-ultraviolet continuum emission, and other activity indicators. The Ca II activity indicators clearly share this evolution: R'_{HK} is clearly tied to L_X/L_\star and P_{rot} . Although the Ca II IR triplet flux is less correlated with P_{rot} , it is strongly correlated with L_X/L_\star .

Differences of the p -values among the pairs of variables illustrates the fickleness of low mass stars. Among stars with the same mass, T_{eff} , and L_\star , some maintain high rotation rates far longer than the rest of their cohort; others spin down more rapidly (e.g., C. P. Johnstone et al. 2021; K. V. Getman et al. 2023; A. R. G. Santos et al. 2025; S. Mathur et al. 2025). Similarly, some stars lose their lithium rapidly while others somehow maintain relatively high lithium abundances compared to the rest of their cohort (e.g., T. Dumont et al. 2021b; A. Rathsam et al. 2023; I. Winnick et al. 2025). While there are clear trends in the evolution of stellar activity with age, individuality introduces profound and sometimes large differences from star to star.

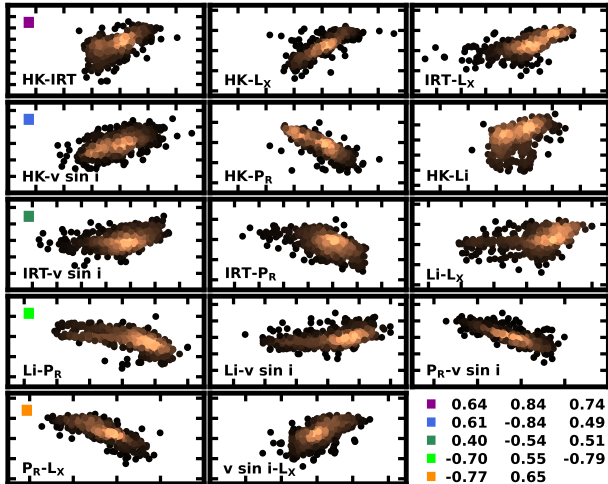


Figure 16. Correlations for 14 pairs of activity indices listed in Table 6 (not shown: R'_{IRT} -[Li/H], which has a negligible correlation coefficient). Text in the lower left corner of each plot indicates the pair of indices; the x-axis (y-axis) plots the first (second) index listed. The lower right corner lists the *Spearman* correlation coefficients from Table 6. For convenience, squares at the start of each row of coefficients correspond to squares in the upper left corners of plots in the first column of the array of plots.

Comparing these results with other estimates is challenging. While many studies show a clear correlation between various activity indicators, they generally do not quote a correlation coefficient (e.g., E. E. Mamajek & L. A. Hillenbrand 2008; T. Dumont et al. 2021b; C. P. Johnstone et al. 2021; A. Núñez et al. 2024; Y. Shan et al. 2024). In general, the correlations look similar to those shown in Fig. 16.

A. C. Lanzafame et al. (2023) consider correlations between the two Ca indices, using unpublished archival data from ESO-FEROS (671 sources) and the extensive S. Boro Saikia et al. (2018) compilation (220 sources). With many CDDS stars in S. Boro Saikia et al. (2018), we focus on this comparison. A. C. Lanzafame et al. (2023) derive a *Pearson* linear correlation coefficient $r = 0.5$ and a relation $\log R'_{IRT} = a \log R'_{HK} - b$, with $a = 0.841$ and $b = 1.661$. The CDDS data yield similar results for 501 stars: $r = 0.63$, $a = 0.817$, and $b = 1.525$. We also infer correlations between T_{eff} and the difference in the two Ca indices, $\delta R_{\text{Ca}} = \log R'_{IRT} - \log R'_{HK}$:

$$\delta R_{\text{Ca}} = \begin{cases} -0.547 T_{1000} + 2.374 & T_{1000} \geq 5 \\ -0.50 & T_{1000} < 5 \end{cases} \quad (7)$$

where $T_{1000} = T_{\text{eff}}/1000$. Both correlations have $r = 0.57$. These results differ from those in J. Martin et al. (2017), who analyze 2274 observations of 82 stars.

S. Freund et al. (2025) consider correlations between L_X/L_\star and R'_{IRT} for a set of 43,200 stars with reliable measurements of *SRG/eROSITA* X-ray and *Gaia* DR3 Ca II IR triplet fluxes. Aside from F-type stars, the smaller set of CDDS stars shows similar trends but with stronger correlations; the Pearson correlation coefficients for CDDS stars are 0.75 (all stars), 0.42 (F), 0.77 (G), 0.86 (K), and 0.74 (M) compared to 0.67 (all), 0.45 (F), 0.69 (G), 0.81 (K), and 0.57 (M) for the S. Freund et al. (2025) sample. Differences could be a result of small number statistics or the overall youth of CDDS stars compared to other stellar samples.

5. MEMBERSHIP IN ASSOCIATIONS, CLUSTERS, AND MOVING GROUPS

To select and to verify targets for observations of moving groups, open clusters, and stellar associations, *Spitzer* programs often relied on published membership lists. For nearby (distant) regions, *Hipparcos* (ground-based) parallaxes and proper motions helped to separate members from the background or foreground. Sometimes, color-magnitude diagrams and stellar activity measures also served to identify cluster stars.

Today, *Gaia* data enable significant improvements in defining the members of associations, clusters, and moving groups. Among Hyades stars, for example, the typical fractional error for ground-based parallax or proper motion measurements is $\sim 10\%$ (e.g., W. F. van Altena et al. 1995; N. Zacharias et al. 2004, and references therein). *Hipparcos* improved on parallax (proper motion) errors by a factor of 2–3 (~ 10). In contrast, the fractional errors for *Gaia* parallax (proper motion) measurements of Hyades stars are $\sim 0.1\%$ (0.02%)! Although the fractional errors increase for more distant stars, the parallax uncertainty for Blanco 1 ($d \approx 237$ pc) is still small, $\sim 1\%$.

To update membership data for CDDS stars, we rely on recent *Gaia*-based studies. These analyses adopt different techniques that include some combination of coordinates on the sky, parallax, proper motion, and radial velocity. *Gaia* or ground-based color-magnitude diagrams often add to the analysis. For CDDS stars, all have a measured or adopted parallax, all but three have a proper motion, and 3568 (97%) have a measured v_{rad} . When the dynamical data are used to construct galactic coordinates (X, Y, Z) and velocities (U, V, W) relative to the galactic center, analyses must account for uncertainties in the solar motion (e.g., V. V. Bobylev & A. T. Bajkova 2016; D. Mikkola et al. 2023). Among the studies we consult, several are all-sky compilations (T. Cantat-Gaudin et al. 2018; W. S. Dias et al. 2021; E. L. Hunt & S. Reffert 2023, 2024). Others focus on 10–20 specific,

well-known regions (e.g., L. Liu & X. Pang 2019; X. Pang et al. 2021; R. J. Jackson et al. 2022). As outlined below, many analyses focus on 1–3 associations, clusters, or groups. When any of these studies include membership probabilities p , we exclude stars with $p < 0.5$.

While the focus of membership analysis is on dynamical properties, we consider comparisons with model stellar isochrones when stars considered members in *Spitzer* studies are rejected as members in *Gaia* dynamical studies. Usually, rejected stars lie well outside the volume of *bona fide* cluster members. Sometimes, rejected stars lie within the cluster; model stellar isochrones are then helpful when deciding cluster membership. For this task, we use version 1.2S of the PAdova and tRieste Stellar Evolutionary Code (PARSEC; Y. Chen et al. 2014; J. Tang et al. 2014; Y. Chen et al. 2015). While other options are available, W. Brandner et al. (2023c,a,b) matched observations of two CDDS clusters, the Hyades and Pleiades, to PARSEC models. In a detailed study of the Castor system (α Gem AB, a CDDS binary system), G. Torres et al. (2022) matched interferometric measures of mass and radius to PARSEC isochrones.

We begin the discussion with a few examples of associations, clusters, and moving groups and then continue with summaries of the remaining clusters. For each system, we briefly outline relevant *Spitzer* programs, *Gaia* analyses, and the number of CDDS stars considered as dynamical members. After describing dynamical measurements that exclude membership for a set of stars, we consider membership based on stellar activity measures. Combining the activity and dynamical information, we close with a best-estimate of CDDS members in each association, cluster, and moving group.

5.1. The Pleiades and Praesepe Open Clusters

The Pleiades and Praesepe are good examples of relatively nearby open clusters with well-defined proper motion distributions and accurate parallaxes. Fig. 17 shows the distribution of proper motions for cluster members (defined below), centered on their median proper motions (J. Alfonso & A. García-Varela 2023). Each has a dense, yellow core of stars close to the median proper motion, a set of gold-colored stars on the outskirts of this core, and a few outliers in black. The Pleiades has a few more outliers than Praesepe, which is probably a result of its smaller distance.

Pleiades. Several *Spitzer* programs targeted the Pleiades (J. R. Stauffer et al. 2005; N. Gorlova et al. 2006; M. R. Meyer et al. 2006; K. Y. L. Su et al. 2006; J. M. Sierchio et al. 2010). Each group selected high probability members based on parallax, proper motion, chromospheric activity, lithium abundance, and position

on the color-magnitude diagram (e.g., J. R. Stauffer & L. W. Hartmann 1987; D. R. Soderblom et al. 1993b,a, and references therein). Across the five programs, the CDDS sample contains 165 stars with spectral types from late B to early M.

Four recent studies of the Pleiades with *Gaia* data place new constraints on likely members. J. Alfonso & A. García-Varela (2023, DR3: 959 stars) and W. Brandner et al. (2023b, DR3: 911 stars) focus on the core regions. The stars in these surveys have a proper motion footprint similar to the CDDS stars in Fig. 17. N. Lodieu et al. (2019a, DR2: 2281 stars) and J. Heyl et al. (2022, eDR3: 1273 stars) cast a much wider net to identify stars in the core and in tidal tails. The combined set of likely members comprises 2313 stars; 146 CDDS stars match entries in all four catalogs.

Of the 19 non-matches in the CDDS, we restore five where the *Gaia* parallax and proper motion data have large errors and the ground-based parallax, proper motion, and radial velocity data suggest membership. For the 14 other non-matches, some combination of the *Gaia*, *Hipparcos*, or ground-based parallaxes and proper motions (and their errors) suggest a star in the foreground, the background, or with a significant velocity relative to Pleiades stars. Some of these stars have strong indicators of youth and thus might be Pleiades-age stars in the vicinity of (but not within) the cluster.

Praesepe. K. Y. L. Su et al. (2006) selected 5 A-type stars in Praesepe from the literature. To construct a more comprehensive view, A. Gáspár et al. (2009) matched a large set of *Spitzer* targets with accurate photometry to high quality proper motion-based membership lists (e.g., J. J. Wang et al. 1995; A. L. Kraus & L. A. Hillenbrand 2007). They collected photometry from the literature, constructed a $g-r, r$ color-magnitude diagram, and focused on a set of high probability members based on proper motions and distance (in magnitudes) from an isochrone delineated by the highest probability cluster members. The final target list includes 193 high probability members with optical, near-infrared, and *Spitzer* photometry (see also L. E. Urban et al. 2012); five of these are in K. Y. L. Su et al. (2006).

From the historical literature, N. Lodieu et al. (2019a) compiled 2078 unique sources among a list of 6479 across all studies. After including *Gaia* DR2 data and applying detailed kinematic and Bayesian procedures to the full compilation, they produce a set of 2199 candidates. From *Gaia* DR3 data, J. Alfonso & A. García-Varela (2023) use two separate analyses to construct a set of 744 likely members within a somewhat smaller volume than those of N. Lodieu et al. (2019a); all but 19 of these are included in the N. Lodieu et al. (2019a) list.

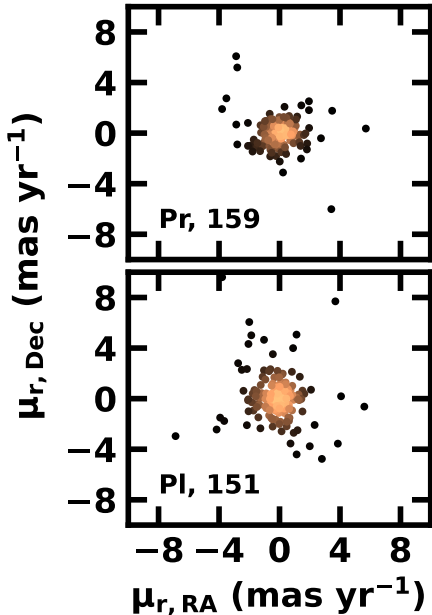


Figure 17. Final proper motion distributions for CDDS stars in Praesepe (upper panel, 160 stars) and the Pleiades (lower panel, 151 stars). Data for each cluster are centered on the median proper motion from J. Alfonso & A. García-Varela (2023): $(\mu_{RA}, \mu_{Dec}) = (19.95, -45.44)$ for the Pleiades and $(-35.93, -12.88)$ for Praesepe. The density of members increases from low (black points) to medium (gold points) to high (bright yellow points).

Of the 193 CDDS stars, 146 match candidates in T. Cantat-Gaudin et al. (2018), N. Lodieu et al. (2019a), J. Alfonso & A. García-Varela (2023), and E. L. Hunt & S. Reffert (2023, 2024). Of the 47 non-matches, 11 (19) are clearly in the foreground (background) of the cluster, closer than (beyond) a few tidal radii from the cluster center. Five stars have distances close to the cluster median, but the proper motions are well outside the cluster limits. Of the remaining stars, (i) three have parallax or proper motion errors too large to make a clear conclusion regarding their membership; (ii) five have parallaxes and proper motions within the bounds of most of the matches; and (iii) another five have no *Gaia* or *Hipparcos* data, have reasonable proper motions from ground-based measurements, and have radial velocities consistent with other cluster members. We assign these last thirteen stars to Praesepe, which brings the number of cluster stars to 159 out of the original 194 cluster members.

Information on stellar activity is insufficient to promote any other non-matches to cluster membership. Stars obviously in the cluster foreground or background have activity levels that place them with older field stars.

Several stars with similar parallax but discrepant proper motion relative to the cluster also have similar activity levels as Praesepe stars, but the proper motions preclude cluster membership. However, all of the 13 non-matches assigned to the cluster and described above have activity levels similar to other Praesepe members with similar spectral types, which supports our assignment of these stars to the cluster.

5.2. The Sco-Cen Association

Of the three stellar associations with more than 100 stars in the CDDS, Upper Scorpius (USco) was the most popular *Spitzer* target (C. H. Chen et al. 2005a; M. R. Meyer et al. 2006; K. Y. L. Su et al. 2006; J. M. Carpenter et al. 2009; C. H. Chen et al. 2011, 2012). Four programs included stars in Upper Centaurus-Lupus (UCL; M. R. Meyer et al. 2006; K. Y. L. Su et al. 2006; C. H. Chen et al. 2011, 2012), while only two focused on Lower Centaurus-Cruce (LCC; C. H. Chen et al. 2011, 2012). These programs selected stars from ground-based optical (A. Blaauw 1964; E. J. de Geus et al. 1989; T. Preibisch et al. 1998), *Hipparcos* (P. T. de Zeeuw et al. 1999), and X-ray (F. M. Walter et al. 1994; S. Sciortino et al. 1998) membership lists. As in P. T. de Zeeuw et al. (1999), we use galactic coordinates to make initial assignments of stars to USco, UCL, and LCC. After eliminating stars with distances $d < 100$ pc, we start with 601 CDDS stars in these associations, 292 in USco, 148 in UCL, and 161 in LCC.

Fig. 18 shows the proper motion distributions of the final set of LCC, UCL, and USco members on an expanded scale compared to Fig. 17. In this space, USco is the most dense, followed by UCL and then LCC. Most stars lie in one of the main concentrations. In addition to some overlap of UCL and USco stars, some stars lie well outside any concentration. In proper motion space, all three associations are much more extended than either the Pleiades or Praesepe.

As summarized in K. L. Luhman (2022), numerous groups have analyzed *Gaia* data to select young stars in the region that includes USco, UCL, and LCC. Here, we match CDDS stars to candidates identified in K. L. Luhman (2022) and several other investigations (B. Goldman et al. 2018; F. Damiani et al. 2019; N. Miret-Roig et al. 2022; G. Briceño-Morales & J. Chanamé 2023; M. L. Wood et al. 2023; S. Ratzenböck et al. 2023). All of these studies, including others listed in K. L. Luhman (2022), apply different techniques to analyze different sets of *Gaia* parallaxes and proper motions (e.g., DR2, eDR3, or DR3) with or without *Gaia* or ground-based radial velocities. While these studies have a set of common candidates, each study has additional candi-

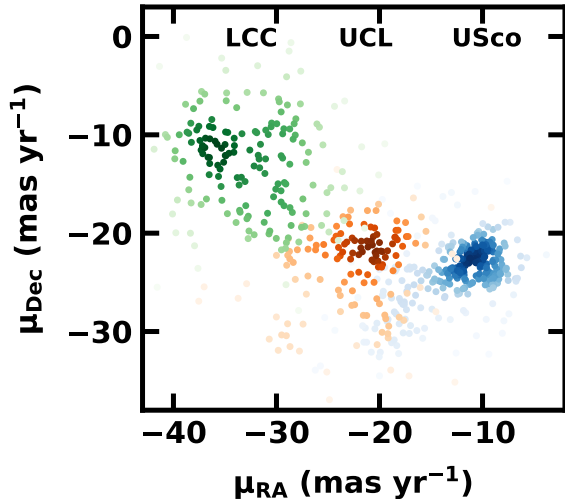


Figure 18. Proper motion distributions for CDDS stars in LCC (179 stars; upper left, green colors), UCL (140 stars, middle, orange colors) and USco (307 stars; lower right, blue colors). The density of members increases from low (light colors) to high (dark colors). There is some overlap in proper motions between UCL and USco and less overlap between LCC and UCL.

dates not included in the others. Our strategy is to (i) compile a set of CDDS stars within a coordinate range that generously encompasses USco, UCL, and LCL, (ii) match CDDS stars to candidates from one of the seven studies listed above, and (iii) eliminate matches from the original list. We then repeat (ii) and (iii) for each of the remaining catalogs. From the distributions of parallax and proper motion for the matches, we remove outliers from the set of non-matches. This exercise results in 617 matches and 44 non-matches with parallaxes and proper motions similar to the matched stars. A few matches have radial velocities that seem discrepant from the rest of the matches; however, these stars have similar measurements of T_{eff} , L_{\star} , and $\log g$ as the rest of the stars in LCL, UCL, and USco.

Among the non-matches, we reject several with sky positions that fall well outside the complete collection of members from sources listed above. We then map the distribution of distances and radial velocities for members across the sky and use this map to include or reject the rest of the non-matches. This exercise results in 28 additional matches with distances and radial velocities close to members with similar sky position and proper motions.

As a final check on membership, we compare the stellar activity measurements of the remaining non-matches with the set of matches. Compared to Sco–Cen stars, all but three of the 16 remaining non-matches have the

activity levels of much older stars. Two stars with moderate activity levels suggestive of a young star lie either too far north or too far south relative to the association boundaries. However, HD 119022 has strong Ca II H&K and X-ray emission, lies on the near side of the bulk of the LCC stars, and has a proper motion on the edge of the LCC proper motion distribution. We include this star in LCC.

The approach outlined above maximizes the number of CDDS stars in the three associations. For each star not included in the original set of assignments to USco, UCL, and LCC or in some other cluster or association, we assign the star to the closest association based on sky position and distance. We then have 645 matches to CDDS stars within or near the galactic coordinate boundaries defined in P. T. de Zeeuw et al. (1999): 308 in USco, 140 in UCL, 179 in LCC, 12 in IC 2602 (discussed below), 5 in TW Hya (discussed below), 1 in ϵ Cha, and 1 in Cha-Near. The full set of 627 Sco–Cen stars includes ~ 25 more stars than the original assignment.

5.3. The 93 Tau Association

The FEPS program targeted eight stars in the general vicinity of the Taurus–Auriga association (M. R. Meyer et al. 2006). As noted in the Appendix, we assign V1299 Tau to the field. Of the remainder, five lie within the 93 Tau association, with distances of 104–122 pc (K. L. Luhman 2023a). Another lies behind 93 Tau at 136 pc and has the low gravity, short P_{rot} , and large R'_{HK} expected for a pre-main sequence star. The final target lies at the appropriate distance but has a much different proper motion. Still, the star has a short rotational period and proper placement in the HR diagram for a young star. We assign five of these stars to 93 Tau and two to the Taurus molecular cloud.

5.4. Nearby Moving Groups

Moving groups, also known as stellar kinematic groups, have a long history (see the discussions in N. G. Roman 1949; O. J. Eggen 1963, 1970; D. R. Soderblom & M. Mayor 1993, and references therein). Based primarily on color-magnitude diagrams, proper motions, and parallaxes for the nearest stars, these studies identified groups of stars with similar ages and space motions. The UMa group (also known as the Sirius group), the Hyades group, the Wolf 630 group, and the Local Association (Pleiades moving group) are good examples of moving groups discovered prior to *Hipparcos* (see also D. Montes et al. 2001).

Hipparcos parallaxes enabled the discovery of new moving groups and the reexamination of older groups (e.g., D. Barrado y Navascues 1998; D. Montes et al.

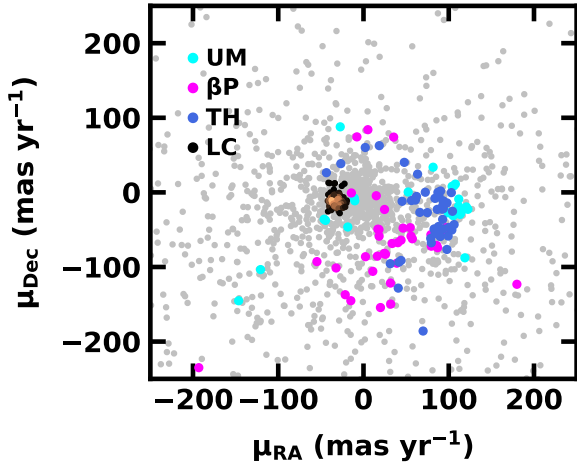


Figure 19. Proper motions for CDDS stars in LCC (black, gold, yellow points as in Fig. 18), β Pic (fuchsia points), Tuc–Hor (dark blue points) and Ursa Major (cyan points). Nearby stars in moving groups have a much larger range of proper motions than stars in associations (e.g., LCC) and clusters (e.g., Pleiades and Praesepe; Fig. 17).

2001; B. Zuckerman et al. 2001a,b,c; J. R. King et al. 2003; J. Bovy et al. 2009; B. Zuckerman et al. 2011, 2013). While many moving groups consist of stars with ages of 100–300 Myr, others have ages as young as 10–20 Myr. The mix of young and old stars among the complete ensemble of moving groups is an interesting outcome of the *Hipparcos* mission.

Various *Spitzer* and *Herschel* programs targeted ~ 210 stars in young moving groups (C. H. Chen et al. 2005b; K. Y. L. Su et al. 2006; L. M. Rebull et al. 2008; P. Plavchan et al. 2009; B. Zuckerman et al. 2011; J. K. Donaldson et al. 2012; C. H. Chen et al. 2014; N. D. Thureau et al. 2014; L. Vican et al. 2016; B. Sibthorpe et al. 2018). Within the CDDS, the AB Dor (47), Tuc–Hor (47), β Pic (30 stars), TW Hya (23), Ursa Major (16), and Columba (16) moving groups are well-represented. There are also stars from the Argus, Her–Lyra, and Octans moving groups.

Recent studies using *Gaia* data suggest 205 CDDS stars as members of the standard moving groups (T. Cantat-Gaudin et al. 2018; J. Gagné et al. 2018; M. Kounkel & K. Covey 2019; N. Miret-Roig et al. 2020; K. Ujjwal et al. 2020; E. L. Hunt & S. Reffert 2023; M. Popinchalk et al. 2023; E. L. Hunt & S. Reffert 2024; R. A. Lee et al. 2024). Of these, most had been listed as moving group members in various *Spitzer* and *Herschel* programs. Others are new identifications. M. Kounkel & K. Covey (2019) recognize 11 other CDDS stars as members of 11 previously unknown groups (e.g.,

Theia 73 and Theia 113). Together, the combined set of old and new candidates includes 259 potential young, nearby moving group members. After analyzing the stellar properties in §4, we reject 46 stars due to (i) more accurate *Gaia* parallaxes and proper motions that result in space velocities inconsistent with other moving group stars, (ii) more accurate T_{eff} , $\log g$, L_* that do not place the stars on the appropriate PARSEC isochrone for their nominal group, and (iii) new activity indicators that imply much older ages than the ages of other nominal group members. Thus, we assign 213 CDDS stars to moving groups (Table 7).

Fig. 19 compares the proper motion distributions of several moving groups with measurements for LCC. Instead of the compact structure observed in open clusters and stellar associations, proper motions for moving groups have a wide spread and do not follow a coherent pattern. Isolating these moving groups requires converting parallaxes, proper motions, radial velocities, and positions on the sky to galactic coordinates and finding their common motions.

5.5. Other Open Clusters

α Per As with other *Spitzer* programs, M. R. Meyer et al. (2006, 13 FGK-type stars) and K. Y. L. Su et al. (2006, 5 A-type stars) selected targets from ground-based proper motion data and measurements of stellar activity. Among recent *Gaia* surveys, T. Cantat-Gaudin et al. (2018), N. Lodieu et al. (2019a), and E. L. Hunt & S. Reffert (2023, 2024) provide extensive membership lists. Thirteen CDDS stars, including one nominal field star, are cluster members. *Gaia* parallaxes for three (two) others place them in the foreground (background) of the cluster.

Blanco 1. Based on studies published prior to 2004, J. R. Stauffer et al. (2010) selected 38 members for *Spitzer* observations. Subsequent photometric and spectroscopic surveys suggest all 38 are members (J. C. Mermilliod et al. 2008; J. F. González & H. Levato 2009). K. Y. L. Su et al. (2006) lists HD 225200 as a member, but this star is not considered a member in more recent dynamical studies. T. Cantat-Gaudin et al. (2018), R. J. Jackson et al. (2020, 2022), Y. Zhang et al. (2020), X. Pang et al. (2021), J. Alfonso & A. García-Varela (2023), and E. L. Hunt & S. Reffert (2023, 2024) analyze *Gaia* data and report new membership lists.

The 38 CDDS members of Blanco 1 have a tight core in proper motion space, similar to those in the Pleiades and Praesepe (Fig. 17). Distances range from 218.2 pc to 241.8 pc; with an inter-quartile range of 4.53 pc, the median distance, $d_{\text{med}} = 234.3$ pc, is identical to the J. Alfonso & A. García-Varela (2023) distance of

236.67±2.10. The dynamical studies quoted above yield 33 (T. Cantat-Gaudin et al. 2018), 31 (Y. Zhang et al. 2020), 33 (X. Pang et al. 2021), 24 (J. Alfonso & A. García-Varela 2023), 27 (E. L. Hunt & S. Reffert 2023), and 34 (E. L. Hunt & S. Reffert 2024) CDDS members. These analyses conclusively reject four stars as members; all are in the cluster background. The remaining 34 are high probability members; all have similar parallaxes, proper motions, and radial velocities.

η Cha. E. E. Mamajek et al. (1999) discovered this cluster from a combination of ROSAT X-ray observations and *Hipparcos* astrometry. Later, I. Gautier et al. (2008) (P. Riviere-Marichalar et al. 2015) reported *Spitzer* (*Herschel*) observations of the brightest cluster members. Among the 16 CDDS stars in η Cha, 15 have *Gaia* parallaxes and proper motions; all but two form a tight cluster with a median distance, $d_{med} \approx 98.4$ pc, close to the $d = 98.2$ pc in E. L. Hunt & S. Reffert (2023, 2024). These stars are clearly cluster members (T. Cantat-Gaudin et al. 2018; J. Gagné et al. 2018; E. L. Hunt & S. Reffert 2023, 2024). EN Cha does not have a *Gaia* parallax. The parallax for ET Cha places it slightly behind the cluster, but the measurement has a large error. With strong X-ray luminosities, EN Cha and ET Cha are certain cluster members.

Coma. Within larger *Spitzer* surveys, K. Y. L. Su et al. (2006) (A. Moór et al. (2011)) assigned five A-type (two F-type) stars to Coma. L. E. Urban et al. (2012) later reported observations of 83 stars that included those discussed in K. Y. L. Su et al. (2006). While all were once considered proper motion members of Coma (e.g., C. Abad & B. Vicente 1999; A. L. Kraus & L. A. Hillenbrand 2007), *Gaia* data place only 18 within the cluster (e.g., S.-Y. Tang et al. 2018, 2019; J. Olivares et al. 2023; E. L. Hunt & S. Reffert 2024). These have a median distance, $d_{med} = 85.3$ pc, close to the nominal distance of 85.8 pc (S.-Y. Tang et al. 2018, 2019; J. Olivares et al. 2023; E. L. Hunt & S. Reffert 2024). Of the remaining stars, four are well in the foreground; five are 10–20 pc more distant than the nominal distance and have proper motions larger than the median cluster proper motion. The rest lie well beyond 130 pc.

Hyades. Four *Spitzer* programs targeted the Hyades, selecting 22 (M. R. Meyer et al. 2006), 11 (K. Y. L. Su et al. 2006), and 45 members (L. A. Cieza et al. 2008). L. E. Urban et al. (2012) reconsidered the full set of 78 stars. Along with a few Hyads from other programs (C. H. Chen et al. 2005b) and later assignments (C. H. Chen et al. 2014), the CDDS sample has 84 nominal members. In addition to a comprehensive series of Hyades studies based on *Gaia* DR3 (W. Brandner et al. 2023c,a,b), N. Lodieu et al. (2019b) combined

Gaia DR2 data with ground-based infrared parallaxes to investigate the core and tidal tails of the cluster. S. Oh & N. W. Evans (2020) made a similar study only with *Gaia* data. E. L. Hunt & S. Reffert (2023, 2024) included the Hyades in a comprehensive *Gaia* DR3 cluster study. Combined, these studies include 76 CDDS stars; S. Oh & N. W. Evans (2020) add two others in the tidal tails. For the six non-matches, four are in the foreground of the cluster, one is in the background, and one has an appropriate parallax but inappropriate proper motions.

IC 2391. N. Sieglér et al. (2007) cast a wide net for possible IC 2391 members from a set of deep *Spitzer* images, ultimately selecting 34 from ground-based proper motion catalogs (D. G. Monet et al. 2003; N. Zacharias et al. 2004). The 34 members have a median distance $d_{med} = 150.6$ pc close to the $d = 150.2$ pc of E. L. Hunt & S. Reffert (2023, 2024). Nearly all of the nominal members lie within 4 mas yr⁻¹ of the median proper motion in RA and Dec. Recent analyses using *Gaia* data yield 100–376 cluster members (T. Cantat-Gaudin et al. 2018; X. Pang et al. 2021; A. H. Nisak et al. 2022; R. J. Jackson et al. 2020, 2022; E. L. Hunt & S. Reffert 2023, 2024). All but two CDDS stars match a cluster member in these surveys. One CDDS star is in the foreground; the other has proper motions inconsistent with other cluster members.

IC 2602. Based on ground-based proper motion catalogs, G. H. Rieke et al. (2005), K. Y. L. Su et al. (2006), and M. R. Meyer et al. (2006) targeted 12 stars in this cluster. *Gaia* analyses suggest all twelve are cluster members (T. Cantat-Gaudin et al. 2018; X. Pang et al. 2021; A. H. Nisak et al. 2022; E. L. Hunt & S. Reffert 2023, 2024).

NGC 2232. Starting with deep *Spitzer* photometry, T. Currie et al. (2008) selected 526 MIPS 24 μ m sources with 2MASS counterparts, matched these with ROSAT X-ray data (W. Voges et al. 1999) and optical photometry (J. J. Claria 1972; W. Lyra et al. 2006), and published a catalog of 209 stars. T. R. Monroe & C. A. Pilachowski (2010) acquired optical spectra of 23 stars with *Spitzer* photometry, concluding that only five are members. From *Gaia*, the distribution of parallaxes and proper motions consists of three groups: (i) ~ 25 foreground stars with $d = 100$ –300 pc, (ii) a group of ~ 50 –60 stars with a small range in proper motions and a median distance $d_{med} = 317.4$ pc, and (iii) a disperse set of ~ 125 stars with $d \gtrsim 360$ pc. We identify the middle group as the cluster; the median distance agrees with the $d = 318$ pc of E. L. Hunt & S. Reffert (2023, 2024). To examine cluster membership in more detail, we consult results from several recent *Gaia* studies (T.

Table 7. Associations, Open Clusters, and Moving Groups^a

Group	N_{SH}	N_g	Age (Myr)	Methods ^b	References
AB Dor	47	33	149	iso	Be15
α Per	18	13	85	Li	B02, B04a, B19, D21
Argus	8	14	40–60	iso, Li	T08, Be15
β Pic	30	41	24	iso	Be15
Blanco 1	38	34	85–125	iso, Li	M07, B19, D21, J22, R22
Carina–Near	3	3	200	act, Li	Z06
Cha–Near	1	1	10	act	Z04, R07
Columba	16	16	42	iso	Be15
Coma	85	18	650	iso	S14, D21
CrA	7	7	4.5	EB	G12
ϵ Cha	1	1	5	iso	DV21
η Cha	16	16	11	iso	Be15
Hyades	84	76	600–850	iso, MSTO, rot	Br15, G18, D21, B23
Her–Lyra	1	1	210–305	Li	E13
IC2391	34	32	40–50	iso, Li	B99, B04b, B19, D21
IC2602	12	12	25–50	iso, Li	S97, D10, B19, D21
LCC	161	179	15	iso	P16
NGC 2232	209	54	18–38	iso, Li	B21, D21, J22, R22
NGC 2422 (M47)	32	28	123–195	iso	B19, D21, L21
NGC 2451a	70	35	35–80	iso, Li	H03, B19, D21, J22, R22
NGC 2451b	131	78	30–50	iso, Li	H03, B19, D21, F22, R22
NGC 2516	50	42	138–265	iso, Li	M93, S02, B19, D21, F22, R22
NGC 2547	30	23	25–40	iso, Li	J03, O03, J05, B19, D21, F22
Oceanus	0	1	400–600	act, iso, rot	G23
Octans	1	1	35	Li	M15
Ori OB1a	9	9	10–11	iso	Br19, H23
Ori OB1b	6	6	3–6	iso	Br19, H23
Pleiades	165	151	100–160	iso, MSTO, rot	S98, B04b, D15, G18, B19, D21
Praesepe	193	159	590–760	iso, MSTO, rot	G18, B19, D21
σ Ori	3	3	3–5	iso	O02, O04
Taurus	7	2	1–3	iso	L23
TW Hya	23	22	10	iso	Be15
Tuc–Hor	46	48	45	iso	Be15
UCL	148	140	16	iso	P16
USco	292	308	10	iso	P16
UMa	16	24	414	int	J15, J17
93 Tau	0	5	20–50	iso	L23

^aAge references: B99: D. Barrado y Navascués et al. (1999); B02: D. Barrado y Navascués et al. (2002); B04a: D. Barrado y Navascués (2004); B04b: D. Barrado y Navascués et al. (2004); Be15: C. P. M. Bell et al. (2015); B19: D. Bossini et al. (2019); B21: A. S. Binks et al. (2021); B23: W. Brandner et al. (2023a); Br15: T. D. Brandt & C. X. Huang (2015); Br19: C. Briceño et al. (2019); D15: S. E. Dahm (2015); D21: W. S. Dias et al. (2021); DV21: D. A. Dickson-Vandervelde et al. (2021); D10: P. D. Dobbie et al. (2010); E13: T. Eisenbeiss et al. (2013); F22: E. Franciosini et al. (2022); G12: M. Gennaro et al. (2012); G18: S. Gossage et al. (2018); G23: J. Gagné et al. (2023); H03: M. Hünsch et al. (2003); H23: J. Hernández et al. (2023); J22: R. J. Jackson et al. (2022); J03: R. D. Jeffries et al. (2003); J04: R. D. Jeffries & J. M. Oliveira (2005); J15: J. Jones et al. (2015); J17: J. Jones et al. (2017); L21: I. Lipartito et al. (2021); L23: K. L. Luhman (2023a); M93: G. Meynet et al. (1993); M07: E. Moraux et al. (2007); M15: S. J. Murphy & W. A. Lawson (2015); O02: J. M. Oliveira et al. (2002); O03: J. M. Oliveira et al. (2003); O04: J. M. Oliveira et al. (2004); P16: M. J. Pecaut & E. E. Mamajek (2016); R07: J. H. Rhee et al. (2007); R22: S. Randich et al. (2022); S14: J. Silaj & J. D. Landstreet (2014); S97: J. R. Stauffer et al. (1997); S98: J. R. Stauffer et al. (1998); S02: H. Sung et al. (2002); T08: C. A. O. Torres et al. (2008); Z04: B. Zuckerman & I. Song (2004); Z06: B. Zuckerman et al. (2006)

^bMethods: act: stellar activity, including X-ray emission; EB: eclipsing binary; int: interferometric sizes of A-type stars; iso: isochronal fitting; Li: Lithium depletion boundary; MSTO: main sequence turnoff; rot: rotation, gyrochronology

Cantat-Gaudin et al. 2018; L. Liu & X. Pang 2019; R. J. Jackson et al. 2020; X. Pang et al. 2021; R. J. Jackson et al. 2022; E. L. Hunt & S. Reffert 2023, 2024). This analysis yields 54 clear members and a few outliers in μ and π that might be part of a tidal tail.

NGC 2422 (M47). Two *Spitzer* programs (N. Gorlova et al. 2004; G. H. Rieke et al. 2005) published observations for 32 stars with spectral types of K0 and earlier and confirmed membership for all but one from ground-based (e.g., S. E. Urban et al. 1998; N. V. Kharchenko 2001; N. Zacharias et al. 2004) and space-based (E. Høg et al. 2000) proper motion catalogs. Using *Gaia* data, all but three of the 32 nominal members form a tight knot in proper motion space within a small range of parallax. The median distance of these stars $d_{med} = 468.6$ pc agrees with the $d = 468.3$ pc derived from 510 members in E. L. Hunt & S. Reffert (2023). From E. L. Hunt & S. Reffert (2023, 2024) and other *Gaia* studies (T. Cantat-Gaudin et al. 2018; L. Liu & X. Pang 2019; X. Pang et al. 2021; R. J. Jackson et al. 2022), at least 28 CDDS stars are members of M47; two others are within 10 pc of the cluster core and almost share the proper motions of cluster members. One candidate lies ~ 30 pc in front of the cluster and has discrepant proper motions. The last candidate is clearly a background star.

NGC 2451. NGC 2451 consists of two clusters, NGC 2451a and NGC 2451b, along the same line of sight. Z. Balog et al. (2009) used a combination of optical photometry, high resolution optical spectroscopy, X-ray emission, and deep IRAC and MIPS images to select 70 (131) members in NGC 2451a (NGC2451b). The CDDS contains 42 cluster stars with MIPS data, 22 in NGC 2451a and 20 in NGC 2451b. Most of the rest have IRAC data. The full set of stars has a broad range in μ and π . Some stars assigned to NGC 2451a (NGC2451b) have $d \sim 190$ pc (360 pc); both have a concentrated group with a common proper motion. Consulting several *Gaia* analyses (T. Cantat-Gaudin et al. 2018; L. Liu & X. Pang 2019; X. Pang et al. 2021; R. J. Jackson et al. 2022; E. L. Hunt & S. Reffert 2023, 2024) results in 35 (78) high probability members in NGC 2451a (NGC 2451b). Of the members in NGC 2451a from Z. Balog et al. (2009), 5 (23) are in the foreground (background); one does not have a *Gaia* parallax. For NGC 2451b, 18 (40) lie in the foreground (background) and one has large *Gaia* parallax errors. The *Gaia* analyses swap several members between the clusters. Among the foreground and background stars, several have parallaxes in the vicinity of one of the clusters but they have discrepant proper motions.

NGC 2516. From ground-based proper motion studies, G. H. Rieke et al. (2005) observed all 50 CDDS stars in NGC 2516. *Gaia* data show a concentrated set of stars with similar proper motion and a small set of outliers. The median distance of 409 pc for the sample agrees with the 407 pc distance derived from more than 500 stars in E. L. Hunt & S. Reffert (2023). Recent *Gaia* surveys classify all but eight stars as members (T. Cantat-Gaudin et al. 2018; L. Liu & X. Pang 2019; X. Pang et al. 2021; R. J. Jackson et al. 2022; E. L. Hunt & S. Reffert 2023, 2024). Several non-members lie within the cluster but have discrepant proper motions. Two others are clear background stars, while another has poor *Gaia* data.

NGC 2547. G. H. Rieke et al. (2005) and N. Gorlova et al. (2007) together selected 30 plausible proper motion members for *Spitzer* observations. The *Gaia* proper motion distribution consists of a tight core similar to that observed in the Pleiades and Praesepe (Fig. 17) with 7–8 outliers. The median distance of stars in the core $d_{med} = 384$ pc is quite close to the E. L. Hunt & S. Reffert (2023, 2024) estimate of 382 pc from analysis of 424 member stars. From a set of detailed *Gaia* analyses, 23 CDDS stars in or close to the proper motion core are cluster members (T. Cantat-Gaudin et al. 2018; L. Liu & X. Pang 2019; X. Pang et al. 2021; R. J. Jackson et al. 2022; E. L. Hunt & S. Reffert 2023, 2024). Of the seven non-members, one (three) star(s) is (are) definitely in the foreground (background). For three others, two are slightly in the foreground; and one has the same parallax as member stars, but has discrepant proper motions with respect to cluster members.

Summary. To conclude this section, Table 7 summarizes several aspects of the set of stellar associations, open clusters, and moving groups in the CDDS. The columns in the table include the group name, number of group members in the CDDS from *Spitzer* and *Herschel* studies (N_{SH}), the number of members suggested by the *Gaia* analyses quoted above (N_g), the range of cluster ages, codes for the age method(s) used, and the appropriate references. As in published *Spitzer* and *Herschel* studies, isochronal methods and the Li-depletion boundary are popular choices to derive cluster ages. The position of the main sequence turn-off and the rotational period distribution are also common methods for estimating ages. Although the age range for several clusters is a factor of ~ 2 , most results from independent approaches agree to within 10% to 25%.

The CDDS contains a representative set of associations and cluster stars with ages ranging from 5–15 Myr (e.g., η Cha, σ Ori, and the Sco-Cen associations) to close to 1 Gyr (the Hyades and Praesepe). Across this

age range, the Sco–Cen associations (10–20 Myr, $\gtrsim 600$ members), Blanco-1 and the Pleiades (~ 100 Myr; 34 and 151 members), and the Hyades and Praesepe (600–850 Myr; 76 and 150 members) are particularly well-represented. The clusters IC 2391, IC 2602, NGC 2232, NGC 2451a, NGC 2451b, and NGC 2547 are intermediate in age between Sco–Cen and the Pleiades. Along with the Coma cluster, NGC 2422 and NGC 2416 span the age range between Blanco-1 and Praesepe.

Moving groups within the CDDS are also well-populated and cover a broad range of ages. Among the younger groups, the CDDS includes most of the stars in Tuc–Hor (45 Myr, 48 members) and β Pic (24 Myr, 41 members). With most members of the TW Hya association discovered since *Spitzer* and *Herschel*, the CDDS contains only ten of 66 possible members (K. L. Luhman 2023b). Although none of the moving groups in the CDDS are as old as the Hyades, AB Dor (149 Myr, 33 members) and UMa (400 Myr, 24 members) provide a useful comparison to the Pleiades and Praesepe.

6. HR DIAGRAMS

For the past 10–20 years, advances in stellar structure calculations together with results from large astrometric and spectroscopic surveys of field stars and open clusters have greatly improved understanding of the evolution of the chromospheric and photospheric properties of main sequence stars. Recent studies illustrate how rotational evolution and internal mixing processes influence Li and Be depletion (e.g., T. Dumont et al. 2021b) and the decline in chromospheric emission (e.g., C. P. Johnstone et al. 2021) as a star evolves. Along with precise cluster membership probabilities from *Gaia*, (e.g., T. Cantat-Gaudin et al. 2020; W. S. Dias et al. 2021; R. J. Jackson et al. 2022; E. L. Hunt & S. Reffert 2024), new model isochrones provide more accurate estimates of cluster ages as a function of metallicity and other physical parameters (e.g., C. P. M. Bell et al. 2015; S. Gossage et al. 2018; W. S. Dias et al. 2021).

Although we defer an extended discussion of age estimates to Paper IV in this series, we conclude our summary of host star properties with HR diagrams for association, cluster, and moving group stars (Fig. 20) and for field stars (Fig. 21). For stars in clusters, a combination of the 3 Myr isochrone for massive stars and the 150 Myr isochrone for lower mass stars roughly corresponds to the zero-age main sequence (ZAMS). Among the lower mass stars with $T_{\text{eff}} \lesssim 10,000$ K, the 3 Myr (150 Myr) isochrone sets a rough upper bound (strict lower bound) to the observed luminosities. Although most stars lie close to the ZAMS, others are starting to turn off the main sequence and evolve towards the red

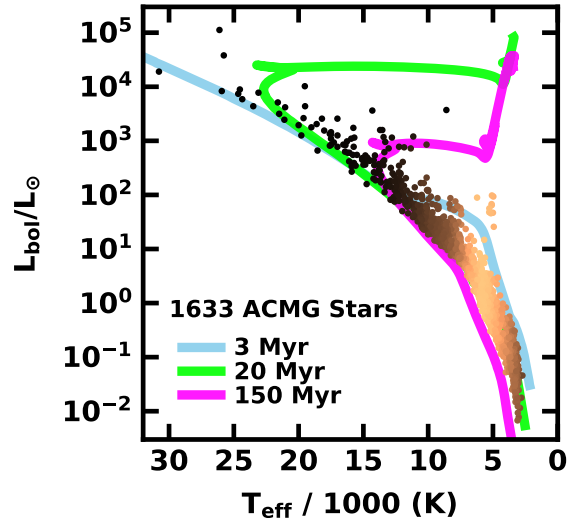


Figure 20. HR diagram for 1633 CDDS stars in stellar associations, clusters, and moving groups (ACMG). The light blue (lime, fuchsia) curves shows the PARSEC 1.2S isochrone for $[\text{Fe}/\text{H}] = 0$ and an age of 3 Myr (20, 150 Myr), displaced by -500 K (0 K, $+750$ K) for clarity. The lower bound of the two curves for $T_{\text{eff}} \gtrsim 15000$ K (light blue) and $T_{\text{eff}} \lesssim 15000$ K (fuchsia) marks the approximate zero-age main sequence; all CDDS stars lie above this locus. For cooler stars, the 3 Myr isochrone sets a strong upper limit to the set of young stars contracting to the main sequence. Some cluster stars lie at the main sequence turnoff for ages 20–150 Myr.

giant branch. Many of these lie on or in between the turnoffs for the 3 Myr and 150 Myr isochrones.

For nearly all of the clusters, an age of 3–150 Myr nicely brackets age estimates for the youngest associations (e.g., LCC, UCL, and Upper Sco; M. J. Pecaut & E. E. Mamajek 2016) to clusters like the Pleiades (e.g., J. R. Stauffer et al. 1998; S. E. Dahm 2015; S. Gossage et al. 2018; D. Bossini et al. 2019; W. S. Dias et al. 2021). Aside from stars on the main sequence turnoff, most stars in older clusters (e.g., Hyades and Praesepe; T. D. Brandt & C. X. Huang 2015; S. Gossage et al. 2018; D. Bossini et al. 2019; W. S. Dias et al. 2021; W. Brandner et al. 2023a) lie on or close to the main sequence. Across all of the clusters, few stars lie on the red giant branch.

The HR diagram for CDDS field stars has a very different morphology (Fig. 21). Most of this group is bound by the 200 Myr and 4.5 Gyr isochrones. Nearly all of the cool stars with $T_{\text{eff}} \lesssim 5000$ K lie on or near the 200 Myr isochrone. Few lie close to the 30 Myr isochrone or the 4.5 Gyr isochrone. Aside from a few stars clearly on the red giant branch, these stars are older than cluster stars of similar T_{eff} , but are much younger than 4.5 Gyr. Among hotter stars with $T_{\text{eff}} = 5000$ – 10000 K, many are either on the main sequence or evolving off the main

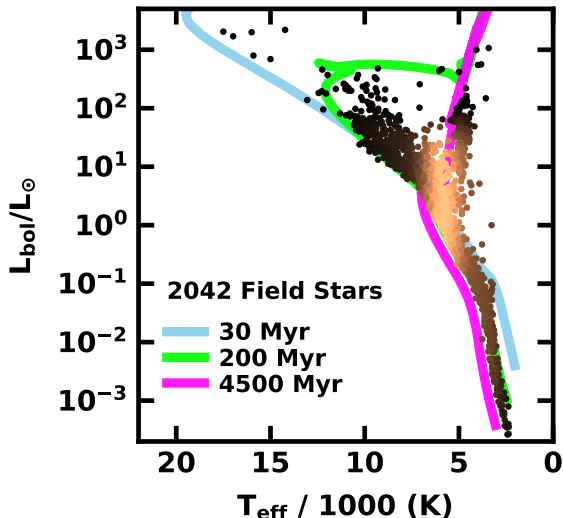


Figure 21. HR diagram for 2042 CDDS field stars. The light blue (lime, fuchsia) curves shows the PARSEC 1.2S isochrone for $[\text{Fe}/\text{H}] = 0$ and an age of 30 Myr (200 Myr, 4.5 Gyr). The lower bound of the light blue and light green curves for $T_{\text{eff}} \gtrsim 10000$ K marks the approximate zero-age main sequence; all CDDS stars lie near or above this locus. Nearly all cooler stars lie near the 200 Myr isochrone; others lie on the giant branch.

sequence. The more evolved stars are bound by the 200 Myr and 4.5 Gyr isochrones. Finally, there are a few very hot stars, $T_{\text{eff}} = 12000\text{--}20000$ K, between the 30 Myr and 200 Myr isochrones that are clearly young. These stars are not quite as young as their cluster counterparts, but they are clearly the youngest stars not obviously associated with an association, cluster, or moving group.

7. DISCUSSION

As described in the previous sections, we have assembled from the literature a sample of 3675 stars that has strong constraints on cold circumstellar dust emission from observations with *Spitzer* and *Herschel*. The stars span a range of spectral types (B5–M9), luminosity classes (V–II), and ages ($\gtrsim 5\text{--}10$ Myr). Most stars are in the field (2042; 56%); the rest (1633; 44%) are members of stellar associations, open clusters, and moving groups. For this sample, we compiled optical-infrared photometry, parallaxes, and proper motions (§2), along with information on planetary and stellar companions (§3); host star properties (spectral type SpT, effective temperature T_{eff} , extinction A_V , luminosity L_* , gravity $\log g$, metallicity $[\text{Fe}/\text{H}]$, Li abundance $A(\text{Li})$, stellar rotation P_{rot} , chromospheric and coronal emission; §4) and their membership in associations, clusters, and moving groups (§5). Several tables report the extent of the compilation; Table 1 summarizes photometric data;

Table 2 outlines the sources of data on stellar multiplicity; Table 3 lists statistics on companions; Table 4 recaps the availability of host star properties; Table 5 reports the frequency of activity measures as a function of spectral type; and Table 6 lists the correlation coefficients for different stellar activity measures within the sample. Table 8 lists properties of candidate common proper motion companions.

Missing Data. Despite efforts to construct a complete compilation, some data are inevitably missing. Among the photometric observations, BVI_C are sometimes unavailable for faint red stars discovered in the 2MASS survey; bright stars saturated in 2MASS and WISE sometimes do not have counterparts in DIRBE or other literature sources. These misses are rare, $\lesssim 1\%$ of the compilation. Deep BVI_C photometry or shallow JHK_s photometry could complete these parts of the compilation. Short time series limit the availability of robust rotational periods for many CDDS stars. Analyses of *TESS* data and additional ground-based programs could alleviate this deficiency.

At longer wavelengths, stars are often too faint for W4 and sometimes too faint for MIPS at $70\ \mu\text{m}$ or *Herschel* PACS and SPIRE at any wavelength. *Herschel* generally observed nearby CDDS stars; 75% (89%) of the stars with *Herschel* 5σ or better detections lie within 50 pc (100 pc). *Herschel* observing time constraints and the large population ($\sim 50\%$) of CDDS stars with distances $\gtrsim 100$ pc precluded a complete set of *Herschel* data. Adding these data require a new and more sensitive space-based mission.

On the rare occasion when *Gaia* misses on a parallax or proper motion, the star is near a much brighter star or is a binary with a period comparable to the lifetime of the satellite. The available data in the rest of the compilation is then sufficient to derive a distance. The activity measures are often helpful in assigning a star to a cluster when proper motion is not available. We anticipate that a future *Gaia* data release will include accurate parallaxes and proper motions for these stars.

Missing spectroscopic diagnostics have several causes. Early type stars with radiative envelopes and $T_{\text{eff}} \gtrsim 6500$ K comprise $\sim 30\%$ of the CDDS and are often too hot or lack the appropriate absorption features to measure $\log g$, $[\text{Fe}/\text{H}]$, $[\text{Li}/\text{H}]$, P_{rot} , R'_{HK} , and R'_{IRT} . Roughly half of the BA and early F stars have measured $v \sin i$ and L_X/L_* . Moderate resolution optical or infrared spectra are sufficient for $v \sin i$. Some of these stars lie in the unpublished half of the *SRG/eROSITA* survey and will at least have improved upper limits once these *SRG/eROSITA* data are published.

Among the late F and G stars, nearly all have measured $\log g$; $\sim 85\%$ have $[\text{Fe}/\text{H}]$; and $\sim 60\text{--}70\%$ have P_{rot} , $v \sin i$, R'_{HK} , R'_{IRT} , and L_X/L_\star . Only $\sim 50\%$ have an $[\text{Li}/\text{H}]$ measurement. The second half of the *SRG/eROSITA* data release should add L_X/L_\star data for many stars. High resolution echelle data can yield $v \sin i$, R'_{HK} , R'_{IRT} , and $[\text{Li}/\text{H}]$. The next *Gaia* data release should add new measurements of $\log R'_{\text{IRT}}$.

Aside from L_X/L_\star , KM stars in the CDDS are less likely to have measurements of $\log g$, abundances, and activity measures than G stars. These stars are often fainter; stronger molecular bands may complicate measures of abundances and activity indicators. The CARMENES project searched many nearby M dwarfs for exoplanets (e.g., F. J. Alonso-Floriano et al. 2015; M. Cortés-Contreras et al. 2017). Future high resolution spectroscopic observations on 4-m class or larger telescopes are required to expand the CDDS collection of M dwarf photospheric and chromospheric properties.

Frequency of CDDS Stars in Associations, Clusters, and Moving Groups. Within the CDDS, stars in open clusters (682) and stellar associations (652) clearly outnumber the stars in moving groups (213). Overall, $\sim 44\%$ of CDDS stars lie within an association, cluster, or moving group. There are another 40–50 on the outskirts of a cluster or association but have discrepant proper motions. Several dozen possibly lie within a moving group.

Compared to the *Hipparcos* data available for *Spitzer* and *Herschel* programs, exquisite *Gaia* data enable much more robust estimates of membership probabilities in associations, clusters, and moving groups at much greater distances (e.g., T. Cantat-Gaudin et al. 2018; T. Cantat-Gaudin & F. Anders 2020; W. S. Dias et al. 2021; E. L. Hunt & S. Reffert 2023, 2024). For the CDDS, *Gaia* data eliminate many potential members in the Pleiades, Praesepe, and other clusters. However, we now have many more CDDS stars in nearby associations. The collection of stars within moving groups is impressive: *Gaia* confirms most of the moving group members discussed in *Spitzer* programs and adds enough new members to replace members lost due to age, distance, and proper motion considerations.

The frequency of cluster stars in the CDDS is much larger than the frequency within 100–200 pc of the Sun. As an example, E. L. Hunt & S. Reffert (2024) identify ~ 2700 cluster members within 100 pc and ~ 19000 within 200 pc. Other analyses yield similar results (e.g., T. Cantat-Gaudin et al. 2018; W. S. Dias et al. 2021; E. L. Hunt & S. Reffert 2023). Within 100 pc, the GCNS contains information on close to 190,000 stars (Gaia Collaboration et al. 2021a). For 200 pc, we scale the

GCNS up by a factor of eight. The frequency of cluster stars is then $\sim 1.25\%$ to 1.5% within 100–200 pc. The CDDS contains a factor of 30–35 more stars in clusters than the solar neighborhood.

Although *Herschel* targeted few cluster stars, *Spitzer* programs focused on young clusters to have a better chance of detecting IR excesses from debris disks and to have a better estimate of stellar ages from analyses of the full cluster instead of individual field stars (see Table 7). With $\sim 44\%$ of CDDS stars in groups with fairly well-defined ages and $\sim 56\%$ in the field, the CDDS sample provides a way to follow the evolution of debris disk emission as a function of environment. When we consider age estimates in Paper IV, we will investigate this issue.

Potential for Gaia–Spitzer Cross-matching.

We have applied many *Gaia* analyses of clusters to assign membership of CDDS stars to associations, clusters, and moving groups. In most cases, *Gaia* parallax and proper motion data coupled with *Gaia* or new ground-based radial velocity data eliminate cluster members from *Spitzer* catalogs. Sometimes the losses are minimal. In the Pleiades, *Gaia* analyses retain 91.5% of Pleiads in the combined *Spitzer* catalog; in Blanco-1, we retain 90% of the *Spitzer* catalog. For other clusters, losses are severe. In Coma (NGC 2451ab), we retain only 21% (56%) of proposed *Spitzer* cluster members.

These results suggest that matching *Gaia* cluster members (e.g., E. L. Hunt & S. Reffert 2024) with the full set of *Spitzer* photometric data for individual clusters might increase the set of cluster members with high quality *Spitzer* photometry. The strategy would be to derive coordinates and photometry for all *Spitzer* sources within the nominal boundary of a cluster, match these to *Gaia* DR3 sources to verify the coordinates and to obtain G, BP, and RP for each *Spitzer* source, and then derive cluster membership probabilities from the detailed *Gaia* cluster studies (e.g., E. L. Hunt & S. Reffert 2024).

As a test of this concept, we consider Blanco-1 which has ~ 800 members from E. L. Hunt & S. Reffert (2024). Matching these to the SEIP Source List (P. Capak 2019) at IPAC recovers 205 matches. While many of these are IRAC measurements, we identify 51 (7) MIPS 24 μm aperture (PSF) measurements. Compared to the 38 measurements reported in J. R. Stauffer et al. (2010), this *Gaia* match adds as many as $\sim 50\%$ more 24 μm measurements from Blanco-1 stars not considered members at the time of the *Spitzer* observations. Considering the high quality requirements for SEIP, it seems plausible that additional *Spitzer* sources might be identified

by reducing the *Spitzer* images from scratch. We set this possibility aside for another day.

Applications As noted in the Introduction, we currently plan three additional studies with the CDDS compilation. Paper II will explore the magnitude and frequency of IR excess emission as a function of the physical properties of the central star, known companions, and membership in a group. In Paper III, we then search for new planetary and stellar companions with *Gaia*. Finally, Paper IV will consider age estimates for the full sample of CDDS stars and examine trends in IR excess emission with age for stars in clusters and the field. Aside from these, CDDS can serve as a starting point for many investigations of stellar physics. We discuss several possibilities.

Although we do not compile information on stellar magnetic fields, the connection between magnetic topology and chromospheric and coronal emission is well-established (e.g., V. See et al. 2016; E. L. Brown et al. 2022; S. V. Jeffers et al. 2023; M. A. Weber et al. 2023). Recent investigations of magnetic field topology in several CDDS stars – τ Boo, 61 Cyg, ϵ Eri, χ Dra, ι Hor, and 18 Sco among others – illustrate the relation between the topology, chromospheric and coronal emission, stellar activity cycles, and the stellar dynamo (e.g., T. S. Metcalfe et al. 2010; S. V. Jeffers et al. 2018, 2022; S. C. Marsden et al. 2023; J. D. do Nascimento et al. 2023). With the success of deriving rotational periods and stellar cycles from ground-based and space-based facilities (e.g., J. D. Hartman et al. 2010; P. A. Cargile et al. 2014; B. L. Canto Martins et al. 2020; L. M. Rebull et al. 2022; M. Popinchalk et al. 2023; S. T. Douglas et al. 2024), it seems plausible that many CDDS stars with high levels of stellar activity will show long-term activity cycles and merit more detailed measurements of their magnetic field topology.

In contrast to the dynamo-produced magnetic fields in the atmospheres of low mass main sequence stars, magnetic fields detected in B-type or A-type stars are probably fossil fields left over from the original molecular cloud (e.g., J. Braithwaite & M. Cantiello 2013; D. R. G. Schleicher et al. 2023). Although the CDDS contains many apparently pristine B-type and A-type stars, there are several with strong metallic lines (SpT: Am or Bm, e.g., 67 UMa) or with magnetic fields (SpT: Ap or Bp, e.g., α Lyr (Vega), α CMa (Sirius), and β UMa (Merak), F. Lignières et al. 2009; P. Petit et al. 2011; A. Blazère et al. 2015). Several others, such as α Aql, α Lyr, and α Lac, have detectable rotation periods, $P_{rot} \lesssim 1$ day, perhaps suggestive of features induced by a weak magnetic field. Detailed studies of other CDDS BA (and perhaps early F) stars might similarly reveal weak fields or short

periods. Enlarging these samples may shed light on the evolution of magnetic and rotational structures observed in massive stars.

8. SUMMARY

We conclude with a synopsis of the compilation, the main results, and the next steps in this study.

The CDDS Compilation. We compile photometric, dynamical, and spectroscopic data for 3675 stars targeted by *Spitzer* and *Herschel* to search for cold circumstellar dust emission from debris disks. We name the compilation the Cold Debris Disk Surveys (CDDS). The photometric data include *Gaia* G, BP, and RP; Tycho $B_T V_T$; Johnson–Cousins BVI_C ; APASS $g'r'i'$, Pan-STARRS and Skymapper $griz$; 2MASS JHK_s; WISE W1–W4; *Spitzer* IRAC B1–B4, IRS 8–25 μm , and MIPS 24–70 μm ; IRAS 12–100 μm ; *Herschel* PACS 70–160 μm and SPIRE 250–500 μm ; and submm 450–1200 μm . Figs. 1–2 and Table 1 show that $\gtrsim 80\%$ of CDDS stars have photometry from B to 25 μm ; the fraction of available data declines at longer wavelengths. Fig. 4 compares the distribution of BP–RP colors of CDDS stars with the colors of main sequence stars in the GCNS; compared to the local solar neighborhood, the compilation has an overabundance of AFG stars and an underabundance of KM stars. When available, the CDDS includes rotational periods P_{rot} measured from photometric time series.

The dynamical data comprise *Hipparcos* and *Gaia* parallaxes and proper motions along with properties of stellar and planetary companions. All but a handful of stars have parallaxes and proper motions. Roughly half (more than 90%) of the sample lies within 100 pc (300 pc). Fig. 3 contrasts the distribution of parallaxes in the CDDS (where the number of stars as a function of distance is approximately $N \propto d$) and the GCNS (where $N \propto d^3$). Approximately 44% (9%) of the stars have at least one stellar (planetary) companion. Figs. 5 and 6 illustrate the broad semimajor axis distributions of stellar and planetary companions to CDDS primary stars. The fraction of non-single FGKM stars in the CDDS is comparable to the fraction in the general field (e.g., S. Gao et al. 2014; Z. Niu et al. 2021; N. Susemihl & M. R. Meyer 2022); the CDDS has a somewhat smaller fraction of non-single BA stars than the field (e.g., Y. Guo et al. 2022). The frequency of planets in the CDDS sample is smaller than the 0.2–1 per star derived for typical field FGKM stars (e.g., E. A. Petigura et al. 2013; R. B. Fernandes et al. 2019; B. J. Fulton et al. 2021; A. Kaminski et al. 2025; L. Mignon et al. 2025).

The spectroscopic data include *Gaia* XP spectra and literature measurements of spectral type SpT, effec-

tive temperature T_{eff} , gravity $\log g$, metallicity $[\text{Fe}/\text{H}]$, lithium abundance $[\text{Li}/\text{H}]$, projected rotational velocity $v \sin i$, the Ca II HK and IR triplet activity indicators R'_{HK} and R'_{IRT} , and the 0.1–3 keV X-ray flux F_X . Combined with the dynamical and photometric data, the measured effective temperatures yield estimates for interstellar extinction A_V and stellar luminosity L_\star . Tables 4–5 summarize the statistics of these measurements as a function of SpT. Data for T_{eff} and L_\star are complete. Approximately 80% (64%, 59%, 54%) of the stars have measured $\log g$ ($[\text{Fe}/\text{H}]$, $v \sin i$, L_X/L_\star). Only $\sim 50\%$ of FGK stars with $T_{\text{eff}} = 4500\text{--}6500$ K have measured $[\text{Li}/\text{H}]$, P_{rot} , R'_{HK} , and R'_{IRT} . Figs. 7–15 illustrate (i) the excellent agreement between T_{eff} , $\log g$, and L_\star estimates from *Gaia* and ground-based data, (ii) a gaussian-like $[\text{Fe}/\text{H}]$ distribution with a median $[\text{Fe}/\text{H}] \approx -0.03$ and a full-width at half maximum of ~ 0.26 , and (iii) the extensive range in $[\text{Li}/\text{H}]$, P_{rot} , $v \sin i$, $\log R'_{HK}$, $\log R'_{IRT}$, and L_X/L_\star as a function of T_{eff} .

Together with detailed studies from the literature, we use the dynamical, photometric, and spectroscopic data to assign CDDS stars to the field (2042 stars; 56% of the sample) or to one of many moving groups, open clusters, or stellar associations (1633 stars; 44%; Table 7). The fraction of CDDS stars within an association, cluster, or moving group is much larger than we would find in a random sample of stars within 100–200 pc, where the fraction is $\sim 1\%$ to 2% (e.g., Gaia Collaboration et al. 2021a; E. L. Hunt & S. Reffert 2024).

Main Results. In parallel with an analysis of *Gaia* data for *Spitzer* and *Herschel* targets, we identify a set of faint stars with nearly identical parallaxes and proper motions as the main target. Table 8 in the Appendix lists G and BP–RP colors, separation from the apparent primary, and velocity difference. The magnitude differences suggest most of these candidate proper motion companions are M dwarfs or brown dwarfs.

Compared to *Spitzer* and *Herschel* studies, *Gaia* data subtract stars from the population of cluster stars, add stars to the population of associations, and add *and* subtract stars from moving groups. Some clusters (e.g., Pleiades and Praesepe) lose few stars; others (e.g., Coma, NGC2232, and NGC2451a,b) lose many. The number of moving group stars with *Spitzer* and *Herschel* data is significant.

The addition of stars to some groups suggests that a full analysis of available *Spitzer* photometry within the footprint of *Gaia* cluster boundaries might result in a larger sample of cluster stars with *Spitzer* photometry. Illustrations with Blanco-1 and Coma imply increases of 25% to 50%. Adding unpublished *Spitzer* photometry to

systems with few members in Table 7 would enhance the *Spitzer* legacy.

Fig. 16 and Table 6 summarize the correlations of pairs of activity indicators. With 467–859 points per correlation, the CDDS provides good statistics for this analysis. The best correlations involve any combination of $\log R'_{HK}$, P_{rot} , and L_X/L_\star (p -values $\lesssim 10^{-137}$ for the probability of no correlation). The strength of most other correlations remains strong, with p -values between 10^{-19} and 10^{-95} . The relation between the Ca II IR triplet and the lithium abundance has the largest probability of no correlation (p -value = 10^{-5}).

The complete HR diagrams for cluster (Fig. 20) and field (Fig. 21) stars indicate that CDDS stars have ages ranging from $\sim 5\text{--}10$ Myr to $\sim 5\text{--}10$ Gyr. Comparisons of $[\text{Li}/\text{H}]$, R'_{HK} , R'_{IRT} , and L_X/L_\star with results for other cluster and field stars in the literature confirm this general conclusion. While the range of ages is a feature for *Spitzer* and *Herschel* targets, few of the field stars are considered as young as 50–100 Myr in *Spitzer* and *Herschel* publications. Some of the young stars might be in extended halos (instead of tidal tails) surrounding the inner cores of the clusters (e.g., T. Currie et al. 2010; H. Yu et al. 2020; X. Pang et al. 2022) or stars ejected from the cluster through dynamical interactions with other cluster members (e.g., P. J. T. Leonard & M. J. Duncan 1990; M. Kounkel et al. 2022; M. Fajrin et al. 2025).

Next Steps. Although the CDDS compilation is extensive, additional data for $\log g$, $[\text{Fe}/\text{H}]$ and $[\text{Li}/\text{H}]$, rotation measures (P_{rot} and $v \sin i$), and activity indicators (R'_{HK} , R'_{IRT} , and L_X/L_\star) would improve understanding of stellar activity evolution and the relationship between stellar activity and the presence of planetary companions and debris disks. Large surveys and focused studies are each responsible for roughly half of the ground-based spectroscopic data in the CDDS. Both approaches are needed to enhance the CDDS.

In paper II of this series, we plan to explore the extent of IR excess emission among CDDS stars. This study will yield the fraction of stars with IR excess as a function of T_{eff} and the age and activity indicators. We will also consider the association of IR excess emission with the presence of stellar and planetary companions.

Paper III will conduct a search for dynamical companions to CDDS stars within *Gaia* DR3. *Gaia* anomalous accelerations have been an important contributor to recent detections of planets and low mass stellar companions (e.g., T. Currie et al. 2023; T. L. Tobin et al. 2024). In addition to isolating accelerating stars within the CDDS, we plan to consider other options for detecting unresolved companions.

Finally, paper IV will consider approaches for deriving ages of CDDS stars and applying these results to the evolution of debris disk emission as a function of stellar age and other physical properties. This analysis will allow tests of various models for the evolution of debris as a function of stellar age (e.g., M. C. Wyatt et al. 2007; S. J. Kenyon & B. C. Bromley 2008; A. V. Krivov & M. C. Wyatt 2021; J. R. Najita et al. 2022).

Acknowledgements.

This project was supported by the NASA Exoplanets Research Program, through contract 80NSSC24K0158. We thank the reviewer for a courteous and constructive report.

This work makes use of data from the ESA missions Hipparcos and Gaia⁴. Gaia data are processed by the Gaia Data Processing and Analysis Consortium⁵ (DPAC). Funding for the DPAC has been provided by national institutions, in particular the institutions participating in the Gaia Multilateral Agreement. Herschel is an ESA space observatory with science instruments provided by European-led Principal Investigator consortia and with important participation from NASA. This research also makes use of data products from (i) the Two Micron All Sky Survey, which is a joint project of the University of Massachusetts and the Infrared Processing and Analysis Center/California Institute of Technology, funded by the National Aeronautics and Space Administration and the National Science Foundation; (ii) the Wide-field Infrared Survey Explorer, which is a joint project of the University of California, Los Angeles, and the Jet Propulsion Laboratory/California Institute of Technology, funded by the National Aeronautics and Space Administration; (iii) the Herschel Space Observatory, which is an ESA space observatory with science instruments provided by European-led Principal Investigator consortia and with important participation from NASA; (iv) AKARI, a JAXA project with the participation of ESA; (v) ISO, an ESA project with instruments funded by ESA Member States (especially the PI countries: France, Germany, the Netherlands and the United Kingdom) and with the participation of ISAS and NASA; and (vi) the Infrared Astronomical Satellite (IRAS), which was a joint project of the US, UK and the Netherlands. We also used the SIMBAD database and VizieR catalogue access tool, CDS, Strasbourg, France (DOI : 10.26093/cds/vizie; F. Ochsenbein et al. 2000); the NASA/IPAC Infrared Science Archive, which is funded by the National Aero-

navics and Space Administration and operated by the California Institute of Technology; the Washington Double Star Catalog maintained at the U.S. Naval Observatory; the NASA *Exoplanet Archive*, which is operated by the California Institute of Technology, under contract with the National Aeronautics and Space Administration under the Exoplanet Exploration Program; and the WEBDA database, operated at the Department of Theoretical Physics and Astrophysics of the Masaryk University. The Pan-STARRS1 Surveys (PS1) and the PS1 public science archive have been made possible through contributions by the Institute for Astronomy, the University of Hawaii, the Pan-STARRS Project Office, the Max-Planck Society and its participating institutes, the Max Planck Institute for Astronomy, Heidelberg and the Max Planck Institute for Extraterrestrial Physics, Garching, The Johns Hopkins University, Durham University, the University of Edinburgh, the Queen's University Belfast, the Harvard-Smithsonian Center for Astrophysics, the Las Cumbres Observatory Global Telescope Network Incorporated, the National Central University of Taiwan, the Space Telescope Science Institute, the National Aeronautics and Space Administration under Grant No. NNX08AR22G issued through the Planetary Science Division of the NASA Science Mission Directorate, the National Science Foundation Grant No. AST-1238877, the University of Maryland, Eotvos Lorand University (ELTE), the Los Alamos National Laboratory, and the Gordon and Betty Moore Foundation. The national facility capability for SkyMapper has been funded through ARC LIEF grant LE130100104 from the Australian Research Council, awarded to the University of Sydney, the Australian National University, Swinburne University of Technology, the University of Queensland, the University of Western Australia, the University of Melbourne, Curtin University of Technology, Monash University and the Australian Astronomical Observatory. SkyMapper is owned and operated by The Australian National University's Research School of Astronomy and Astrophysics. The survey data were processed and provided by the SkyMapper Team at ANU. The SkyMapper node of the All-Sky Virtual Observatory (ASVO) is hosted at the National Computational Infrastructure (NCI). Development and support of the SkyMapper node of the ASVO has been funded in part by Astronomy Australia Limited (AAL) and the Australian Government through the Commonwealth's Education Investment Fund (EIF) and National Collaborative Research Infrastructure Strategy (NCRIS), particularly the National eResearch Collaboration Tools and Resources (NeCTAR) and the Australian National Data Service Projects (ANDS).

⁴ <https://www.cosmos.esa.int/gaia>

⁵ <https://www.cosmos.esa.int/web/gaia/dpac/consortium>

Data Availability. All of the data discussed in this paper are publicly available from the websites noted above and within the literature quoted throughout. We

plan to publish the full compilation in parallel with Paper IV of this series.

APPENDIX

While building this compilation, we encountered several confusing source identifications and derived distances for stars with uncertain or unknown parallaxes. For investigations of stellar or planetary companions, we needed to separate physically associated companions from those along the same line-of-sight. For all CDDS stars, we used *Gaia* sky positions, parallaxes, and proper motions to distinguish physical pairs from chance alignments. By gathering sources that lie at a parallax within $3\text{-}\sigma$ of each star and comparing inferred physical separation and relative speed, we identified plausible common-proper motion companions of the CDDS stars. Table 8 lists some of these companions, chosen as a result of their low relative velocity (< 2 km/s at the physical distance inferred from the CDDS stars' parallax), their small physical separation ($< 1,000$ au), their large distance from a known star cluster, and their failure to appear as a known companion in the double star catalogs considered here.

Stars with special circumstances. Some CDDS stars have no measured parallax. Several others have an interesting history in the literature. Here we outline approaches to derive distances and provide summaries for mis-classified stars.

EN Cha. Within the uncertainties, EN Cha has the same radial velocity and proper motion as other members of the η Cha cluster, but it has no distance. Adopting a distance $d = 98.2$ pc (E. L. Hunt & S. Reffert 2023, 2024) yields a similar L_\star as other M4–M5 stars in the group.

HIP 59154. Far away from any association or cluster, this star has an appropriate $L_X/L_\star \sim 5 \times 10^{-4}$ for a moderately young star on the main sequence. The adopted distance is then 27 pc.

2MASS J06434532-6424396. The $\log g$ and $v \sin i$ suggest a star contracting to the main sequence. Adopting $M_\star = 0.32 M_\odot$ for $T_{\text{eff}} = 3350$ K implies $d = 37.7$ pc.

2MASS J07453282-3751230. The T_{eff} , $\log g$, $v \sin i$, and [Li/H] suggest an old M3–M4 star on the main sequence. Adopting $M_\star = 0.32 M_\odot$ for $T_{\text{eff}} = 3350$ K implies $d = 139$ pc.

Pleiades. The B star Cl* Melotte 22 HII 1432 (η Tau) is assigned to the Pleiades, but has large errors in parallax and proper motion. The nominal parallax places it on the near side of the cluster. Within the large uncertainties, the M star Cl* Melotte 22 HCG 0277 (QV

Tau) has similar proper motion and radial velocity to η Tau; with no distance estimate, we use $\log g$, T_{eff} , and a mass estimate ($0.27 M_\odot$) to derive L_\star and a distance of 95 pc. *Gaia* studies place the star in the field, which agrees with our distance estimate.

Praesepe. Five stars assigned to Praesepe on dynamical grounds have no distance measurement (Cl* NGC 2632 KW 236, BD+20 2162, Cl* NGC 2632 WJJP 607, BD+19 2076, and Cl* NGC 2632 JC 243; see §5). Adopting the median distance of Praesepe stars, $d = 183.43$ pc, places all five on or close to the 600–700 Myr PARSEC isochrones appropriate for Praesepe (S. Gosage et al. 2018; D. Bossini et al. 2019; W. S. Dias et al. 2021).

Sco-Cen Association. Several stars (CD–22° 11432, HD 128242, 2MASS J15571674-2529192, 2MASS J15572986-2258438, 2MASS J16080157-1927579, 2MASS J16082387-1935518, 2MASS J16082751-1949047, 2MASS J16084309-1900519, and V1154 Sco) have appropriate radial velocities and proper motions for LCC, UCL, or USco, but have no distance estimate. They also have some combination of $\log g$, P_{rot} , and L_X/L_\star indicative of very young stars. Adopting a median distance to LCC, UCL, or USco places these stars on a 10–20 Myr PARSEC isochrone. As a check, we adopt a mass appropriate for the spectral type and derive L_\star (and then a distance similar to the median distance) from $\log g$ and T_{eff} . For ScoPMS 13, ScoPMS 23, and ScoPMS 31 (no distance estimates and large proper motion errors), their $\log g$, P_{rot} , and L_X/L_\star are consistent with other USco stars that have ages of ~ 10 Myr. Adopting the 10 Myr age implies $d = 96$ pc for ScoPMS 13 and ScoPMS 31 and $d = 107$ pc for ScoPMS 23. These stars lie in the foreground of most association stars.

TYC 654-1274-1 (also known as 1E0307.4+1424, 1E0307.5+1424, and 2E0307.4+1424). In SIMBAD, 1E0307.4+1424 has J2000.0 coordinates shifted by $\delta\text{RA} = 1.64$ sec and $\delta\text{Dec} = 15.95$ arcsec relative to the *Gaia* coordinates for TYC 654-1274-1 (which are almost identical to the 2MASS and WISE coordinates). However, they are the same star; on the Digitized Sky Survey, PanSTARRS DR1, 2MASS, and allWISE available with Aladin Lite, there is no star at the coordinates listed for 1E0307.4+1424, but there is clearly a star at the coordi-

Table 8. Binary and triple star candidates from Gaia astrometry

SIMBAD main_id	Gaia DR3 source_id	G-band (mag)	BP-RP (mag)	companion source_id	G-band (mag)	BP-RP (mag)	sep. (au)	vel. (km/s)
HD 109536	6146899611411058304	5.067	0.313	6146899611411103360	13.841	2.786	15.7	0.62
G 54-20	625740966539620096	13.479	2.506	625740966539596032	15.447	2.987	5.2	1.48
* phi For	4967177781457918976	5.112	0.109	4967153630858709120	7.465	0.683	391.1	0.21
HD 20759	4854737122493173760	7.595	0.628	4854737122493187200	14.469	nan	3.5	1.56
HD 37548	2971060398858087168	7.451	0.764	2971060330138611968	15.234	2.855	44.0	0.17
HD 40540	2889357751382815872	7.495	0.379	2889357751382248704	15.269	2.944	40.6	0.52
HD 46190	5478200622494775552	6.599	0.118	5478200588135044096	14.849	2.776	82.2	0.11
HD 71722	5321368860896990720	6.044	0.080	5321369406350033664	11.076	1.366	268.9	0.12
HD 71722	5321368860896990720	6.044	0.080	5321368860896992000	15.644	2.437	9.9	1.06
HD 77052	686698960631875968	8.708	0.814	686698891912397696	14.130	2.545	55.4	0.23
HD 101259	3491774880840574464	6.167	1.040	3491774880840574208	15.395	1.974	8.0	0.81
HD 109391	3703459387769393920	8.485	0.601	3703459387768058624	15.962	nan	3.5	1.30
HD 113319	1467164096785657088	7.367	0.820	1467167257881586816	15.657	3.558	175.1	0.13
HD 150697	4326683743996162432	7.933	0.690	4326683743996161408	16.884	3.242	21.3	0.31
* b Oph	4111251723554095104	4.105	0.394	4111251689120620160	14.566	3.122	18.1	1.92
HD 220150	1910520582770593792	8.231	0.548	1910520544116627840	13.652	1.674	4.0	0.81
HD 33283	2955981936912654592	7.912	0.767	2955981696394487296	16.972	3.194	55.7	0.33
HD 107148	3693358861640279296	7.864	0.827	3693358792919145600	17.413	0.649	35.0	1.07
HD 188015	2028419118720795392	8.078	0.848	2028419118720966912	15.434	3.084	13.0	0.75
BD-20 638	5101544806816778752	10.194	0.815	5101544802521433216	17.951	4.091	40.0	0.20
HD 279788	179245207355823232	10.482	1.083	179244760679229184	13.484	2.098	93.5	0.33
HD 285840	3410633602770942464	10.554	1.054	3410633980728058624	13.448	2.242	154.2	1.42
BD+08 742	329261710558895104	10.772	0.984	3292617041166009216	14.703	2.741	15.7	0.18
HD 245567	3341551046679446016	9.386	0.963	3341556922194703232	13.726	2.576	49.8	1.22
HD 90712	5447414606155987200	7.375	0.758	5447414606155987840	11.970	2.294	33.3	0.47
HD 157664	1638293082964887424	7.847	0.691	1638293082964794880	13.831	2.317	16.5	1.80
HD 170778	2112083741571086592	7.344	0.762	2112083741570227072	12.555	2.765	20.2	1.29
HD 193017	4219087666404378624	7.148	0.705	4219087700764115840	16.643	3.911	53.6	0.35
BD+22 4792	2839360861722307200	10.009	0.738	2839360861721116416	13.675	nan	1.4	1.31
HD 104731	6148648281576023424	5.033	0.574	6148648281576023552	10.537	nan	2.2	1.24
HD 202884	1743504800870418432	7.149	0.655	1743504525992505600	15.086	2.953	89.5	0.24
HD 40335	3315163867123687808	6.890	0.298	3315169399041560832	5.869	0.317	177.8	0.84
HD 45557	5481786576589734400	5.773	-0.004	5481833477632605056	14.185	2.382	33.2	0.34
HD 65517	5194852249768916224	7.482	0.304	5194852249769630976	12.102	nan	2.2	0.63
HD 114905	1522893908790675456	6.721	0.630	1522893908790675584	12.606	1.941	6.6	0.48
HD 73487	664329465285221248	9.003	1.073	664329465285129856	16.473	2.331	32.1	0.07
HD 146569	6037205940527834624	8.243	0.165	6037206692130852352	17.854	3.019	30.0	0.55
* eta Aps	5772879737424829184	4.835	0.325	5772878981507554048	15.219	-0.136	24.9	0.16
HD 102956	845335158256083584	7.619	1.097	845335158256818176	15.319	2.543	31.9	0.39
HD 108863	3952692457305436800	7.467	1.147	3952693281939158144	10.004	0.725	115.4	0.17
BD+26 2339	4008339427981993088	9.927	0.592	4008339359262516224	14.000	1.513	13.1	0.18
BD+28 2091	4009747107807825664	9.933	0.658	4009747146463096192	15.748	2.186	22.8	0.58
HD 105898	4003139184658921472	7.264	1.059	4003139180364904064	17.331	2.091	13.1	0.13
HD 107086	4008609736043668864	7.454	0.589	4008609731748472192	17.080	3.368	19.0	0.58
HD 108956	3959079382912168320	6.979	0.778	3959079382911362944	14.099	2.260	7.0	1.02

nates for TYC 654-1274-1. Curiously, there is no X-ray source coincident with either coordinate in ROSAT data.

TIC 454363834 (also known as *CHX 18N*, *CHX 18*, and *RXJ1111.7-7620*). Like TYC 654-1274-1, this K5 star has two entries in SIMBAD, one for CHX 18N (TIC 454363834) and another for CHX 18 (RXJ1111.7-7620), but the information in the two entries corresponds to the same star. The coordinates for CHX 18 are shifted by $\delta\text{RA} = 3.46$ sec and $\delta\text{Dec} = +20.9$ arcsec relative to CHX 18N. Although this field is too far south for PAN-

STARRS, CHX 18N is visible on Digitized Sky Survey, 2MASS, and allWISE images on Aladin Lite; CHX 18 is not visible. With ROSAT and eROSITA, there is an obvious X-ray source associated with CHX 18N and none associated with the position of CHX 18.

V1299 Tau. The negligible reddening, $\log g = 4.273$, and $T_{\text{eff}} = 5775$ K place the star on a PARSEC isochrone for an age of ~ 15 Myr and yields $L_{\star} \approx 2 L_{\odot}$ and $d = 103.5$ pc. Younger isochrones are precluded. Stellar activity diagnostics, $v \sin i \approx 70$ km s $^{-1}$ and L_X/L_{\star}

$\sim 10^{-3}$, are consistent with a young age. Although the star might be in the greater Taurus region (A. L. Kraus et al. 2017), we assign it to the field.

Candidate Common Proper Motion Companions. To construct a set of candidate common proper motion stars, we consider possible companion stars that satisfy three constraints: (i) the projected separation s at the distance of the nominal CDDS primary star is $s \leq s_{max} = 1000$ au, (ii) the parallax difference between the candidate companion and the primary is zero within the $3\text{-}\sigma$ errors, and (iii) the difference in relative tangential velocities is $\delta v \leq 2$ km s $^{-1}$, where the tangential velocity of each component is $v = 4.74 \mu/\pi$ (units of km s $^{-1}$, mas yr $^{-1}$, and mas, respectively) and $\delta v = |v_1 - v_2|$. As a final cut, we eliminate stars where the parallax error is too large to make a reliable estimate of the projected separation; typically, this constraint precludes companions to stars in the vicinity of associations or clusters with distances larger than ~ 300 pc. Once we have a final set of possible common proper motion companions, we remove those previously reported in the literature (see Table 2).

For all of the candidates, uncertainties in the parallax preclude an accurate assessment of the 3D separation. Typical errors in the relative positions are $\lesssim 0.1$ arcsec, which corresponds to ~ 5 au at the 50 pc median distance of CDDS stars. Parallax uncertainties are $\sim 0.2\%$ (0.5%) for primary (secondary) stars; at 50 pc, the line-of-sight separation then has a minimum uncertainty of a few thousand au. For orbits randomly oriented in space, large line-of-sight separations and small projected separations are rare. Thus, we only consider the projected separation.

Table 8 lists the candidates. The first four columns list the nominal ID of the CDDS primary along with its *Gaia* ID, G-band magnitude, and BP–RP color. The next three columns lists the *Gaia* ID, G, and BP–RP for the proposed companion. The table concludes with the projected separation in au and velocity difference in km s $^{-1}$. The candidates fall into three broad classes. Some have no entries in SIMBAD; others have an entry with only a *Gaia* DR3 identification, the G-magnitude, and sometimes 2MASS JHK $_s$ data. Several have information on spectral types that we discuss below. All of the candidates are consistent with main sequence or white dwarf companions to brighter primary stars. Additional information, such as supplementary epochs of imaging, BVI $_C$ photometry, and optical or infrared spectroscopy would test the possibility that these companions are physical pairs.

η *Apodis*. The possible companion to this A-type star is a DA white dwarf (F. M. Jiménez-Esteban et al. 2023),

one of many discovered with *Gaia*. The stars are not obviously known as a binary pair.

b Ophiuchi. With a magnitude difference $\Delta G \approx 10.4$, this pair consists of an A-type primary and an M-type secondary. The magnitude difference implies a middle M spectral type for the fainter star. Infrared colors (2MASS J17262200-2410487) and G–K paint an inconsistent picture: G–K and H–K suggest a late type star, while J–H is more consistent with an early K star.

HD 33283. Although the companion is included in J. González-Payo et al. (2024), it merits inclusion due to uncertainties in the quoted separation. The primary HD 33283 A is a solar-type star with $d \approx 90$ pc. The secondary HD 33283 B is listed in SIMBAD and has the G–K and J–K colors of a middle M-type star. J. González-Payo et al. (2024) show a schematic with a planet orbiting A inside 1 au and the companion star beyond 10^4 au. With a projected separation of 50–60 au, most of the quoted separation is due to differences in a parallax which has large uncertainties of ~ 5000 au. Optical or infrared spectra would establish the spectral type of component B; IR imaging over several years would constrain the orbit.

HD 77052. This G-type star has companion with a magnitude difference $\Delta G \approx 5.8$. For the M. J. Pecaut & E. E. Mamajek (2013) main sequence locus, the G-magnitude difference implies a spectral type, $\approx M3$ V, that is consistent with the spectral type of M2.5 V listed in SIMBAD. The companion is also listed as TIC 203226434.

HD 104731. The middle F primary is roughly 5.5 mag brighter than the potential companion at G, which implies a spectral type of M0–M1 for a main sequence companion. The lack of BP–RP precludes a consistency check. Aside from listings in catalogs of nearby stars (Gaia Collaboration et al. 2021a; A. Golovin et al. 2023), the companion appears in SIMBAD as HD 104731 B without any additional information

HD 107148. The early G-type primary is $\sim 10\%$ more luminous than the Sun and approximately 9.5 mag brighter than the white dwarf companion at G (F. M. Jiménez-Esteban et al. 2023). Although SIMBAD does not list the white dwarf as a companion, J. González-Payo et al. (2024) place the star at a separation of $\sim 10^4$ au and note the two planets within 1 au of the primary. The projected separation is only ~ 35 au; the line-of-sight separation has an uncertainty of $\sim 2 \times 10^4$ au.

HD 202884. The companion to this F5 star has an M4 spectral type in SIMBAD (TIC 262277113). The G-magnitude difference implies a spectral type of M3–M5 (M. J. Pecaut & E. E. Mamajek 2013). 2MASS data quoted in SIMBAD (2MASS J21184222+085645, TIC

262277113) are consistent with an M4 main sequence star.

REFERENCES

- Abad, C., & Vicente, B. 1999, *A&AS*, 136, 307, doi: [10.1051/aas:1999216](https://doi.org/10.1051/aas:1999216)
- Abdurro'uf, Accetta, K., Aerts, C., et al. 2022, *ApJS*, 259, 35, doi: [10.3847/1538-4365/ac4414](https://doi.org/10.3847/1538-4365/ac4414)
- Abt, H. A. 2004, *ApJS*, 155, 175, doi: [10.1086/423803](https://doi.org/10.1086/423803)
- Abt, H. A., Levato, H., & Grosso, M. 2002, *ApJ*, 573, 359, doi: [10.1086/340590](https://doi.org/10.1086/340590)
- Abt, H. A., & Morrell, N. I. 1995, *ApJS*, 99, 135, doi: [10.1086/192182](https://doi.org/10.1086/192182)
- Aguilera-Gómez, C., Ramírez, I., & Chanamé, J. 2018, *A&A*, 614, A55, doi: [10.1051/0004-6361/201732209](https://doi.org/10.1051/0004-6361/201732209)
- Akeson, R., Beichman, C., Kervella, P., Fomalont, E., & Benedict, G. F. 2021, *AJ*, 162, 14, doi: [10.3847/1538-3881/abfaff](https://doi.org/10.3847/1538-3881/abfaff)
- Alfonso, J., & García-Varela, A. 2023, *A&A*, 677, A163, doi: [10.1051/0004-6361/202346569](https://doi.org/10.1051/0004-6361/202346569)
- Alonso, A., Arribas, S., & Martínez-Roger, C. 1999, *A&AS*, 140, 261, doi: [10.1051/aas:1999521](https://doi.org/10.1051/aas:1999521)
- Alonso-Floriano, F. J., Morales, J. C., Caballero, J. A., et al. 2015, *A&A*, 577, A128, doi: [10.1051/0004-6361/201525803](https://doi.org/10.1051/0004-6361/201525803)
- Andrae, R., Rix, H.-W., & Chandra, V. 2023a, *ApJS*, 267, 8, doi: [10.3847/1538-4365/acd53e](https://doi.org/10.3847/1538-4365/acd53e)
- Andrae, R., Fouesneau, M., Sordo, R., et al. 2023b, *A&A*, 674, A27, doi: [10.1051/0004-6361/202243462](https://doi.org/10.1051/0004-6361/202243462)
- Andretta, V., Busà, I., Gomez, M. T., & Terranegra, L. 2005, *A&A*, 430, 669, doi: [10.1051/0004-6361:20041745](https://doi.org/10.1051/0004-6361:20041745)
- Anthoz, F., Ménéard, F., Pinte, C., et al. 2015, *A&A*, 574, A41, doi: [10.1051/0004-6361/201424520](https://doi.org/10.1051/0004-6361/201424520)
- Argiroffi, C., Caramazza, M., Micela, G., et al. 2016, *A&A*, 589, A113, doi: [10.1051/0004-6361/201526539](https://doi.org/10.1051/0004-6361/201526539)
- Argiroffi, C., Favata, F., Flaccomio, E., et al. 2006, *A&A*, 459, 199, doi: [10.1051/0004-6361:20065674](https://doi.org/10.1051/0004-6361:20065674)
- Aschenbach, B., Bräuninger, H., Briel, U., et al. 1981, *SSRv*, 30, 569, doi: [10.1007/BF01246075](https://doi.org/10.1007/BF01246075)
- Asplund, M., Grevesse, N., Sauval, A. J., & Scott, P. 2009, *ARA&A*, 47, 481, doi: [10.1146/annurev.astro.46.060407.145222](https://doi.org/10.1146/annurev.astro.46.060407.145222)
- Astudillo-Defru, N., Delfosse, X., Bonfils, X., et al. 2017, *A&A*, 600, A13, doi: [10.1051/0004-6361/201527078](https://doi.org/10.1051/0004-6361/201527078)
- Aumann, H. H., Gillett, F. C., Beichman, C. A., et al. 1984, *ApJL*, 278, L23, doi: [10.1086/184214](https://doi.org/10.1086/184214)
- Bailer-Jones, C. A. L., Rybizki, J., Fouesneau, M., Demleitner, M., & Andrae, R. 2021, *AJ*, 161, 147, doi: [10.3847/1538-3881/abd806](https://doi.org/10.3847/1538-3881/abd806)
- Bailer-Jones, C. A. L., Andrae, R., Arcay, B., et al. 2013, *A&A*, 559, A74, doi: [10.1051/0004-6361/201322344](https://doi.org/10.1051/0004-6361/201322344)
- Bailey, J. I., Mateo, M., White, R. J., Shectman, S. A., & Crane, J. D. 2018, *MNRAS*, 475, 1609, doi: [10.1093/mnras/stx3266](https://doi.org/10.1093/mnras/stx3266)
- Balog, Z., Kiss, L. L., Vinkó, J., et al. 2009, *ApJ*, 698, 1989, doi: [10.1088/0004-637X/698/2/1989](https://doi.org/10.1088/0004-637X/698/2/1989)
- Barenfeld, S. A., Carpenter, J. M., Ricci, L., & Isella, A. 2016, *ApJ*, 827, 142, doi: [10.3847/0004-637X/827/2/142](https://doi.org/10.3847/0004-637X/827/2/142)
- Baron, F., Monnier, J. D., Pedretti, E., et al. 2012, *ApJ*, 752, 20, doi: [10.1088/0004-637X/752/1/20](https://doi.org/10.1088/0004-637X/752/1/20)
- Barrado y Navascués, D. 1998, *A&A*, 339, 831, doi: [10.48550/arXiv.astro-ph/9905243](https://doi.org/10.48550/arXiv.astro-ph/9905243)
- Barrado Y Navascués, D. 2004, in *ESA Special Publication*, Vol. 538, *Stellar Structure and Habitable Planet Finding*, ed. F. Favata, S. Aigrain, & A. Wilson (ESA Publications Division), 269–271
- Barrado y Navascués, D., Bouvier, J., Stauffer, J. R., Lodieu, N., & McCaughrean, M. J. 2002, *A&A*, 395, 813, doi: [10.1051/0004-6361:20021262](https://doi.org/10.1051/0004-6361:20021262)
- Barrado y Navascués, D., Stauffer, J. R., & Jayawardhana, R. 2004, *ApJ*, 614, 386, doi: [10.1086/423485](https://doi.org/10.1086/423485)
- Barrado y Navascués, D., Stauffer, J. R., & Patten, B. M. 1999, *ApJL*, 522, L53, doi: [10.1086/312212](https://doi.org/10.1086/312212)
- Beichman, C. A., Bryden, G., Rieke, G. H., et al. 2005, *ApJ*, 622, 1160, doi: [10.1086/428115](https://doi.org/10.1086/428115)
- Beichman, C. A., Tanner, A., Bryden, G., et al. 2006, *ApJ*, 639, 1166, doi: [10.1086/499424](https://doi.org/10.1086/499424)
- Beichmann, C. A. 1985, *Infrared Astronomical Satellite (IRAS) catalogs and atlases. Explanatory supplement (Jet Propulsion Laboratory, Pasadena, CA USA)*
- Bell, C. P. M., Mamajek, E. E., & Naylor, T. 2015, *MNRAS*, 454, 593, doi: [10.1093/mnras/stv1981](https://doi.org/10.1093/mnras/stv1981)
- Bensby, T., & Lind, K. 2018, *A&A*, 615, A151, doi: [10.1051/0004-6361/201833118](https://doi.org/10.1051/0004-6361/201833118)
- Berdugina, S. V., Jankov, S., Ilyin, I., Tuominen, I., & Fekel, F. C. 1998, *A&A*, 334, 863
- Bessel, M. S. 1990, *A&AS*, 83, 357
- Bessell, M., & Murphy, S. 2012, *PASP*, 124, 140, doi: [10.1086/664083](https://doi.org/10.1086/664083)
- Binks, A. S., Jeffries, R. D., Jackson, R. J., et al. 2021, *MNRAS*, 505, 1280, doi: [10.1093/mnras/stab1351](https://doi.org/10.1093/mnras/stab1351)
- Blaauw, A. 1964, *ARA&A*, 2, 213, doi: [10.1146/annurev.aa.02.090164.001241](https://doi.org/10.1146/annurev.aa.02.090164.001241)

- Blazère, A., Petit, P., Lignières, F., et al. 2015, in IAU Symposium, Vol. 305, Polarimetry, ed. K. N. Nagendra, S. Bagnulo, R. Centeno, & M. Jesús Martínez González, 67–72, doi: [10.1017/S1743921315004536](https://doi.org/10.1017/S1743921315004536)
- Bobylev, V. V., & Bajkova, A. T. 2016, *Astronomy Letters*, 42, 90, doi: [10.1134/S1063773716020018](https://doi.org/10.1134/S1063773716020018)
- Boesgaard, A. M., Armengaud, E., & King, J. R. 2003, *ApJ*, 583, 955, doi: [10.1086/345410](https://doi.org/10.1086/345410)
- Boesgaard, A. M., Deliyannis, C. P., Lum, M. G., & Chontos, A. 2022, *ApJ*, 941, 21, doi: [10.3847/1538-4357/ac9625](https://doi.org/10.3847/1538-4357/ac9625)
- Boller, T., Freyberg, M. J., Trümper, J., et al. 2016, *A&A*, 588, A103, doi: [10.1051/0004-6361/201525648](https://doi.org/10.1051/0004-6361/201525648)
- Bonsor, A., Kennedy, G. M., Wyatt, M. C., Johnson, J. A., & Sibthorpe, B. 2014, *MNRAS*, 437, 3288, doi: [10.1093/mnras/stt2128](https://doi.org/10.1093/mnras/stt2128)
- Booth, M., Schulz, M., Krivov, A. V., et al. 2021, *MNRAS*, 500, 1604, doi: [10.1093/mnras/staa3362](https://doi.org/10.1093/mnras/staa3362)
- Boro Saikia, S., Marvin, C. J., Jeffers, S. V., et al. 2018, *A&A*, 616, A108, doi: [10.1051/0004-6361/201629518](https://doi.org/10.1051/0004-6361/201629518)
- Borsenberger, J., de Batz, B., Derriere, S., et al. 2006, in *Visions for Infrared Astronomy, Instrumentation, Measurement, Metrology*, ed. V. Coudé du Foresto, D. Rouan, & G. Rousset, 135–138
- Bossini, D., Vallenari, A., Bragaglia, A., et al. 2019, *A&A*, 623, A108, doi: [10.1051/0004-6361/201834693](https://doi.org/10.1051/0004-6361/201834693)
- Bouchaud, K., Domiciano de Souza, A., Rieutord, M., Reese, D. R., & Kervella, P. 2020, *A&A*, 633, A78, doi: [10.1051/0004-6361/201936830](https://doi.org/10.1051/0004-6361/201936830)
- Bouma, L. G., Curtis, J. L., Hartman, J. D., Winn, J. N., & Bakos, G. Á. 2021, *AJ*, 162, 197, doi: [10.3847/1538-3881/ac18cd](https://doi.org/10.3847/1538-3881/ac18cd)
- Bouvier, J., Barrado, D., Moraux, E., et al. 2018, *A&A*, 613, A63, doi: [10.1051/0004-6361/201731881](https://doi.org/10.1051/0004-6361/201731881)
- Bovy, J., Hogg, D. W., & Roweis, S. T. 2009, *ApJ*, 700, 1794, doi: [10.1088/0004-637X/700/2/1794](https://doi.org/10.1088/0004-637X/700/2/1794)
- Boyle, A. W., & Bouma, L. G. 2023, *AJ*, 166, 14, doi: [10.3847/1538-3881/acd3e8](https://doi.org/10.3847/1538-3881/acd3e8)
- Braithwaite, J., & Cantiello, M. 2013, *MNRAS*, 428, 2789, doi: [10.1093/mnras/sts109](https://doi.org/10.1093/mnras/sts109)
- Brandner, W., Calissendorff, P., & Kopytova, T. 2023a, *AJ*, 165, 108, doi: [10.3847/1538-3881/acb208](https://doi.org/10.3847/1538-3881/acb208)
- Brandner, W., Calissendorff, P., & Kopytova, T. 2023b, *A&A*, 677, A162, doi: [10.1051/0004-6361/202346790](https://doi.org/10.1051/0004-6361/202346790)
- Brandner, W., Calissendorff, P., & Kopytova, T. 2023c, *MNRAS*, 518, 662, doi: [10.1093/mnras/stac2247](https://doi.org/10.1093/mnras/stac2247)
- Brandt, T. D., & Huang, C. X. 2015, *ApJ*, 807, 58, doi: [10.1088/0004-637X/807/1/58](https://doi.org/10.1088/0004-637X/807/1/58)
- Briceño, C., Calvet, N., Hernández, J., et al. 2019, *AJ*, 157, 85, doi: [10.3847/1538-3881/aaf79b](https://doi.org/10.3847/1538-3881/aaf79b)
- Briceño-Morales, G., & Chanamé, J. 2023, *MNRAS*, 522, 1288, doi: [10.1093/mnras/stad608](https://doi.org/10.1093/mnras/stad608)
- Briggs, K. R., & Pye, J. P. 2003, *MNRAS*, 345, 714, doi: [10.1046/j.1365-8711.2003.06991.x](https://doi.org/10.1046/j.1365-8711.2003.06991.x)
- Brown, E. L., Jeffers, S. V., Marsden, S. C., et al. 2022, *MNRAS*, 514, 4300, doi: [10.1093/mnras/stac1291](https://doi.org/10.1093/mnras/stac1291)
- Bryden, G., Beichman, C. A., Trilling, D. E., et al. 2006, *ApJ*, 636, 1098, doi: [10.1086/498093](https://doi.org/10.1086/498093)
- Bryden, G., Beichman, C. A., Carpenter, J. M., et al. 2009, *ApJ*, 705, 1226, doi: [10.1088/0004-637X/705/2/1226](https://doi.org/10.1088/0004-637X/705/2/1226)
- Buder, S., Sharma, S., Kos, J., et al. 2021, *MNRAS*, 506, 150, doi: [10.1093/mnras/stab1242](https://doi.org/10.1093/mnras/stab1242)
- Buder, S., Lind, K., Ness, M. K., et al. 2022, *MNRAS*, 510, 2407, doi: [10.1093/mnras/stab3504](https://doi.org/10.1093/mnras/stab3504)
- Busà, I., Aznar Cuadrado, R., Terranegra, L., Andretta, V., & Gomez, M. T. 2007, *A&A*, 466, 1089, doi: [10.1051/0004-6361:20065588](https://doi.org/10.1051/0004-6361:20065588)
- Cakirli, O., Ibanoglu, C., Frasca, A., & Catalano, S. 2003, *A&A*, 400, 257, doi: [10.1051/0004-6361:20021885](https://doi.org/10.1051/0004-6361:20021885)
- Calvet, N., & Gullbring, E. 1998, *ApJ*, 509, 802, doi: [10.1086/306527](https://doi.org/10.1086/306527)
- Cameron, A. C., Hearnshaw, J. B., & Austin, R. R. D. 1981, *MNRAS*, 197, 769, doi: [10.1093/mnras/197.3.769](https://doi.org/10.1093/mnras/197.3.769)
- Campelo, J. P. S., Canto Martins, B. L., Leão, I. C., et al. 2025, *ApJ*, 989, 177, doi: [10.3847/1538-4357/ade2f](https://doi.org/10.3847/1538-4357/ade2f)
- Cannon, A. J., & Pickering, E. C. 1924, *Henry Draper (HD) catalog and HD extension (Harvard College Observatory, Cambridge, MA USA)*
- Cantat-Gaudin, T., & Anders, F. 2020, *A&A*, 633, A99, doi: [10.1051/0004-6361/201936691](https://doi.org/10.1051/0004-6361/201936691)
- Cantat-Gaudin, T., & Brandt, T. D. 2021, *A&A*, 649, A124, doi: [10.1051/0004-6361/202140807](https://doi.org/10.1051/0004-6361/202140807)
- Cantat-Gaudin, T., Jordi, C., Vallenari, A., et al. 2018, *A&A*, 618, A93, doi: [10.1051/0004-6361/201833476](https://doi.org/10.1051/0004-6361/201833476)
- Cantat-Gaudin, T., Anders, F., Castro-Ginard, A., et al. 2020, *A&A*, 640, A1, doi: [10.1051/0004-6361/202038192](https://doi.org/10.1051/0004-6361/202038192)
- Canto Martins, B. L., Gomes, R. L., Messias, Y. S., et al. 2020, *ApJS*, 250, 20, doi: [10.3847/1538-4365/aba73f](https://doi.org/10.3847/1538-4365/aba73f)
- Cao, Z., Jiang, B., Wang, S., & Li, J. 2024, *arXiv e-prints*, arXiv:2410.02731, doi: [10.48550/arXiv.2410.02731](https://doi.org/10.48550/arXiv.2410.02731)
- Cao, Z., Jiang, B., Zhao, H., & Sun, M. 2023, *ApJ*, 945, 132, doi: [10.3847/1538-4357/acbbc7](https://doi.org/10.3847/1538-4357/acbbc7)
- Capak, P. 2019, *Spitzer Enhanced Imaging Products (SEIP) Source List*, NASA IPAC DataSet, IRSA3 doi: [10.26131/IRSA3](https://doi.org/10.26131/IRSA3)
- Cardelli, J. A., Clayton, G. C., & Mathis, J. S. 1989, *ApJ*, 345, 245, doi: [10.1086/167900](https://doi.org/10.1086/167900)
- Cargile, P. A., James, D. J., Pepper, J., et al. 2014, *ApJ*, 782, 29, doi: [10.1088/0004-637X/782/1/29](https://doi.org/10.1088/0004-637X/782/1/29)

- Cargile, P. A., James, D. J., & Platais, I. 2009, *AJ*, 137, 3230, doi: [10.1088/0004-6256/137/2/3230](https://doi.org/10.1088/0004-6256/137/2/3230)
- Carlos, M., Meléndez, J., Spina, L., et al. 2019, *MNRAS*, 485, 4052, doi: [10.1093/mnras/stz681](https://doi.org/10.1093/mnras/stz681)
- Carlsson, M., De Pontieu, B., & Hansteen, V. H. 2019, *ARA&A*, 57, 189, doi: [10.1146/annurev-astro-081817-052044](https://doi.org/10.1146/annurev-astro-081817-052044)
- Carpenter, J. M., Esplin, T. L., Luhman, K. L., Mamajek, E. E., & Andrews, S. M. 2025, *ApJ*, 978, 117, doi: [10.3847/1538-4357/ad8ebc](https://doi.org/10.3847/1538-4357/ad8ebc)
- Carpenter, J. M., Mamajek, E. E., Hillenbrand, L. A., & Meyer, M. R. 2009, *ApJ*, 705, 1646, doi: [10.1088/0004-637X/705/2/1646](https://doi.org/10.1088/0004-637X/705/2/1646)
- Carpenter, J. M., Ricci, L., & Isella, A. 2014, *ApJ*, 787, 42, doi: [10.1088/0004-637X/787/1/42](https://doi.org/10.1088/0004-637X/787/1/42)
- Carpenter, J. M., Bouwman, J., Silverstone, M. D., et al. 2008, *ApJS*, 179, 423, doi: [10.1086/592274](https://doi.org/10.1086/592274)
- Cayrel, R., de Strobel, G. C., Campbell, B., et al. 1983, *A&A*, 123, 89
- Chambers, K. C., Magnier, E. A., Metcalfe, N., et al. 2016, arXiv e-prints, arXiv:1612.05560, doi: [10.48550/arXiv.1612.05560](https://doi.org/10.48550/arXiv.1612.05560)
- Chapman, N. L., Mundy, L. G., Lai, S.-P., & Evans, Neal J., I. 2009, *ApJ*, 690, 496, doi: [10.1088/0004-637X/690/1/496](https://doi.org/10.1088/0004-637X/690/1/496)
- Chavero, C., de la Reza, R., Ghezzi, L., et al. 2019, *MNRAS*, 487, 3162, doi: [10.1093/mnras/stz1496](https://doi.org/10.1093/mnras/stz1496)
- Chen, C. H., Jura, M., Gordon, K. D., & Blaylock, M. 2005a, *ApJ*, 623, 493, doi: [10.1086/428607](https://doi.org/10.1086/428607)
- Chen, C. H., Mamajek, E. E., Bitner, M. A., et al. 2011, *ApJ*, 738, 122, doi: [10.1088/0004-637X/738/2/122](https://doi.org/10.1088/0004-637X/738/2/122)
- Chen, C. H., Mittal, T., Kuchner, M., et al. 2014, *ApJS*, 211, 25, doi: [10.1088/0067-0049/211/2/25](https://doi.org/10.1088/0067-0049/211/2/25)
- Chen, C. H., Pecaut, M., Mamajek, E. E., Su, K. Y. L., & Bitner, M. 2012, *ApJ*, 756, 133, doi: [10.1088/0004-637X/756/2/133](https://doi.org/10.1088/0004-637X/756/2/133)
- Chen, C. H., Sheehan, P., Watson, D. M., Manoj, P., & Najita, J. R. 2009, *ApJ*, 701, 1367, doi: [10.1088/0004-637X/701/2/1367](https://doi.org/10.1088/0004-637X/701/2/1367)
- Chen, C. H., Su, K. Y. L., & Xu, S. 2020, *Nature Astronomy*, 4, 328, doi: [10.1038/s41550-020-1067-6](https://doi.org/10.1038/s41550-020-1067-6)
- Chen, C. H., Patten, B. M., Werner, M. W., et al. 2005b, *ApJ*, 634, 1372, doi: [10.1086/497124](https://doi.org/10.1086/497124)
- Chen, C. H., Sargent, B. A., Bohac, C., et al. 2006, *ApJS*, 166, 351, doi: [10.1086/505751](https://doi.org/10.1086/505751)
- Chen, Y., Bressan, A., Girardi, L., et al. 2015, *MNRAS*, 452, 1068, doi: [10.1093/mnras/stv1281](https://doi.org/10.1093/mnras/stv1281)
- Chen, Y., Girardi, L., Bressan, A., et al. 2014, *MNRAS*, 444, 2525, doi: [10.1093/mnras/stu1605](https://doi.org/10.1093/mnras/stu1605)
- Chmielewski, Y. 2000, *A&A*, 353, 666
- Cieza, L. A., Cochran, W. D., & Augereau, J.-C. 2008, *ApJ*, 679, 720, doi: [10.1086/586887](https://doi.org/10.1086/586887)
- Cieza, L. A., Kessler-Silacci, J. E., Jaffe, D. T., Harvey, P. M., & Evans, Neal J., I. 2005, *ApJ*, 635, 422, doi: [10.1086/497325](https://doi.org/10.1086/497325)
- Cieza, L. A., Olofsson, J., Harvey, P. M., et al. 2013, *ApJ*, 762, 100, doi: [10.1088/0004-637X/762/2/100](https://doi.org/10.1088/0004-637X/762/2/100)
- Cifuentes, C., Caballero, J. A., González-Payo, J., et al. 2025, *A&A*, 693, A228, doi: [10.1051/0004-6361/202452527](https://doi.org/10.1051/0004-6361/202452527)
- Claria, J. J. 1972, *A&A*, 19, 303
- Colman, I. L., Angus, R., David, T., et al. 2024, *AJ*, 167, 189, doi: [10.3847/1538-3881/ad2c86](https://doi.org/10.3847/1538-3881/ad2c86)
- Correia, A. C. M., Udry, S., Mayor, M., et al. 2005, *A&A*, 440, 751, doi: [10.1051/0004-6361:20042376](https://doi.org/10.1051/0004-6361:20042376)
- Cortés-Contreras, M., Béjar, V. J. S., Caballero, J. A., et al. 2017, *A&A*, 597, A47, doi: [10.1051/0004-6361/201629056](https://doi.org/10.1051/0004-6361/201629056)
- Costa, E., Méndez, R. A., Jao, W. C., et al. 2006, *AJ*, 132, 1234, doi: [10.1086/505706](https://doi.org/10.1086/505706)
- Creevey, O. L., Sordo, R., Pailer, F., et al. 2023, *A&A*, 674, A26, doi: [10.1051/0004-6361/202243688](https://doi.org/10.1051/0004-6361/202243688)
- Cummings, J. D., Deliyannis, C. P., Maderak, R. M., & Steinhauer, A. 2017, *AJ*, 153, 128, doi: [10.3847/1538-3881/aa5b86](https://doi.org/10.3847/1538-3881/aa5b86)
- Currie, T., Plavchan, P., & Kenyon, S. J. 2008, *ApJ*, 688, 597, doi: [10.1086/591842](https://doi.org/10.1086/591842)
- Currie, T., Hernandez, J., Irwin, J., et al. 2010, *ApJS*, 186, 191, doi: [10.1088/0067-0049/186/2/191](https://doi.org/10.1088/0067-0049/186/2/191)
- Currie, T., Brandt, G. M., Brandt, T. D., et al. 2023, *Science*, 380, 198, doi: [10.1126/science.abo6192](https://doi.org/10.1126/science.abo6192)
- Cutri, R. M., Skrutskie, M. F., van Dyk, S., et al. 2003, 2MASS All Sky Catalog of point sources. (NASA/IPAC Infrared Science Archive)
- Cutri, R. M., Wright, E. L., Conrow, T., et al. 2013, Explanatory Supplement to the AllWISE Data Release Products., Explanatory Supplement to the AllWISE Data Release Products, by R. M. Cutri et al. IPAC, Caltech
- Czekala, I., Chiang, E., Andrews, S. M., et al. 2019, *ApJ*, 883, 22, doi: [10.3847/1538-4357/ab287b](https://doi.org/10.3847/1538-4357/ab287b)
- da Silva, L., Torres, C. A. O., de La Reza, R., et al. 2009, *A&A*, 508, 833, doi: [10.1051/0004-6361/200911736](https://doi.org/10.1051/0004-6361/200911736)
- Dahm, S. E. 2015, *ApJ*, 813, 108, doi: [10.1088/0004-637X/813/2/108](https://doi.org/10.1088/0004-637X/813/2/108)
- Damiani, F., Flaccomio, E., Micela, G., et al. 2003, *ApJ*, 588, 1009, doi: [10.1086/374214](https://doi.org/10.1086/374214)
- Damiani, F., Prisinzano, L., Pillitteri, I., Micela, G., & Sciortino, S. 2019, *A&A*, 623, A112, doi: [10.1051/0004-6361/201833994](https://doi.org/10.1051/0004-6361/201833994)
- Daniel, K. J., Linsky, J. L., & Gagné, M. 2002, *ApJ*, 578, 486, doi: [10.1086/340553](https://doi.org/10.1086/340553)

- David, T. J., & Hillenbrand, L. A. 2015, *ApJ*, 804, 146, doi: [10.1088/0004-637X/804/2/146](https://doi.org/10.1088/0004-637X/804/2/146)
- De Angeli, F., Weiler, M., Montegriffo, P., et al. 2023, *A&A*, 674, A2, doi: [10.1051/0004-6361/202243680](https://doi.org/10.1051/0004-6361/202243680)
- de Geus, E. J., de Zeeuw, P. T., & Lub, J. 1989, *A&A*, 216, 44
- de Grijs, R., & Kamath, D. 2021, *Universe*, 7, 440, doi: [10.3390/universe7110440](https://doi.org/10.3390/universe7110440)
- De Moortel, I., & Browning, P. 2015, *Philosophical Transactions of the Royal Society of London Series A*, 373, 20140269, doi: [10.1098/rsta.2014.0269](https://doi.org/10.1098/rsta.2014.0269)
- de Zeeuw, P. T., Hoogerwerf, R., de Bruijne, J. H. J., Brown, A. G. A., & Blaauw, A. 1999, *AJ*, 117, 354, doi: [10.1086/300682](https://doi.org/10.1086/300682)
- Declair, M., Gordon, K. D., Andrews, J. E., et al. 2022, *ApJ*, 930, 15, doi: [10.3847/1538-4357/ac5dbe](https://doi.org/10.3847/1538-4357/ac5dbe)
- Delgado Mena, E., Israelian, G., González Hernández, J. I., et al. 2014, *A&A*, 562, A92, doi: [10.1051/0004-6361/201321493](https://doi.org/10.1051/0004-6361/201321493)
- Delgado Mena, E., Bertrán de Lis, S., Adibekyan, V. Z., et al. 2015, *A&A*, 576, A69, doi: [10.1051/0004-6361/201425433](https://doi.org/10.1051/0004-6361/201425433)
- Deliyannis, C. P., Pinsonneault, M. H., & Charbonnel, C. 2000, in *IAU Symposium*, Vol. 198, *The Light Elements and their Evolution*, ed. L. da Silva, R. de Medeiros, & M. Spite, 61
- Delorme, P., Collier Cameron, A., Hebb, L., et al. 2011, *MNRAS*, 413, 2218, doi: [10.1111/j.1365-2966.2011.18299.x](https://doi.org/10.1111/j.1365-2966.2011.18299.x)
- Delorme, P., Gagné, J., Girard, J. H., et al. 2013, *A&A*, 553, L5, doi: [10.1051/0004-6361/201321169](https://doi.org/10.1051/0004-6361/201321169)
- Denis, C. 2005, *VizieR Online Data Catalog: The DENIS database (DENIS Consortium, 2005)*, *VizieR On-line Data Catalog: B/denis*. Originally published in: *The DENIS consortium (2005)*
- Dias, W. S., Monteiro, H., Moitinho, A., et al. 2021, *MNRAS*, 504, 356, doi: [10.1093/mnras/stab770](https://doi.org/10.1093/mnras/stab770)
- Dickson-Vandervelde, D. A., Wilson, E. C., & Kastner, J. H. 2021, *AJ*, 161, 87, doi: [10.3847/1538-3881/abd0fd](https://doi.org/10.3847/1538-3881/abd0fd)
- Díez Alonso, E., Caballero, J. A., Montes, D., et al. 2019, *A&A*, 621, A126, doi: [10.1051/0004-6361/201833316](https://doi.org/10.1051/0004-6361/201833316)
- Dineva, E., Pearson, J., Ilyin, I., et al. 2022, *Astronomische Nachrichten*, 343, e23996, doi: [10.1002/asna.20223996](https://doi.org/10.1002/asna.20223996)
- Distefano, E., Lanzafame, A. C., Brugaletta, E., et al. 2023, *A&A*, 674, A20, doi: [10.1051/0004-6361/202244178](https://doi.org/10.1051/0004-6361/202244178)
- Dittmann, J. A., Irwin, J. M., Charbonneau, D., & Berta-Thompson, Z. K. 2014, *ApJ*, 784, 156, doi: [10.1088/0004-637X/784/2/156](https://doi.org/10.1088/0004-637X/784/2/156)
- do Nascimento, J. D., Barnes, S. A., Saar, S. H., et al. 2023, *ApJ*, 958, 57, doi: [10.3847/1538-4357/acfc1a](https://doi.org/10.3847/1538-4357/acfc1a)
- Dobbie, P. D., Lodieu, N., & Sharp, R. G. 2010, *MNRAS*, 409, 1002, doi: [10.1111/j.1365-2966.2010.17355.x](https://doi.org/10.1111/j.1365-2966.2010.17355.x)
- Dodson-Robinson, S. E., Su, K. Y. L., Bryden, G., Harvey, P., & Green, J. D. 2016, *ApJ*, 833, 183, doi: [10.3847/1538-4357/833/2/183](https://doi.org/10.3847/1538-4357/833/2/183)
- Donaldson, J. K., Roberge, A., Chen, C. H., et al. 2012, *ApJ*, 753, 147, doi: [10.1088/0004-637X/753/2/147](https://doi.org/10.1088/0004-637X/753/2/147)
- Douglas, S. T., Agüeros, M. A., Covey, K. R., & Kraus, A. 2017, *ApJ*, 842, 83, doi: [10.3847/1538-4357/aa6e52](https://doi.org/10.3847/1538-4357/aa6e52)
- Douglas, S. T., Cargile, P. A., Matt, S. P., et al. 2024, *ApJ*, 962, 16, doi: [10.3847/1538-4357/ad0fe3](https://doi.org/10.3847/1538-4357/ad0fe3)
- Douglas, S. T., Curtis, J. L., Agüeros, M. A., et al. 2019, *ApJ*, 879, 100, doi: [10.3847/1538-4357/ab2468](https://doi.org/10.3847/1538-4357/ab2468)
- Draper, Z. H., Matthews, B., Venn, K., et al. 2018, *ApJ*, 857, 93, doi: [10.3847/1538-4357/aab1fd](https://doi.org/10.3847/1538-4357/aab1fd)
- Ducati, J. R., Bevilacqua, C. M., Rembold, S. B., & Ribeiro, D. 2001, *ApJ*, 558, 309, doi: [10.1086/322439](https://doi.org/10.1086/322439)
- Dumont, T. 2023, *A&A*, 677, A119, doi: [10.1051/0004-6361/202346915](https://doi.org/10.1051/0004-6361/202346915)
- Dumont, T., Charbonnel, C., Palacios, A., & Borisov, S. 2021a, *A&A*, 654, A46, doi: [10.1051/0004-6361/202141094](https://doi.org/10.1051/0004-6361/202141094)
- Dumont, T., Palacios, A., Charbonnel, C., et al. 2021b, *A&A*, 646, A48, doi: [10.1051/0004-6361/202039515](https://doi.org/10.1051/0004-6361/202039515)
- Duncan, D. K., Vaughan, A. H., Wilson, O. C., et al. 1991, *ApJS*, 76, 383, doi: [10.1086/191572](https://doi.org/10.1086/191572)
- Edenhofer, G., Zucker, C., Frank, P., et al. 2024, *A&A*, 685, A82, doi: [10.1051/0004-6361/202347628](https://doi.org/10.1051/0004-6361/202347628)
- Egan, M. P., & Price, S. D. 1996, *AJ*, 112, 2862, doi: [10.1086/118227](https://doi.org/10.1086/118227)
- Egeland, R., Soon, W., Baliunas, S., et al. 2017, *ApJ*, 835, 25, doi: [10.3847/1538-4357/835/1/25](https://doi.org/10.3847/1538-4357/835/1/25)
- Eggen, O. J. 1963, *AJ*, 68, 697, doi: [10.1086/109198](https://doi.org/10.1086/109198)
- Eggen, O. J. 1970, *Vistas in Astronomy*, 12, 367, doi: [10.1016/0083-6656\(70\)90049-8](https://doi.org/10.1016/0083-6656(70)90049-8)
- Eiroa, C., Marshall, J. P., Mora, A., et al. 2013, *A&A*, 555, A11, doi: [10.1051/0004-6361/201321050](https://doi.org/10.1051/0004-6361/201321050)
- Eisenbeiss, T., Ammler-von Eiff, M., Roell, T., et al. 2013, *A&A*, 556, A53, doi: [10.1051/0004-6361/201118362](https://doi.org/10.1051/0004-6361/201118362)
- Eker, Z., Bilir, S., Soyduğan, F., et al. 2014, *PASA*, 31, e024, doi: [10.1017/pasa.2014.17](https://doi.org/10.1017/pasa.2014.17)
- Engels, D., Sherwood, W. A., Wamsteker, W., & Schultz, G. V. 1981, *A&AS*, 45, 5
- Evans, D. W., Riello, M., De Angeli, F., et al. 2018, *A&A*, 616, A4, doi: [10.1051/0004-6361/201832756](https://doi.org/10.1051/0004-6361/201832756)
- Evans, I. N., Primini, F. A., Glotfelty, K. J., et al. 2010, *ApJS*, 189, 37, doi: [10.1088/0067-0049/189/1/37](https://doi.org/10.1088/0067-0049/189/1/37)
- Fabrizius, C., Luri, X., Arenou, F., et al. 2021, *A&A*, 649, A5, doi: [10.1051/0004-6361/202039834](https://doi.org/10.1051/0004-6361/202039834)

- Fajrin, M., Armstrong, J. J., Tan, J. C., Farias, J. P., & Eyer, L. 2025, *MNRAS*, 537, 1320, doi: [10.1093/mnras/staf074](https://doi.org/10.1093/mnras/staf074)
- Fang, X.-S., Zhao, G., Zhao, J.-K., & Bharat Kumar, Y. 2018, *MNRAS*, 476, 908, doi: [10.1093/mnras/sty212](https://doi.org/10.1093/mnras/sty212)
- Faramaz, V., Krist, J., Stapelfeldt, K. R., et al. 2019, *AJ*, 158, 162, doi: [10.3847/1538-3881/ab3ec1](https://doi.org/10.3847/1538-3881/ab3ec1)
- Faramaz, V., Marino, S., Booth, M., et al. 2021, *AJ*, 161, 271, doi: [10.3847/1538-3881/abf4e0](https://doi.org/10.3847/1538-3881/abf4e0)
- Farihi, J. 2016, *NewAR*, 71, 9, doi: [10.1016/j.newar.2016.03.001](https://doi.org/10.1016/j.newar.2016.03.001)
- Fazio, G. G., Hora, J. L., Allen, L. E., et al. 2004, *ApJS*, 154, 10, doi: [10.1086/422843](https://doi.org/10.1086/422843)
- Fekel, F. C. 1996, *AJ*, 112, 269, doi: [10.1086/118010](https://doi.org/10.1086/118010)
- Fekel, F. C. 1997, *AJ*, 114, 2747, doi: [10.1086/118683](https://doi.org/10.1086/118683)
- Fekel, F. C., Dadonas, V., Sperauskas, J., Vaccaro, T. R., & Patterson, L. R. 1994, *AJ*, 108, 1936, doi: [10.1086/117207](https://doi.org/10.1086/117207)
- Fekel, F. C., Gillies, K., Africano, J., & Quigley, R. 1988, *AJ*, 96, 1426, doi: [10.1086/114893](https://doi.org/10.1086/114893)
- Fekel, F. C., Henry, G. W., & Alston, F. M. 2004, *AJ*, 127, 2303, doi: [10.1086/382718](https://doi.org/10.1086/382718)
- Fernandes, R. B., Mulders, G. D., Pascucci, I., Mordasini, C., & Emsenhuber, A. 2019, *ApJ*, 874, 81, doi: [10.3847/1538-4357/ab0300](https://doi.org/10.3847/1538-4357/ab0300)
- Fitzpatrick, E. L. 1999, *PASP*, 111, 63, doi: [10.1086/316293](https://doi.org/10.1086/316293)
- Foing, B. H., Crivellari, L., Vladilo, G., Rebolo, R., & Beckman, J. E. 1989, *A&AS*, 80, 189
- Follette, K. B., Rameau, J., Dong, R., et al. 2017, *AJ*, 153, 264, doi: [10.3847/1538-3881/aa6d85](https://doi.org/10.3847/1538-3881/aa6d85)
- Ford, A., Jeffries, R. D., James, D. J., & Barnes, J. R. 2001, *A&A*, 369, 871, doi: [10.1051/0004-6361:20010235](https://doi.org/10.1051/0004-6361:20010235)
- Fouesneau, M., Frémat, Y., Andrae, R., et al. 2023, *A&A*, 674, A28, doi: [10.1051/0004-6361/202243919](https://doi.org/10.1051/0004-6361/202243919)
- Franciosini, E., Randich, S., & Pallavicini, R. 2003, *A&A*, 405, 551, doi: [10.1051/0004-6361:20030623](https://doi.org/10.1051/0004-6361:20030623)
- Franciosini, E., Randich, S., de Laverny, P., et al. 2022, *A&A*, 668, A49, doi: [10.1051/0004-6361/202244854](https://doi.org/10.1051/0004-6361/202244854)
- Freund, S., Czesla, S., Fuhrmeister, B., et al. 2025, *A&A*, 697, A230, doi: [10.1051/0004-6361/202451421](https://doi.org/10.1051/0004-6361/202451421)
- Freund, S., Czesla, S., Robrade, J., Schneider, P. C., & Schmitt, J. H. M. M. 2022, *A&A*, 664, A105, doi: [10.1051/0004-6361/202142573](https://doi.org/10.1051/0004-6361/202142573)
- Freund, S., Robrade, J., Schneider, P. C., & Schmitt, J. H. M. M. 2018, *A&A*, 614, A125, doi: [10.1051/0004-6361/201732009](https://doi.org/10.1051/0004-6361/201732009)
- Freund, S., Czesla, S., Predehl, P., et al. 2024, *A&A*, 684, A121, doi: [10.1051/0004-6361/202348278](https://doi.org/10.1051/0004-6361/202348278)
- Frisch, P. C., & York, D. G. 1983, *ApJL*, 271, L59, doi: [10.1086/184095](https://doi.org/10.1086/184095)
- Fritzewski, D. J., Barnes, S. A., James, D. J., & Strassmeier, K. G. 2020, *A&A*, 641, A51, doi: [10.1051/0004-6361/201936860](https://doi.org/10.1051/0004-6361/201936860)
- Fuhrmann, K. 2008, *MNRAS*, 384, 173, doi: [10.1111/j.1365-2966.2007.12671.x](https://doi.org/10.1111/j.1365-2966.2007.12671.x)
- Fuhrmann, K., & Chini, R. 2015, *ApJ*, 809, 107, doi: [10.1088/0004-637X/809/1/107](https://doi.org/10.1088/0004-637X/809/1/107)
- Fuhrmann, K., Chini, R., Hoffmeister, V. H., et al. 2011, *MNRAS*, 411, 2311, doi: [10.1111/j.1365-2966.2010.17850.x](https://doi.org/10.1111/j.1365-2966.2010.17850.x)
- Fulton, B. J., Rosenthal, L. J., Hirsch, L. A., et al. 2021, *ApJS*, 255, 14, doi: [10.3847/1538-4365/abfcc1](https://doi.org/10.3847/1538-4365/abfcc1)
- Furlan, E., Hartmann, L., Calvet, N., et al. 2006, *ApJS*, 165, 568, doi: [10.1086/505468](https://doi.org/10.1086/505468)
- Gagné, J., Moranta, L., Faherty, J. K., et al. 2023, *ApJ*, 945, 119, doi: [10.3847/1538-4357/acb8b7](https://doi.org/10.3847/1538-4357/acb8b7)
- Gagné, J., Mamajek, E. E., Malo, L., et al. 2018, *ApJ*, 856, 23, doi: [10.3847/1538-4357/aaae09](https://doi.org/10.3847/1538-4357/aaae09)
- Gaia Collaboration, Smart, R. L., Sarro, L. M., et al. 2021a, *A&A*, 649, A6, doi: [10.1051/0004-6361/202039498](https://doi.org/10.1051/0004-6361/202039498)
- Gaia Collaboration, Brown, A. G. A., Vallenari, A., et al. 2021b, *A&A*, 649, A1, doi: [10.1051/0004-6361/202039657](https://doi.org/10.1051/0004-6361/202039657)
- Gaia Collaboration, Vallenari, A., Brown, A. G. A., et al. 2023a, *A&A*, 674, A1, doi: [10.1051/0004-6361/202243940](https://doi.org/10.1051/0004-6361/202243940)
- Gaia Collaboration, Montegriffo, P., Bellazzini, M., et al. 2023b, *A&A*, 674, A33, doi: [10.1051/0004-6361/202243709](https://doi.org/10.1051/0004-6361/202243709)
- Gaia Collaboration, Arenou, F., Babusiaux, C., et al. 2023c, *A&A*, 674, A34, doi: [10.1051/0004-6361/202243782](https://doi.org/10.1051/0004-6361/202243782)
- Gaidos, E., Mann, A. W., Lépine, S., et al. 2014, *MNRAS*, 443, 2561, doi: [10.1093/mnras/stu1313](https://doi.org/10.1093/mnras/stu1313)
- Gallenne, A., Mérand, A., Kervella, P., et al. 2023, *A&A*, 672, A119, doi: [10.1051/0004-6361/202245712](https://doi.org/10.1051/0004-6361/202245712)
- Gallet, F., & Bouvier, J. 2015, *A&A*, 577, A98, doi: [10.1051/0004-6361/201525660](https://doi.org/10.1051/0004-6361/201525660)
- Gao, S., Liu, C., Zhang, X., et al. 2014, *ApJL*, 788, L37, doi: [10.1088/2041-8205/788/2/L37](https://doi.org/10.1088/2041-8205/788/2/L37)
- Gao, X., Lind, K., Amarsi, A. M., et al. 2020, *MNRAS*, 497, L30, doi: [10.1093/mnras/laaa109](https://doi.org/10.1093/mnras/laaa109)
- Gáspár, A., Rieke, G. H., & Ballering, N. 2016, *ApJ*, 826, 171, doi: [10.3847/0004-637X/826/2/171](https://doi.org/10.3847/0004-637X/826/2/171)
- Gáspár, A., Rieke, G. H., Su, K. Y. L., et al. 2009, *ApJ*, 697, 1578, doi: [10.1088/0004-637X/697/2/1578](https://doi.org/10.1088/0004-637X/697/2/1578)
- Gautier, Thomas N., I., Rebull, L. M., Stapelfeldt, K. R., & Mainzer, A. 2008, *ApJ*, 683, 813, doi: [10.1086/589708](https://doi.org/10.1086/589708)
- Gautier, Thomas N., I., Rieke, G. H., Stansberry, J., et al. 2007, *ApJ*, 667, 527, doi: [10.1086/520667](https://doi.org/10.1086/520667)
- Gennaro, M., Prada Moroni, P. G., & Tognelli, E. 2012, *MNRAS*, 420, 986, doi: [10.1111/j.1365-2966.2011.19945.x](https://doi.org/10.1111/j.1365-2966.2011.19945.x)

- Getman, K. V., Feigelson, E. D., & Garmire, G. P. 2023, *ApJ*, 952, 63, doi: [10.3847/1538-4357/acd690](https://doi.org/10.3847/1538-4357/acd690)
- Gezari, D. Y., Schmitz, M., Pitts, P. S., & Mead, J. M. 1993, *Catalog of infrared observations (NASA, Greenbelt, MD USA)*
- Ghezzi, L., Cunha, K., Smith, V. V., & de la Reza, R. 2010, *ApJ*, 724, 154, doi: [10.1088/0004-637X/724/1/154](https://doi.org/10.1088/0004-637X/724/1/154)
- Ghezzi, L., Montet, B. T., & Johnson, J. A. 2018, *ApJ*, 860, 109, doi: [10.3847/1538-4357/aac37c](https://doi.org/10.3847/1538-4357/aac37c)
- Gillen, E., Briegal, J. T., Hodgkin, S. T., et al. 2020, *MNRAS*, 492, 1008, doi: [10.1093/mnras/stz3251](https://doi.org/10.1093/mnras/stz3251)
- Gillon, M., Jehin, E., Lederer, S. M., et al. 2016, *Nature*, 533, 221, doi: [10.1038/nature17448](https://doi.org/10.1038/nature17448)
- Glebocki, R., Gnacinski, P., & Stawikowski, A. 2000, *AcA*, 50, 509
- Gliese, W. 1969, *Veroeffentlichungen des Astronomischen Rechen-Instituts Heidelberg*, 22, 1
- Gliese, W., & Jahreiß, H. 1991, *Preliminary Version of the Third Catalogue of Nearby Stars,, On: The Astronomical Data Center CD-ROM: Selected Astronomical Catalogs, Vol. I; L.E. Brotzmann, S.E. Gesser (eds.), NASA/Astronomical Data Center, Goddard Space Flight Center, Greenbelt, MD*
- Goldman, B., Röser, S., Schilbach, E., Moór, A. C., & Henning, T. 2018, *ApJ*, 868, 32, doi: [10.3847/1538-4357/aae64c](https://doi.org/10.3847/1538-4357/aae64c)
- Golimowski, D. A., Ardila, D. R., Krist, J. E., et al. 2006, *AJ*, 131, 3109, doi: [10.1086/503801](https://doi.org/10.1086/503801)
- Golovin, A., Reffert, S., Just, A., et al. 2023, *A&A*, 670, A19, doi: [10.1051/0004-6361/202244250](https://doi.org/10.1051/0004-6361/202244250)
- Gomes da Silva, J., Santos, N. C., Boisse, I., Dumusque, X., & Lovis, C. 2014, *A&A*, 566, A66, doi: [10.1051/0004-6361/201322697](https://doi.org/10.1051/0004-6361/201322697)
- Gomes da Silva, J., Santos, N. C., Adibekyan, V., et al. 2021, *A&A*, 646, A77, doi: [10.1051/0004-6361/202039765](https://doi.org/10.1051/0004-6361/202039765)
- Gondoin, P. 2020, *A&A*, 641, A110, doi: [10.1051/0004-6361/202038291](https://doi.org/10.1051/0004-6361/202038291)
- González, J. F., & Levato, H. 2009, *A&A*, 507, 541, doi: [10.1051/0004-6361/200912772](https://doi.org/10.1051/0004-6361/200912772)
- González-Payo, J., Caballero, J. A., Gorgas, J., et al. 2024, *A&A*, 689, A302, doi: [10.1051/0004-6361/202450048](https://doi.org/10.1051/0004-6361/202450048)
- Gordon, K. D., Misselt, K. A., Bouwman, J., et al. 2021, *ApJ*, 916, 33, doi: [10.3847/1538-4357/ac00b7](https://doi.org/10.3847/1538-4357/ac00b7)
- Gorlova, N., Balog, Z., Rieke, G. H., et al. 2007, *ApJ*, 670, 516, doi: [10.1086/521671](https://doi.org/10.1086/521671)
- Gorlova, N., Rieke, G. H., Muzerolle, J., et al. 2006, *ApJ*, 649, 1028, doi: [10.1086/506373](https://doi.org/10.1086/506373)
- Gorlova, N., Padgett, D. L., Rieke, G. H., et al. 2004, *ApJS*, 154, 448, doi: [10.1086/422822](https://doi.org/10.1086/422822)
- Gossage, S., Conroy, C., Dotter, A., et al. 2018, *ApJ*, 863, 67, doi: [10.3847/1538-4357/aad0a0](https://doi.org/10.3847/1538-4357/aad0a0)
- Gosset, E., Damerdji, Y., Morel, T., et al. 2024, *arXiv e-prints*, arXiv:2410.14372, doi: [10.48550/arXiv.2410.14372](https://doi.org/10.48550/arXiv.2410.14372)
- Gray, R. O., Corbally, C. J., Garrison, R. F., et al. 2006, *AJ*, 132, 161, doi: [10.1086/504637](https://doi.org/10.1086/504637)
- Gray, R. O., Corbally, C. J., Garrison, R. F., McFadden, M. T., & Robinson, P. E. 2003, *AJ*, 126, 2048, doi: [10.1086/378365](https://doi.org/10.1086/378365)
- Greaves, J. S., Wyatt, M. C., Holland, W. S., & Dent, W. R. F. 2004, *MNRAS*, 351, L54, doi: [10.1111/j.1365-2966.2004.07957.x](https://doi.org/10.1111/j.1365-2966.2004.07957.x)
- Greaves, J. S., Holland, W. S., Moriarty-Schieven, G., et al. 1998, *ApJL*, 506, L133, doi: [10.1086/311652](https://doi.org/10.1086/311652)
- Green, G. M., Schlafly, E., Zucker, C., Speagle, J. S., & Finkbeiner, D. 2019, *ApJ*, 887, 93, doi: [10.3847/1538-4357/ab5362](https://doi.org/10.3847/1538-4357/ab5362)
- Griffin, M. J., Abergel, A., Abreu, A., et al. 2010, *A&A*, 518, L3, doi: [10.1051/0004-6361/201014519](https://doi.org/10.1051/0004-6361/201014519)
- Griffin, R. E. M., & Griffin, R. F. 2011, *Astronomische Nachrichten*, 332, 105, doi: [10.1002/asna.201011514](https://doi.org/10.1002/asna.201011514)
- Groenewegen, M. A. T. 2021, *A&A*, 654, A20, doi: [10.1051/0004-6361/202140862](https://doi.org/10.1051/0004-6361/202140862)
- Gruner, D., Barnes, S. A., & Weingrill, J. 2023, *A&A*, 672, A159, doi: [10.1051/0004-6361/202345942](https://doi.org/10.1051/0004-6361/202345942)
- Güdel, M. 2004, *A&A Rv*, 12, 71, doi: [10.1007/s00159-004-0023-2](https://doi.org/10.1007/s00159-004-0023-2)
- Guiglion, G., de Laverny, P., Recio-Blanco, A., et al. 2016, *A&A*, 595, A18, doi: [10.1051/0004-6361/201628919](https://doi.org/10.1051/0004-6361/201628919)
- Guo, Y., Liu, C., Wang, L., et al. 2022, *A&A*, 667, A44, doi: [10.1051/0004-6361/202244300](https://doi.org/10.1051/0004-6361/202244300)
- Gutiérrez Albarrán, M. L., Montes, D., Tabernero, H. M., et al. 2024, *A&A*, 685, A83, doi: [10.1051/0004-6361/202348438](https://doi.org/10.1051/0004-6361/202348438)
- Hahlin, A., Kochukhov, O., Alecian, E., Morin, J., & BinaMIcS Collaboration. 2021, *A&A*, 650, A197, doi: [10.1051/0004-6361/202140832](https://doi.org/10.1051/0004-6361/202140832)
- Halbwachs, J.-L., Pourbaix, D., Arenou, F., et al. 2023, *A&A*, 674, A9, doi: [10.1051/0004-6361/202243969](https://doi.org/10.1051/0004-6361/202243969)
- Hales, A. S., Marino, S., Sheehan, P. D., et al. 2022, *ApJ*, 940, 161, doi: [10.3847/1538-4357/ac9cd3](https://doi.org/10.3847/1538-4357/ac9cd3)
- Hall, J. C. 2008, *Living Reviews in Solar Physics*, 5, 2, doi: [10.12942/lrsp-2008-2](https://doi.org/10.12942/lrsp-2008-2)
- Hamdy, M. A., Abo Elazm, M. S., & Saad, S. M. 1993, *Ap&SS*, 203, 53, doi: [10.1007/BF00659414](https://doi.org/10.1007/BF00659414)
- Hartigan, P., Hartmann, L., Kenyon, S., Hewett, R., & Stauffer, J. 1989, *ApJS*, 70, 899, doi: [10.1086/191361](https://doi.org/10.1086/191361)
- Hartkopf, W. I., Mason, B. D., & Worley, C. E. 2001, *AJ*, 122, 3472, doi: [10.1086/323921](https://doi.org/10.1086/323921)

- Hartman, J. D., Bakos, G. Á., Kovács, G., & Noyes, R. W. 2010, *MNRAS*, 408, 475, doi: [10.1111/j.1365-2966.2010.17147.x](https://doi.org/10.1111/j.1365-2966.2010.17147.x)
- Hartmann, L., Herczeg, G., & Calvet, N. 2016, *ARA&A*, 54, 135, doi: [10.1146/annurev-astro-081915-023347](https://doi.org/10.1146/annurev-astro-081915-023347)
- Hegedűs, V., Mészáros, S., Jofré, P., et al. 2023, *A&A*, 670, A107, doi: [10.1051/0004-6361/202244813](https://doi.org/10.1051/0004-6361/202244813)
- Helminiak, K. G., Konacki, M., Muterspaugh, M. W., et al. 2012, *MNRAS*, 419, 1285, doi: [10.1111/j.1365-2966.2011.19785.x](https://doi.org/10.1111/j.1365-2966.2011.19785.x)
- Henden, A., & Munari, U. 2014, *Contributions of the Astronomical Observatory Skalnaté Pleso*, 43, 518
- Henden, A. A., Levine, S., Terrell, D., et al. 2018, in *American Astronomical Society Meeting Abstracts*, Vol. 232, American Astronomical Society Meeting Abstracts #232, 223.06
- Hengst, S., Marshall, J. P., Horner, J., & Marsden, S. C. 2017, *MNRAS*, 468, 4725, doi: [10.1093/mnras/stx753](https://doi.org/10.1093/mnras/stx753)
- Henry, T. J., Soderblom, D. R., Donahue, R. A., & Baliunas, S. L. 1996, *AJ*, 111, 439, doi: [10.1086/117796](https://doi.org/10.1086/117796)
- Henry, T. J., Jao, W.-C., Winters, J. G., et al. 2018, *AJ*, 155, 265, doi: [10.3847/1538-3881/aac262](https://doi.org/10.3847/1538-3881/aac262)
- Herczeg, G. J., Chen, Y., Donati, J.-F., et al. 2023, *ApJ*, 956, 102, doi: [10.3847/1538-4357/acf468](https://doi.org/10.3847/1538-4357/acf468)
- Hernández, J., Briceño, C., Calvet, N., et al. 2006, *ApJ*, 652, 472, doi: [10.1086/507942](https://doi.org/10.1086/507942)
- Hernández, J., Hartmann, L., Megeath, T., et al. 2007, *ApJ*, 662, 1067, doi: [10.1086/513735](https://doi.org/10.1086/513735)
- Hernández, J., Zamudio, L. F., Briceño, C., et al. 2023, *AJ*, 165, 205, doi: [10.3847/1538-3881/acc467](https://doi.org/10.3847/1538-3881/acc467)
- Heyl, J., Caiazzo, I., & Richer, H. B. 2022, *ApJ*, 926, 132, doi: [10.3847/1538-4357/ac45fc](https://doi.org/10.3847/1538-4357/ac45fc)
- Hillenbrand, L. A., Carpenter, J. M., Kim, J. S., et al. 2008, *ApJ*, 677, 630, doi: [10.1086/529027](https://doi.org/10.1086/529027)
- Hinkel, N. R., Timmes, F. X., Young, P. A., Pagano, M. D., & Turnbull, M. C. 2014, *AJ*, 148, 54, doi: [10.1088/0004-6256/148/3/54](https://doi.org/10.1088/0004-6256/148/3/54)
- Hinkel, N. R., Mamajek, E. E., Turnbull, M. C., et al. 2017, *ApJ*, 848, 34, doi: [10.3847/1538-4357/aa8b0f](https://doi.org/10.3847/1538-4357/aa8b0f)
- Hoffleit, D., & Jaschek, C. 1991, *The Bright star catalogue* (Yale University Observatory, New Haven, CT USA)
- Høg, E., Bässgen, G., Bastian, U., et al. 1997, *A&A*, 323, L57
- Høg, E., Fabricius, C., Makarov, V. V., et al. 2000, *A&A*, 355, L27
- Holland, W. S., Matthews, B. C., Kennedy, G. M., et al. 2017, *MNRAS*, 470, 3606, doi: [10.1093/mnras/stx1378](https://doi.org/10.1093/mnras/stx1378)
- Holmberg, J., Nordström, B., & Andersen, J. 2009, *A&A*, 501, 941, doi: [10.1051/0004-6361/200811191](https://doi.org/10.1051/0004-6361/200811191)
- Houck, J. R., Roellig, T. L., van Cleve, J., et al. 2004, *ApJS*, 154, 18, doi: [10.1086/423134](https://doi.org/10.1086/423134)
- Houdebine, E. R. 2009, *MNRAS*, 397, 2133, doi: [10.1111/j.1365-2966.2009.15112.x](https://doi.org/10.1111/j.1365-2966.2009.15112.x)
- Houdebine, E. R. 2011, *MNRAS*, 416, 2233, doi: [10.1111/j.1365-2966.2011.19199.x](https://doi.org/10.1111/j.1365-2966.2011.19199.x)
- Houdebine, E. R., & Mullan, D. J. 2015, *ApJ*, 801, 106, doi: [10.1088/0004-637X/801/2/106](https://doi.org/10.1088/0004-637X/801/2/106)
- Houdebine, E. R., Mullan, D. J., Bercu, B., Paletou, F., & Gebran, M. 2017, *ApJ*, 837, 96, doi: [10.3847/1538-4357/aa5cad](https://doi.org/10.3847/1538-4357/aa5cad)
- Houdebine, É. R., Mullan, D. J., Doyle, J. G., et al. 2019, *AJ*, 158, 56, doi: [10.3847/1538-3881/ab23fe](https://doi.org/10.3847/1538-3881/ab23fe)
- Houdebine, E. R., Mullan, D. J., Paletou, F., & Gebran, M. 2016, *ApJ*, 822, 97, doi: [10.3847/0004-637X/822/2/97](https://doi.org/10.3847/0004-637X/822/2/97)
- Houk, N. 1978, *Michigan catalogue of two-dimensional spectral types for the HD stars* (Department of Astronomy, University of Michigan, Ann Arbor, MI USA)
- Hourihane, A., François, P., Worley, C. C., et al. 2023, *A&A*, 676, A129, doi: [10.1051/0004-6361/202345910](https://doi.org/10.1051/0004-6361/202345910)
- Huang, B., Yuan, H., Xiang, M., et al. 2024, *ApJS*, 271, 13, doi: [10.3847/1538-4365/ad18b1](https://doi.org/10.3847/1538-4365/ad18b1)
- Hughes, A. M., Duchêne, G., & Matthews, B. C. 2018, *ARA&A*, 56, 541, doi: [10.1146/annurev-astro-081817-052035](https://doi.org/10.1146/annurev-astro-081817-052035)
- Hummel, C. A., Armstrong, J. T., Buscher, D. F., et al. 1995, *AJ*, 110, 376, doi: [10.1086/117528](https://doi.org/10.1086/117528)
- Hummel, C. A., Monnier, J. D., Roettenbacher, R. M., et al. 2017, *ApJ*, 844, 115, doi: [10.3847/1538-4357/aa7b87](https://doi.org/10.3847/1538-4357/aa7b87)
- Hünsch, M., Weidner, C., & Schmitt, J. H. M. M. 2003, *A&A*, 402, 571, doi: [10.1051/0004-6361:20030268](https://doi.org/10.1051/0004-6361:20030268)
- Hunt, E. L., & Reffert, S. 2023, *A&A*, 673, A114, doi: [10.1051/0004-6361/202346285](https://doi.org/10.1051/0004-6361/202346285)
- Hunt, E. L., & Reffert, S. 2024, *A&A*, 686, A42, doi: [10.1051/0004-6361/202348662](https://doi.org/10.1051/0004-6361/202348662)
- Jackson, R. J., Jeffries, R. D., Wright, N. J., et al. 2020, *MNRAS*, 496, 4701, doi: [10.1093/mnras/staa1749](https://doi.org/10.1093/mnras/staa1749)
- Jackson, R. J., Jeffries, R. D., Wright, N. J., et al. 2022, *MNRAS*, 509, 1664, doi: [10.1093/mnras/stab3032](https://doi.org/10.1093/mnras/stab3032)
- Jang-Condell, H., Chen, C. H., Mittal, T., et al. 2015, *ApJ*, 808, 167, doi: [10.1088/0004-637X/808/2/167](https://doi.org/10.1088/0004-637X/808/2/167)
- Jansen, F., Lumb, D., Altieri, B., et al. 2001, *A&A*, 365, L1, doi: [10.1051/0004-6361:20000036](https://doi.org/10.1051/0004-6361:20000036)
- Janson, M., Gratton, R., Rodet, L., et al. 2021, *Nature*, 600, 231, doi: [10.1038/s41586-021-04124-8](https://doi.org/10.1038/s41586-021-04124-8)
- Jeffers, S. V., Kiefer, R., & Metcalfe, T. S. 2023, *SSRv*, 219, 54, doi: [10.1007/s11214-023-01000-x](https://doi.org/10.1007/s11214-023-01000-x)
- Jeffers, S. V., Mengel, M., Moutou, C., et al. 2018, *MNRAS*, 479, 5266, doi: [10.1093/mnras/sty1717](https://doi.org/10.1093/mnras/sty1717)

- Jeffers, S. V., Cameron, R. H., Marsden, S. C., et al. 2022, *A&A*, 661, A152, doi: [10.1051/0004-6361/202142202](https://doi.org/10.1051/0004-6361/202142202)
- Jeffries, R. D. 1999, *MNRAS*, 304, 821, doi: [10.1046/j.1365-8711.1999.02347.x](https://doi.org/10.1046/j.1365-8711.1999.02347.x)
- Jeffries, R. D., Evans, P. A., Pye, J. P., & Briggs, K. R. 2006, *MNRAS*, 367, 781, doi: [10.1111/j.1365-2966.2005.09988.x](https://doi.org/10.1111/j.1365-2966.2005.09988.x)
- Jeffries, R. D., & Oliveira, J. M. 2005, *MNRAS*, 358, 13, doi: [10.1111/j.1365-2966.2005.08820.x](https://doi.org/10.1111/j.1365-2966.2005.08820.x)
- Jeffries, R. D., Oliveira, J. M., Barrado y Navascués, D., & Stauffer, J. R. 2003, *MNRAS*, 343, 1271, doi: [10.1046/j.1365-8711.2003.06768.x](https://doi.org/10.1046/j.1365-8711.2003.06768.x)
- Jeffries, R. D., Jackson, R. J., Wright, N. J., et al. 2023, *MNRAS*, 523, 802, doi: [10.1093/mnras/stad1293](https://doi.org/10.1093/mnras/stad1293)
- Jenkins, J. S., Ramsey, L. W., Jones, H. R. A., et al. 2009, *ApJ*, 704, 975, doi: [10.1088/0004-637X/704/2/975](https://doi.org/10.1088/0004-637X/704/2/975)
- Jiménez-Esteban, F. M., Torres, S., Rebassa-Mansergas, A., et al. 2023, *MNRAS*, 518, 5106, doi: [10.1093/mnras/stac3382](https://doi.org/10.1093/mnras/stac3382)
- Johnstone, C. P., Bartel, M., & Güdel, M. 2021, *A&A*, 649, A96, doi: [10.1051/0004-6361/202038407](https://doi.org/10.1051/0004-6361/202038407)
- Jones, J., White, R. J., Boyajian, T. S., et al. 2017, in *American Astronomical Society Meeting Abstracts*, Vol. 229, American Astronomical Society Meeting Abstracts #229, 131.05
- Jones, J., White, R. J., Boyajian, T., et al. 2015, *ApJ*, 813, 58, doi: [10.1088/0004-637X/813/1/58](https://doi.org/10.1088/0004-637X/813/1/58)
- Jones, N. K., Wang, J. J., Nielsen, E. L., et al. 2025, *ApJL*, 995, L41, doi: [10.3847/2041-8213/ae2007](https://doi.org/10.3847/2041-8213/ae2007)
- Jørgensen, J. K., Harvey, P. M., Evans, Neal J., I., et al. 2006, *ApJ*, 645, 1246, doi: [10.1086/504373](https://doi.org/10.1086/504373)
- Judge, P. G., Solomon, S. C., & Ayres, T. R. 2003, *ApJ*, 593, 534, doi: [10.1086/376405](https://doi.org/10.1086/376405)
- Jura, M., Chen, C. H., Furlan, E., et al. 2004, *ApJS*, 154, 453, doi: [10.1086/422975](https://doi.org/10.1086/422975)
- Kaiser, N., Burgett, W., Chambers, K., et al. 2010, in *Society of Photo-Optical Instrumentation Engineers (SPIE) Conference Series*, Vol. 7733, *Ground-based and Airborne Telescopes III*, ed. L. M. Stepp, R. Gilmozzi, & H. J. Hall, 77330E, doi: [10.1117/12.859188](https://doi.org/10.1117/12.859188)
- Kalas, P., Graham, J. R., & Clampin, M. 2005, *Nature*, 435, 1067, doi: [10.1038/nature03601](https://doi.org/10.1038/nature03601)
- Kamai, B. L., Vrba, F. J., Stauffer, J. R., & Stassun, K. G. 2014, *AJ*, 148, 30, doi: [10.1088/0004-6256/148/2/30](https://doi.org/10.1088/0004-6256/148/2/30)
- Kaminski, A., Sabotta, S., Kemmer, J., et al. 2025, *A&A*, 696, A101, doi: [10.1051/0004-6361/202453381](https://doi.org/10.1051/0004-6361/202453381)
- Keller, S. C., Schmidt, B. P., Bessell, M. S., et al. 2007, *PASA*, 24, 1, doi: [10.1071/AS07001](https://doi.org/10.1071/AS07001)
- Kennedy, G. M., Bryden, G., Ardila, D., et al. 2018, *MNRAS*, 476, 4584, doi: [10.1093/mnras/sty492](https://doi.org/10.1093/mnras/sty492)
- Kenyon, S. J., & Bromley, B. C. 2002, *ApJL*, 577, L35, doi: [10.1086/344084](https://doi.org/10.1086/344084)
- Kenyon, S. J., & Bromley, B. C. 2004, *ApJL*, 602, L133, doi: [10.1086/382693](https://doi.org/10.1086/382693)
- Kenyon, S. J., & Bromley, B. C. 2008, *ApJS*, 179, 451, doi: [10.1086/591794](https://doi.org/10.1086/591794)
- Kenyon, S. J., & Hartmann, L. 1995, *ApJS*, 101, 117, doi: [10.1086/192235](https://doi.org/10.1086/192235)
- Kenyon, S. J., & Hartmann, L. W. 1990, *ApJ*, 349, 197, doi: [10.1086/168306](https://doi.org/10.1086/168306)
- Kenyon, S. J., Najita, J. R., & Bromley, B. C. 2016, *ApJ*, 831, 8, doi: [10.3847/0004-637X/831/1/8](https://doi.org/10.3847/0004-637X/831/1/8)
- Kessler, M. F., Steinz, J. A., Anderegg, M. E., et al. 1996, *A&A*, 315, L27
- Kharchenko, N. V. 2001, *Kinematika i Fizika Nebesnykh Tel*, 17, 409
- Kharchenko, N. V., Piskunov, A. E., Röser, S., Schilbach, E., & Scholz, R. D. 2005, *A&A*, 438, 1163, doi: [10.1051/0004-6361:20042523](https://doi.org/10.1051/0004-6361:20042523)
- Kiefer, F., Halbwegs, J.-L., Lebreton, Y., et al. 2018, *MNRAS*, 474, 731, doi: [10.1093/mnras/stx2794](https://doi.org/10.1093/mnras/stx2794)
- Kim, J. S., Hines, D. C., Backman, D. E., et al. 2005, *ApJ*, 632, 659, doi: [10.1086/432863](https://doi.org/10.1086/432863)
- Kimeswenger, S., Lederle, C., Richichi, A., et al. 2004, *A&A*, 413, 1037, doi: [10.1051/0004-6361:20031576](https://doi.org/10.1051/0004-6361:20031576)
- King, J. R., Villarreal, A. R., Soderblom, D. R., Gulliver, A. F., & Adelman, S. J. 2003, *AJ*, 125, 1980, doi: [10.1086/368241](https://doi.org/10.1086/368241)
- Kiraga, M. 2012, *AcA*, 62, 67, doi: [10.48550/arXiv.1204.3825](https://doi.org/10.48550/arXiv.1204.3825)
- Kiraga, M., & Stepień, K. 2013, *AcA*, 63, 53, doi: [10.48550/arXiv.1304.3236](https://doi.org/10.48550/arXiv.1304.3236)
- Kochukhov, O., & Shulyak, D. 2019, *ApJ*, 873, 69, doi: [10.3847/1538-4357/ab06c5](https://doi.org/10.3847/1538-4357/ab06c5)
- Koen, C., Kilkenny, D., van Wyk, F., & Marang, F. 2010, *MNRAS*, 403, 1949, doi: [10.1111/j.1365-2966.2009.16182.x](https://doi.org/10.1111/j.1365-2966.2009.16182.x)
- Koerner, D. W., Kim, S., Trilling, D. E., et al. 2010, *ApJL*, 710, L26, doi: [10.1088/2041-8205/710/1/L26](https://doi.org/10.1088/2041-8205/710/1/L26)
- Koornneef, J. 1983, *A&AS*, 51, 489
- Kounkel, M., & Covey, K. 2019, *AJ*, 158, 122, doi: [10.3847/1538-3881/ab339a](https://doi.org/10.3847/1538-3881/ab339a)
- Kounkel, M., McBride, A., Stassun, K. G., & Leigh, N. 2022, *MNRAS*, 517, 1946, doi: [10.1093/mnras/stac2829](https://doi.org/10.1093/mnras/stac2829)
- Kovács, G., Hartman, J. D., Bakos, G. Á., et al. 2014, *MNRAS*, 442, 2081, doi: [10.1093/mnras/stu946](https://doi.org/10.1093/mnras/stu946)
- Kraus, A. L., Herczeg, G. J., Rizzuto, A. C., et al. 2017, *ApJ*, 838, 150, doi: [10.3847/1538-4357/aa62a0](https://doi.org/10.3847/1538-4357/aa62a0)
- Kraus, A. L., & Hillenbrand, L. A. 2007, *AJ*, 134, 2340, doi: [10.1086/522831](https://doi.org/10.1086/522831)

- Krivov, A. V., & Wyatt, M. C. 2021, *MNRAS*, 500, 718, doi: [10.1093/mnras/staa2385](https://doi.org/10.1093/mnras/staa2385)
- Küker, M., Rüdiger, G., Olah, K., & Strassmeier, K. G. 2019, *A&A*, 622, A40, doi: [10.1051/0004-6361/201833173](https://doi.org/10.1051/0004-6361/201833173)
- Lallement, R., Babusiaux, C., Vergely, J. L., et al. 2019, *A&A*, 625, A135, doi: [10.1051/0004-6361/201834695](https://doi.org/10.1051/0004-6361/201834695)
- Lambert, D. L., & Reddy, B. E. 2004, *MNRAS*, 349, 757, doi: [10.1111/j.1365-2966.2004.07557.x](https://doi.org/10.1111/j.1365-2966.2004.07557.x)
- Lanzafame, A. C., Brugaletta, E., Frémat, Y., et al. 2023, *A&A*, 674, A30, doi: [10.1051/0004-6361/202244156](https://doi.org/10.1051/0004-6361/202244156)
- Lawson, W. A., & Crause, L. A. 2005, *MNRAS*, 357, 1399, doi: [10.1111/j.1365-2966.2005.08793.x](https://doi.org/10.1111/j.1365-2966.2005.08793.x)
- Lee, R. A., Gaidos, E., van Saders, J., Feiden, G. A., & Gagné, J. 2024, *MNRAS*, 528, 4760, doi: [10.1093/mnras/stae007](https://doi.org/10.1093/mnras/stae007)
- Leonard, P. J. T., & Duncan, M. J. 1990, *AJ*, 99, 608, doi: [10.1086/115354](https://doi.org/10.1086/115354)
- Lépine, S., Thorstensen, J. R., Shara, M. M., & Rich, R. M. 2009, *AJ*, 137, 4109, doi: [10.1088/0004-6256/137/5/4109](https://doi.org/10.1088/0004-6256/137/5/4109)
- Lestrade, J. F., Matthews, B. C., Kennedy, G. M., et al. 2025, *A&A*, 694, A123, doi: [10.1051/0004-6361/202451673](https://doi.org/10.1051/0004-6361/202451673)
- Li, L., Wang, S., Chen, X., & Jiang, Q. 2023, *ApJ*, 956, 26, doi: [10.3847/1538-4357/aced8a](https://doi.org/10.3847/1538-4357/aced8a)
- Lieman-Sifry, J., Hughes, A. M., Carpenter, J. M., et al. 2016, *ApJ*, 828, 25, doi: [10.3847/0004-637X/828/1/25](https://doi.org/10.3847/0004-637X/828/1/25)
- Lignières, F., Petit, P., Böhm, T., & Aurière, M. 2009, *A&A*, 500, L41, doi: [10.1051/0004-6361/200911996](https://doi.org/10.1051/0004-6361/200911996)
- Lindgren, L., Klioner, S. A., Hernández, J., et al. 2021, *A&A*, 649, A2, doi: [10.1051/0004-6361/202039709](https://doi.org/10.1051/0004-6361/202039709)
- Linsky, J. L. 2017, *ARA&A*, 55, 159, doi: [10.1146/annurev-astro-091916-055327](https://doi.org/10.1146/annurev-astro-091916-055327)
- Linsky, J. L., Hunten, D. M., Sowell, R., Glackin, D. L., & Kelch, W. L. 1979, *ApJS*, 41, 481, doi: [10.1086/190627](https://doi.org/10.1086/190627)
- Linsky, J. L., & Redfield, S. 2021, *ApJ*, 920, 75, doi: [10.3847/1538-4357/ac1feb](https://doi.org/10.3847/1538-4357/ac1feb)
- Lipartito, I., Bailey, III, J. I., Brandt, T. D., et al. 2021, *AJ*, 162, 285, doi: [10.3847/1538-3881/ac2ccd](https://doi.org/10.3847/1538-3881/ac2ccd)
- Liseau, R., Risacher, C., Brandeker, A., et al. 2008, *A&A*, 480, L47, doi: [10.1051/0004-6361:20079276](https://doi.org/10.1051/0004-6361:20079276)
- Liu, L., & Pang, X. 2019, *ApJS*, 245, 32, doi: [10.3847/1538-4365/ab530a](https://doi.org/10.3847/1538-4365/ab530a)
- Liu, M. C., Matthews, B. C., Williams, J. P., & Kalas, P. G. 2004, *ApJ*, 608, 526, doi: [10.1086/392531](https://doi.org/10.1086/392531)
- Llorrente de Andrés, F., Chavero, C., de la Reza, R., Roca-Fàbrega, S., & Cifuentes, C. 2021, *A&A*, 654, A137, doi: [10.1051/0004-6361/202141339](https://doi.org/10.1051/0004-6361/202141339)
- Lodieu, N., Pérez-Garrido, A., Smart, R. L., & Silvotti, R. 2019a, *A&A*, 628, A66, doi: [10.1051/0004-6361/201935533](https://doi.org/10.1051/0004-6361/201935533)
- Lodieu, N., Smart, R. L., Pérez-Garrido, A., & Silvotti, R. 2019b, *A&A*, 623, A35, doi: [10.1051/0004-6361/201834045](https://doi.org/10.1051/0004-6361/201834045)
- López-Valdivia, R., Hernández-Águila, J. B., Bertone, E., et al. 2015, *MNRAS*, 451, 4368, doi: [10.1093/mnras/stv1222](https://doi.org/10.1093/mnras/stv1222)
- Lorenzo-Oliveira, D., Porto de Mello, G. F., Dutra-Ferreira, L., & Ribas, I. 2016, *A&A*, 595, A11, doi: [10.1051/0004-6361/201628825](https://doi.org/10.1051/0004-6361/201628825)
- Lorenzo-Oliveira, D., Freitas, F. C., Meléndez, J., et al. 2018, *A&A*, 619, A73, doi: [10.1051/0004-6361/201629294](https://doi.org/10.1051/0004-6361/201629294)
- Lovell, J. B., Marino, S., Wyatt, M. C., et al. 2021, *MNRAS*, 506, 1978, doi: [10.1093/mnras/stab1678](https://doi.org/10.1093/mnras/stab1678)
- Low, F. J., Smith, P. S., Werner, M., et al. 2005, *ApJ*, 631, 1170, doi: [10.1086/432640](https://doi.org/10.1086/432640)
- Lubin, D., Holden, B. P., Stock, C., Melis, C., & Tytler, D. 2024, *AJ*, 168, 240, doi: [10.3847/1538-3881/ad823d](https://doi.org/10.3847/1538-3881/ad823d)
- Luhman, K. L. 2022, *AJ*, 163, 24, doi: [10.3847/1538-3881/ac35e2](https://doi.org/10.3847/1538-3881/ac35e2)
- Luhman, K. L. 2023a, *AJ*, 165, 37, doi: [10.3847/1538-3881/ac9da3](https://doi.org/10.3847/1538-3881/ac9da3)
- Luhman, K. L. 2023b, *AJ*, 165, 269, doi: [10.3847/1538-3881/accf19](https://doi.org/10.3847/1538-3881/accf19)
- Luhman, K. L., & Esplin, T. L. 2022, *AJ*, 163, 26, doi: [10.3847/1538-3881/ac35e4](https://doi.org/10.3847/1538-3881/ac35e4)
- Lurie, J. C., Henry, T. J., Jao, W.-C., et al. 2014, *AJ*, 148, 91, doi: [10.1088/0004-6256/148/5/91](https://doi.org/10.1088/0004-6256/148/5/91)
- Lyra, W., Moitinho, A., van der Blik, N. S., & Alves, J. 2006, *A&A*, 453, 101, doi: [10.1051/0004-6361:20053894](https://doi.org/10.1051/0004-6361:20053894)
- MacGregor, M. A., Wilner, D. J., Chandler, C., et al. 2016, *ApJ*, 823, 79, doi: [10.3847/0004-637X/823/2/79](https://doi.org/10.3847/0004-637X/823/2/79)
- MacGregor, M. A., Matrà, L., Kalas, P., et al. 2017, *ApJ*, 842, 8, doi: [10.3847/1538-4357/aa71ae](https://doi.org/10.3847/1538-4357/aa71ae)
- MacGregor, M. A., Hurt, S. A., Stark, C. C., et al. 2022, *ApJL*, 933, L1, doi: [10.3847/2041-8213/ac7729](https://doi.org/10.3847/2041-8213/ac7729)
- Magaudda, E., Stelzer, B., Covey, K. R., et al. 2020, *A&A*, 638, A20, doi: [10.1051/0004-6361/201937408](https://doi.org/10.1051/0004-6361/201937408)
- Magaudda, E., Stelzer, B., Raetz, S., et al. 2022, *A&A*, 661, A29, doi: [10.1051/0004-6361/202141617](https://doi.org/10.1051/0004-6361/202141617)
- Malo, L., Artigau, É., Doyon, R., et al. 2014, *ApJ*, 788, 81, doi: [10.1088/0004-637X/788/1/81](https://doi.org/10.1088/0004-637X/788/1/81)
- Mamajek, E. E., & Hillenbrand, L. A. 2008, *ApJ*, 687, 1264, doi: [10.1086/591785](https://doi.org/10.1086/591785)
- Mamajek, E. E., Lawson, W. A., & Feigelson, E. D. 1999, *ApJL*, 516, L77, doi: [10.1086/312005](https://doi.org/10.1086/312005)
- Manara, C. F., Ansdell, M., Rosotti, G. P., et al. 2023, in *Astronomical Society of the Pacific Conference Series*, Vol. 534, *Protostars and Planets VII*, ed. S. Inutsuka, Y. Aikawa, T. Muto, K. Tomida, & M. Tamura, 539, doi: [10.48550/arXiv.2203.09930](https://doi.org/10.48550/arXiv.2203.09930)

- Manara, C. F., Testi, L., Rigliaco, E., et al. 2013, *A&A*, 551, A107, doi: [10.1051/0004-6361/201220921](https://doi.org/10.1051/0004-6361/201220921)
- Marino, S., Wyatt, M. C., Kennedy, G. M., et al. 2017, *MNRAS*, 469, 3518, doi: [10.1093/mnras/stx1102](https://doi.org/10.1093/mnras/stx1102)
- Marino, S., Yelverton, B., Booth, M., et al. 2019, *MNRAS*, 484, 1257, doi: [10.1093/mnras/stz049](https://doi.org/10.1093/mnras/stz049)
- Marino, S., Carpenter, J., Wyatt, M. C., et al. 2018, *MNRAS*, 479, 5423, doi: [10.1093/mnras/sty1790](https://doi.org/10.1093/mnras/sty1790)
- Marino, S., Zurlo, A., Faramaz, V., et al. 2020, *MNRAS*, 498, 1319, doi: [10.1093/mnras/staa2386](https://doi.org/10.1093/mnras/staa2386)
- Marino, S., Matrà, L., Hughes, A. M., et al. 2026, *A&A*, 705, A195, doi: [10.1051/0004-6361/202556489](https://doi.org/10.1051/0004-6361/202556489)
- Marsden, S. C., Evensberger, D., Brown, E. L., et al. 2023, *MNRAS*, 522, 792, doi: [10.1093/mnras/stad925](https://doi.org/10.1093/mnras/stad925)
- Marshall, J. P., Maddison, S. T., Thilliez, E., et al. 2017, *MNRAS*, 468, 2719, doi: [10.1093/mnras/stx645](https://doi.org/10.1093/mnras/stx645)
- Marshall, J. P., Milli, J., Choquet, E., et al. 2023, *MNRAS*, 521, 5940, doi: [10.1093/mnras/stad913](https://doi.org/10.1093/mnras/stad913)
- Martin, J., Fuhrmeister, B., Mittag, M., et al. 2017, *A&A*, 605, A113, doi: [10.1051/0004-6361/201630298](https://doi.org/10.1051/0004-6361/201630298)
- Martínez-Arnáiz, R., Maldonado, J., Montes, D., Eiroa, C., & Montesinos, B. 2010, *A&A*, 520, A79, doi: [10.1051/0004-6361/200913725](https://doi.org/10.1051/0004-6361/200913725)
- Marvin, C. J., Reiners, A., Anglada-Escudé, G., Jeffers, S. V., & Boro Saikia, S. 2023, *A&A*, 671, A162, doi: [10.1051/0004-6361/201937306](https://doi.org/10.1051/0004-6361/201937306)
- Mason, B. D., Wycoff, G. L., Hartkopf, W. I., Douglass, G. G., & Worley, C. E. 2001, *AJ*, 122, 3466, doi: [10.1086/323920](https://doi.org/10.1086/323920)
- Mathews, G. S., Pinte, C., Duchêne, G., Williams, J. P., & Ménard, F. 2013, *A&A*, 558, A66, doi: [10.1051/0004-6361/201321228](https://doi.org/10.1051/0004-6361/201321228)
- Mathews, G. S., Williams, J. P., Ménard, F., et al. 2012, *ApJ*, 745, 23, doi: [10.1088/0004-637X/745/1/23](https://doi.org/10.1088/0004-637X/745/1/23)
- Mathur, S., Santos, Â. R. G., Claytor, Z. R., et al. 2025, *ApJ*, 982, 114, doi: [10.3847/1538-4357/adb8cc](https://doi.org/10.3847/1538-4357/adb8cc)
- Matrà, L., Dent, W. R. F., Wilner, D. J., et al. 2020, *ApJ*, 898, 146, doi: [10.3847/1538-4357/aba0a4](https://doi.org/10.3847/1538-4357/aba0a4)
- Matrà, L., Marino, S., Wilner, D. J., et al. 2025, *A&A*, 693, A151, doi: [10.1051/0004-6361/202451397](https://doi.org/10.1051/0004-6361/202451397)
- Matthews, B. C., Krivov, A. V., Wyatt, M. C., Bryden, G., & Eiroa, C. 2014, in *Protostars and Planet VI*, ed. Beuther, H., Klessen, R. S., Dullemond, C. P., & Henning, T. (The University of Arizona Press, Tucson, AZ), 521–544
- Matthews, B. C., Sibthorpe, B., Kennedy, G., et al. 2010, *A&A*, 518, L135, doi: [10.1051/0004-6361/201014667](https://doi.org/10.1051/0004-6361/201014667)
- McQuillan, A., Mazeh, T., & Aigrain, S. 2014, *ApJS*, 211, 24, doi: [10.1088/0067-0049/211/2/24](https://doi.org/10.1088/0067-0049/211/2/24)
- Mellon, S. N., Mamajek, E. E., Oberst, T. E., & Pecaut, M. J. 2017, *ApJ*, 844, 66, doi: [10.3847/1538-4357/aa77fb](https://doi.org/10.3847/1538-4357/aa77fb)
- Merloni, A., Lamer, G., Liu, T., et al. 2024, *A&A*, 682, A34, doi: [10.1051/0004-6361/202347165](https://doi.org/10.1051/0004-6361/202347165)
- Mermilliod, J. C. 1987a, *A&AS*, 71, 413
- Mermilliod, J. C. 1987b, *A&AS*, 71, 119
- Mermilliod, J.-C. 1995, in *Information & On-Line Data in Astronomy*, ed. D. Egret & M. A. Albrecht, Vol. 203 (Springer), 127, doi: [10.1007/978-94-011-0397-8_12](https://doi.org/10.1007/978-94-011-0397-8_12)
- Mermilliod, J. C., Platais, I., James, D. J., Grenon, M., & Cargile, P. A. 2008, *A&A*, 485, 95, doi: [10.1051/0004-6361:20079072](https://doi.org/10.1051/0004-6361:20079072)
- Messina, S., Millward, M., Buccino, A., et al. 2017, *A&A*, 600, A83, doi: [10.1051/0004-6361/201629152](https://doi.org/10.1051/0004-6361/201629152)
- Metcalfe, T. S., Basu, S., Henry, T. J., et al. 2010, *ApJL*, 723, L213, doi: [10.1088/2041-8205/723/2/L213](https://doi.org/10.1088/2041-8205/723/2/L213)
- Meunier, N., Kretzschmar, M., Gravet, R., Mignon, L., & Delfosse, X. 2022, *A&A*, 658, A57, doi: [10.1051/0004-6361/202142120](https://doi.org/10.1051/0004-6361/202142120)
- Meunier, N., & Lagrange, A.-M. 2022, *A&A*, 659, A104, doi: [10.1051/0004-6361/202142702](https://doi.org/10.1051/0004-6361/202142702)
- Meyer, M. R., Hillenbrand, L. A., Backman, D., et al. 2006, *PASP*, 118, 1690, doi: [10.1086/510099](https://doi.org/10.1086/510099)
- Meyer, M. R., Carpenter, J. M., Mamajek, E. E., et al. 2008, *ApJL*, 673, L181, doi: [10.1086/527470](https://doi.org/10.1086/527470)
- Meynet, G., Mermilliod, J. C., & Maeder, A. 1993, *A&AS*, 98, 477
- Micela, G., Sciortino, S., Harnden, F. R., J., et al. 1999, *A&A*, 341, 751
- Middelkoop, F. 1982, *A&A*, 107, 31
- Mignon, L., Meunier, N., Delfosse, X., et al. 2023, *A&A*, 675, A168, doi: [10.1051/0004-6361/202244249](https://doi.org/10.1051/0004-6361/202244249)
- Mignon, L., Delfosse, X., Meunier, N., et al. 2025, *A&A*, 700, A146, doi: [10.1051/0004-6361/202451142](https://doi.org/10.1051/0004-6361/202451142)
- Mikkola, D., McMillan, P. J., & Hobbs, D. 2023, *MNRAS*, 519, 1989, doi: [10.1093/mnras/stac3649](https://doi.org/10.1093/mnras/stac3649)
- Miret-Roig, N., Galli, P. A. B., Olivares, J., et al. 2022, *A&A*, 667, A163, doi: [10.1051/0004-6361/202244709](https://doi.org/10.1051/0004-6361/202244709)
- Miret-Roig, N., Galli, P. A. B., Brandner, W., et al. 2020, *A&A*, 642, A179, doi: [10.1051/0004-6361/202038765](https://doi.org/10.1051/0004-6361/202038765)
- Monet, D. G., Levine, S. E., Canzian, B., et al. 2003, *AJ*, 125, 984, doi: [10.1086/345888](https://doi.org/10.1086/345888)
- Monroe, T. R., & Pilachowski, C. A. 2010, *AJ*, 140, 2109, doi: [10.1088/0004-6256/140/6/2109](https://doi.org/10.1088/0004-6256/140/6/2109)
- Montegriffo, P., De Angeli, F., Andrae, R., et al. 2023, *A&A*, 674, A3, doi: [10.1051/0004-6361/202243880](https://doi.org/10.1051/0004-6361/202243880)
- Montes, D., López-Santiago, J., Gálvez, M. C., et al. 2001, *MNRAS*, 328, 45, doi: [10.1046/j.1365-8711.2001.04781.x](https://doi.org/10.1046/j.1365-8711.2001.04781.x)
- Montesinos, B., Eiroa, C., Krivov, A. V., et al. 2016, *A&A*, 593, A51, doi: [10.1051/0004-6361/201628329](https://doi.org/10.1051/0004-6361/201628329)

- Moór, A., Pascucci, I., Kóspál, Á., et al. 2011, *ApJS*, 193, 4, doi: [10.1088/0067-0049/193/1/4](https://doi.org/10.1088/0067-0049/193/1/4)
- Morales, F. Y., Bryden, G., Werner, M. W., & Stapelfeldt, K. R. 2016, *ApJ*, 831, 97, doi: [10.3847/0004-637X/831/1/97](https://doi.org/10.3847/0004-637X/831/1/97)
- Morales, F. Y., Werner, M. W., Bryden, G., et al. 2009, *ApJ*, 699, 1067, doi: [10.1088/0004-637X/699/2/1067](https://doi.org/10.1088/0004-637X/699/2/1067)
- Moraux, E., Bouvier, J., Stauffer, J. R., Barrado y Navascués, D., & Cuillandre, J. C. 2007, *A&A*, 471, 499, doi: [10.1051/0004-6361:20066308](https://doi.org/10.1051/0004-6361:20066308)
- Moshir, M., Kopman, G., & Conrow, T. A. O. 1992, *IRAS Faint Source Survey, Explanatory supplement version 2* (Caltech Infrared Processing and Analysis Center, Pasadena, CA USA)
- Mucciarelli, A., Bellazzini, M., & Massari, D. 2021, *A&A*, 653, A90, doi: [10.1051/0004-6361/202140979](https://doi.org/10.1051/0004-6361/202140979)
- Muirhead, P. S., Nordhaus, J., & Drout, M. R. 2022, *AJ*, 163, 34, doi: [10.3847/1538-3881/ac390f](https://doi.org/10.3847/1538-3881/ac390f)
- Murakami, H., Baba, H., Barthel, P., et al. 2007, *PASJ*, 59, S369, doi: [10.1093/pasj/59.sp2.S369](https://doi.org/10.1093/pasj/59.sp2.S369)
- Murphy, S. J., & Lawson, W. A. 2015, *MNRAS*, 447, 1267, doi: [10.1093/mnras/stu2450](https://doi.org/10.1093/mnras/stu2450)
- Najita, J., & Williams, J. P. 2005, *ApJ*, 635, 625, doi: [10.1086/497159](https://doi.org/10.1086/497159)
- Najita, J. R., Kenyon, S. J., & Bromley, B. C. 2022, *ApJ*, 925, 45, doi: [10.3847/1538-4357/ac37b6](https://doi.org/10.3847/1538-4357/ac37b6)
- Nandakumar, G., Schultheis, M., Hayden, M., et al. 2017, *A&A*, 606, A97, doi: [10.1051/0004-6361/201731099](https://doi.org/10.1051/0004-6361/201731099)
- Naylor, T., Totten, E. J., Jeffries, R. D., et al. 2002, *MNRAS*, 335, 291, doi: [10.1046/j.1365-8711.2002.05592.x](https://doi.org/10.1046/j.1365-8711.2002.05592.x)
- Niederlander, A., Hughes, A. M., Fehr, A. J., et al. 2021, *ApJ*, 917, 5, doi: [10.3847/1538-4357/abdd32](https://doi.org/10.3847/1538-4357/abdd32)
- Neugebauer, G., Habing, H. J., van Duinen, R., et al. 1984, *ApJL*, 278, L1, doi: [10.1086/184209](https://doi.org/10.1086/184209)
- Newton, E. R., Charbonneau, D., Irwin, J., et al. 2014, *AJ*, 147, 20, doi: [10.1088/0004-6256/147/1/20](https://doi.org/10.1088/0004-6256/147/1/20)
- Newton, E. R., Irwin, J., Charbonneau, D., et al. 2017, *ApJ*, 834, 85, doi: [10.3847/1538-4357/834/1/85](https://doi.org/10.3847/1538-4357/834/1/85)
- Newton, E. R., Irwin, J., Charbonneau, D., et al. 2016, *ApJ*, 821, 93, doi: [10.3847/0004-637X/821/2/93](https://doi.org/10.3847/0004-637X/821/2/93)
- Newton, E. R., Mondrik, N., Irwin, J., Winters, J. G., & Charbonneau, D. 2018, *AJ*, 156, 217, doi: [10.3847/1538-3881/aad73b](https://doi.org/10.3847/1538-3881/aad73b)
- Nilsson, R., Liseau, R., Brandeker, A., et al. 2010, *A&A*, 518, A40, doi: [10.1051/0004-6361/201014444](https://doi.org/10.1051/0004-6361/201014444)
- Nisak, A. H., White, R. J., Yep, A., et al. 2022, *AJ*, 163, 278, doi: [10.3847/1538-3881/ac63c3](https://doi.org/10.3847/1538-3881/ac63c3)
- Niu, Z., Yuan, H., Wang, S., & Liu, J. 2021, *ApJ*, 922, 211, doi: [10.3847/1538-4357/ac2573](https://doi.org/10.3847/1538-4357/ac2573)
- Nordström, B., Mayor, M., Andersen, J., et al. 2004, *A&A*, 418, 989, doi: [10.1051/0004-6361:20035959](https://doi.org/10.1051/0004-6361:20035959)
- Norfolk, B. J., Maddison, S. T., Marshall, J. P., et al. 2021, *MNRAS*, 507, 3139, doi: [10.1093/mnras/stab1901](https://doi.org/10.1093/mnras/stab1901)
- Noyes, R. W., Hartmann, L. W., Baliunas, S. L., Duncan, D. K., & Vaughan, A. H. 1984, *ApJ*, 279, 763, doi: [10.1086/161945](https://doi.org/10.1086/161945)
- Núñez, A., Agüeros, M. A., Covey, K. R., et al. 2022, *ApJ*, 931, 45, doi: [10.3847/1538-4357/ac6517](https://doi.org/10.3847/1538-4357/ac6517)
- Núñez, A., Agüeros, M. A., Curtis, J. L., et al. 2024, *ApJ*, 962, 12, doi: [10.3847/1538-4357/ad117e](https://doi.org/10.3847/1538-4357/ad117e)
- Ochsenbein, F., Bauer, P., & Marcout, J. 2000, *A&AS*, 143, 23, doi: [10.1051/aas:2000169](https://doi.org/10.1051/aas:2000169)
- Oelkers, R. J., Macri, L. M., Marshall, J. L., et al. 2016, *AJ*, 152, 75, doi: [10.3847/0004-6256/152/3/75](https://doi.org/10.3847/0004-6256/152/3/75)
- Oh, S., & Evans, N. W. 2020, *MNRAS*, 498, 1920, doi: [10.1093/mnras/staa2381](https://doi.org/10.1093/mnras/staa2381)
- Olivares, J., Lodieu, N., Bejar, V. J. S., et al. 2023, *A&A*, 675, A28, doi: [10.1051/0004-6361/202244703](https://doi.org/10.1051/0004-6361/202244703)
- Oliveira, J. M., Jeffries, R. D., Devey, C. R., et al. 2003, *MNRAS*, 342, 651, doi: [10.1046/j.1365-8711.2003.06592.x](https://doi.org/10.1046/j.1365-8711.2003.06592.x)
- Oliveira, J. M., Jeffries, R. D., Kenyon, M. J., Thompson, S. A., & Naylor, T. 2002, *A&A*, 382, L22, doi: [10.1051/0004-6361:20011778](https://doi.org/10.1051/0004-6361:20011778)
- Oliveira, J. M., Jeffries, R. D., & van Loon, J. T. 2004, *MNRAS*, 347, 1327, doi: [10.1111/j.1365-2966.2004.07315.x](https://doi.org/10.1111/j.1365-2966.2004.07315.x)
- Olofsson, J., van Holstein, R. G., Boccaletti, A., et al. 2018, *A&A*, 617, A109, doi: [10.1051/0004-6361/201832583](https://doi.org/10.1051/0004-6361/201832583)
- O'Neill, T. J., Goodman, A. A., Soler, J. D., Zucker, C., & Han, J. J. 2025, *ApJ*, 988, 191, doi: [10.3847/1538-4357/ade306](https://doi.org/10.3847/1538-4357/ade306)
- O'Neill, T. J., Zucker, C., Goodman, A. A., & Edenhofer, G. 2024, arXiv e-prints, arXiv:2403.04961, doi: [10.48550/arXiv.2403.04961](https://doi.org/10.48550/arXiv.2403.04961)
- Onken, C. A., Wolf, C., Bessell, M. S., et al. 2024, arXiv e-prints, arXiv:2402.02015, doi: [10.48550/arXiv.2402.02015](https://doi.org/10.48550/arXiv.2402.02015)
- Pace, G., Castro, M., Meléndez, J., Théado, S., & do Nascimento, J. D., J. 2012, *A&A*, 541, A150, doi: [10.1051/0004-6361/201117704](https://doi.org/10.1051/0004-6361/201117704)
- Padgett, D. L., Rebull, L. M., Stapelfeldt, K. R., et al. 2008, *ApJ*, 672, 1013, doi: [10.1086/523883](https://doi.org/10.1086/523883)
- Pang, X., Li, Y., Yu, Z., et al. 2021, *ApJ*, 912, 162, doi: [10.3847/1538-4357/abeaac](https://doi.org/10.3847/1538-4357/abeaac)
- Pang, X., Tang, S.-Y., Li, Y., et al. 2022, *ApJ*, 931, 156, doi: [10.3847/1538-4357/ac674e](https://doi.org/10.3847/1538-4357/ac674e)
- Pawellek, N., Wyatt, M., Matrà, L., Kennedy, G., & Yelverton, B. 2021, *MNRAS*, 502, 5390, doi: [10.1093/mnras/stab269](https://doi.org/10.1093/mnras/stab269)

- Pearce, T. D., Launhardt, R., Ostermann, R., et al. 2022, *A&A*, 659, A135, doi: [10.1051/0004-6361/202142720](https://doi.org/10.1051/0004-6361/202142720)
- Pecaut, M. J., & Mamajek, E. E. 2013, *ApJS*, 208, 9, doi: [10.1088/0067-0049/208/1/9](https://doi.org/10.1088/0067-0049/208/1/9)
- Pecaut, M. J., & Mamajek, E. E. 2016, *MNRAS*, 461, 794, doi: [10.1093/mnras/stw1300](https://doi.org/10.1093/mnras/stw1300)
- Perdelwitz, V., Mittag, M., Tal-Or, L., et al. 2021, *A&A*, 652, A116, doi: [10.1051/0004-6361/202140889](https://doi.org/10.1051/0004-6361/202140889)
- Perryman, M. A. C., Lindegren, L., Kovalevsky, J., et al. 1997, *A&A*, 323, L49
- Petigura, E. A., Howard, A. W., & Marcy, G. W. 2013, *Proceedings of the National Academy of Science*, 110, 19273, doi: [10.1073/pnas.1319909110](https://doi.org/10.1073/pnas.1319909110)
- Petit, P., Böhm, T., Folsom, C. P., Lignières, F., & Cang, T. 2022, *A&A*, 666, A20, doi: [10.1051/0004-6361/202143000](https://doi.org/10.1051/0004-6361/202143000)
- Petit, P., Lignières, F., Aurière, M., et al. 2011, *A&A*, 532, L13, doi: [10.1051/0004-6361/201117573](https://doi.org/10.1051/0004-6361/201117573)
- Phillips, N. M., Greaves, J. S., Dent, W. R. F., et al. 2010, *MNRAS*, 403, 1089, doi: [10.1111/j.1365-2966.2009.15641.x](https://doi.org/10.1111/j.1365-2966.2009.15641.x)
- Piccotti, L., Docobo, J. Á., Carini, R., et al. 2020, *MNRAS*, 492, 2709, doi: [10.1093/mnras/stz3616](https://doi.org/10.1093/mnras/stz3616)
- Pillitteri, I., Micela, G., Damiani, F., & Sciortino, S. 2006, *A&A*, 450, 993, doi: [10.1051/0004-6361:20054003](https://doi.org/10.1051/0004-6361:20054003)
- Pillitteri, I., Micela, G., Sciortino, S., Damiani, F., & Harnden, F. R., J. 2004, *A&A*, 421, 175, doi: [10.1051/0004-6361:20035869](https://doi.org/10.1051/0004-6361:20035869)
- Pinsonneault, M. 1997, *ARA&A*, 35, 557, doi: [10.1146/annurev.astro.35.1.557](https://doi.org/10.1146/annurev.astro.35.1.557)
- Pittman, C. V., Espaillat, C. C., Robinson, C. E., et al. 2025, *ApJ*, 992, 134, doi: [10.3847/1538-4357/ade335](https://doi.org/10.3847/1538-4357/ade335)
- Plavchan, P., Werner, M. W., Chen, C. H., et al. 2009, *ApJ*, 698, 1068, doi: [10.1088/0004-637X/698/2/1068](https://doi.org/10.1088/0004-637X/698/2/1068)
- Poglitsch, A., Waelkens, C., Geis, N., et al. 2010, *A&A*, 518, L2, doi: [10.1051/0004-6361/201014535](https://doi.org/10.1051/0004-6361/201014535)
- Popinchalk, M., Faherty, J. K., Curtis, J. L., et al. 2023, *ApJ*, 945, 114, doi: [10.3847/1538-4357/acb055](https://doi.org/10.3847/1538-4357/acb055)
- Popper, D. M. 1990, *AJ*, 100, 247, doi: [10.1086/115511](https://doi.org/10.1086/115511)
- Pourbaix, D., Tokovinin, A. A., Batten, A. H., et al. 2004, *A&A*, 424, 727, doi: [10.1051/0004-6361:20041213](https://doi.org/10.1051/0004-6361:20041213)
- Predehl, P., Hasinger, G., Böhringer, H., et al. 2006, in *Society of Photo-Optical Instrumentation Engineers (SPIE) Conference Series*, Vol. 6266, *Space Telescopes and Instrumentation II: Ultraviolet to Gamma Ray*, ed. M. J. L. Turner & G. Hasinger, 62660P, doi: [10.1117/12.670249](https://doi.org/10.1117/12.670249)
- Preibisch, T., Brown, A. G. A., Bridges, T., Guenther, E., & Zinnecker, H. 2002, *AJ*, 124, 404, doi: [10.1086/341174](https://doi.org/10.1086/341174)
- Preibisch, T., Guenther, E., Zinnecker, H., et al. 1998, *A&A*, 333, 619
- Prisinzano, L., Micela, G., Sciortino, S., & Favata, F. 2003, *A&A*, 404, 927, doi: [10.1051/0004-6361:20030524](https://doi.org/10.1051/0004-6361:20030524)
- Queiroz, A. B. A., Anders, F., Chiappini, C., et al. 2023, *A&A*, 673, A155, doi: [10.1051/0004-6361/202245399](https://doi.org/10.1051/0004-6361/202245399)
- Raghavan, D., McAlister, H. A., Torres, G., et al. 2009, *ApJ*, 690, 394, doi: [10.1088/0004-637X/690/1/394](https://doi.org/10.1088/0004-637X/690/1/394)
- Rainer, M., Desidera, S., Borsa, F., et al. 2023, *A&A*, 676, A90, doi: [10.1051/0004-6361/202245564](https://doi.org/10.1051/0004-6361/202245564)
- Ramírez, I., Fish, J. R., Lambert, D. L., & Allende Prieto, C. 2012, *ApJ*, 756, 46, doi: [10.1088/0004-637X/756/1/46](https://doi.org/10.1088/0004-637X/756/1/46)
- Ramírez, I., Meléndez, J., Bean, J., et al. 2014, *A&A*, 572, A48, doi: [10.1051/0004-6361/201424244](https://doi.org/10.1051/0004-6361/201424244)
- Rampalli, R., Agüeros, M. A., Curtis, J. L., et al. 2021, *ApJ*, 921, 167, doi: [10.3847/1538-4357/ac0c1e](https://doi.org/10.3847/1538-4357/ac0c1e)
- Randich, S., Schmitt, J. H. M. M., Prosser, C. F., & Stauffer, J. R. 1996, *A&A*, 305, 785
- Randich, S., Gilmore, G., Magrini, L., et al. 2022, *A&A*, 666, A121, doi: [10.1051/0004-6361/202243141](https://doi.org/10.1051/0004-6361/202243141)
- Rathsam, A., Meléndez, J., & Carvalho Silva, G. 2023, *MNRAS*, 525, 4642, doi: [10.1093/mnras/stad2589](https://doi.org/10.1093/mnras/stad2589)
- Ratzenböck, S., Großschedl, J. E., Möller, T., et al. 2023, *A&A*, 677, A59, doi: [10.1051/0004-6361/202243690](https://doi.org/10.1051/0004-6361/202243690)
- Rebull, L. M., Stauffer, J. R., Cody, A. M., et al. 2020, *AJ*, 159, 273, doi: [10.3847/1538-3881/ab893c](https://doi.org/10.3847/1538-3881/ab893c)
- Rebull, L. M., Stauffer, J. R., Cody, A. M., et al. 2018, *AJ*, 155, 196, doi: [10.3847/1538-3881/aab605](https://doi.org/10.3847/1538-3881/aab605)
- Rebull, L. M., Stauffer, J. R., Hillenbrand, L. A., et al. 2017, *ApJ*, 839, 92, doi: [10.3847/1538-4357/aa6aa4](https://doi.org/10.3847/1538-4357/aa6aa4)
- Rebull, L. M., Stauffer, J. R., Hillenbrand, L. A., et al. 2022, *AJ*, 164, 80, doi: [10.3847/1538-3881/ac75f1](https://doi.org/10.3847/1538-3881/ac75f1)
- Rebull, L. M., Wolff, S. C., & Strom, S. E. 2004, *AJ*, 127, 1029, doi: [10.1086/380931](https://doi.org/10.1086/380931)
- Rebull, L. M., Stapelfeldt, K. R., Werner, M. W., et al. 2008, *ApJ*, 681, 1484, doi: [10.1086/588182](https://doi.org/10.1086/588182)
- Rebull, L. M., Stauffer, J. R., Bouvier, J., et al. 2016, *AJ*, 152, 113, doi: [10.3847/0004-6256/152/5/113](https://doi.org/10.3847/0004-6256/152/5/113)
- Reid, I. N., Kilkenny, D., & Cruz, K. L. 2002, *AJ*, 123, 2822, doi: [10.1086/339700](https://doi.org/10.1086/339700)
- Reiners, A., Joshi, N., & Goldman, B. 2012, *AJ*, 143, 93, doi: [10.1088/0004-6256/143/4/93](https://doi.org/10.1088/0004-6256/143/4/93)
- Reiners, A., Zechmeister, M., Caballero, J. A., et al. 2018, *A&A*, 612, A49, doi: [10.1051/0004-6361/201732054](https://doi.org/10.1051/0004-6361/201732054)
- Reiners, A., Shulyak, D., Käpylä, P. J., et al. 2022, *A&A*, 662, A41, doi: [10.1051/0004-6361/202243251](https://doi.org/10.1051/0004-6361/202243251)
- Rhee, J. H., Song, I., & Zuckerman, B. 2007, *ApJ*, 671, 616, doi: [10.1086/520760](https://doi.org/10.1086/520760)
- Riaz, B., Mullan, D. J., & Gizis, J. E. 2006, *ApJ*, 650, 1133, doi: [10.1086/507446](https://doi.org/10.1086/507446)

- Riedel, A. R., Finch, C. T., Henry, T. J., et al. 2014, *AJ*, 147, 85, doi: [10.1088/0004-6256/147/4/85](https://doi.org/10.1088/0004-6256/147/4/85)
- Rieke, G. H., Young, E. T., Engelbracht, C. W., et al. 2004, *ApJS*, 154, 25, doi: [10.1086/422717](https://doi.org/10.1086/422717)
- Rieke, G. H., Su, K. Y. L., Stansberry, J. A., et al. 2005, *ApJ*, 620, 1010, doi: [10.1086/426937](https://doi.org/10.1086/426937)
- Riello, M., De Angeli, F., Evans, D. W., et al. 2021, *A&A*, 649, A3, doi: [10.1051/0004-6361/202039587](https://doi.org/10.1051/0004-6361/202039587)
- Riviere-Marichalar, P., Pinte, C., Barrado, D., et al. 2013, *A&A*, 555, A67, doi: [10.1051/0004-6361/201321506](https://doi.org/10.1051/0004-6361/201321506)
- Riviere-Marichalar, P., Barrado, D., Montesinos, B., et al. 2014, *A&A*, 565, A68, doi: [10.1051/0004-6361/201322901](https://doi.org/10.1051/0004-6361/201322901)
- Riviere-Marichalar, P., Elliott, P., Rebollido, I., et al. 2015, *A&A*, 584, A22, doi: [10.1051/0004-6361/201526584](https://doi.org/10.1051/0004-6361/201526584)
- Robrade, J., Czesla, S., Freund, S., Schmitt, J. H. M. M., & Schneider, P. C. 2022, *A&A*, 661, A34, doi: [10.1051/0004-6361/202141124](https://doi.org/10.1051/0004-6361/202141124)
- Roccatagliata, V., Henning, T., Wolf, S., et al. 2009, *A&A*, 497, 409, doi: [10.1051/0004-6361/200811018](https://doi.org/10.1051/0004-6361/200811018)
- Roccatagliata, V., Sicilia-Aguilar, A., Kim, M., et al. 2024, *A&A*, 682, A63, doi: [10.1051/0004-6361/202346655](https://doi.org/10.1051/0004-6361/202346655)
- Rojas-Ayala, B., Covey, K. R., Muirhead, P. S., & Lloyd, J. P. 2012, *ApJ*, 748, 93, doi: [10.1088/0004-637X/748/2/93](https://doi.org/10.1088/0004-637X/748/2/93)
- Roman, N. G. 1949, *ApJ*, 110, 205, doi: [10.1086/145199](https://doi.org/10.1086/145199)
- Romano, D., Magrini, L., Randich, S., et al. 2021, *A&A*, 653, A72, doi: [10.1051/0004-6361/202141340](https://doi.org/10.1051/0004-6361/202141340)
- Royer, F., Gerbaldi, M., Faraggiana, R., & Gómez, A. E. 2002a, *A&A*, 381, 105, doi: [10.1051/0004-6361:20011422](https://doi.org/10.1051/0004-6361:20011422)
- Royer, F., Grenier, S., Baylac, M. O., Gómez, A. E., & Zorec, J. 2002b, *A&A*, 393, 897, doi: [10.1051/0004-6361:20020943](https://doi.org/10.1051/0004-6361:20020943)
- Royer, F., Zorec, J., & Gómez, A. E. 2007, *A&A*, 463, 671, doi: [10.1051/0004-6361:20065224](https://doi.org/10.1051/0004-6361:20065224)
- Rugel, M., Fedele, D., & Herczeg, G. 2018, *A&A*, 609, A70, doi: [10.1051/0004-6361/201630111](https://doi.org/10.1051/0004-6361/201630111)
- Ryabchikova, T., Zvyagintsev, S., Tkachenko, A., et al. 2022, *MNRAS*, 509, 202, doi: [10.1093/mnras/stab2891](https://doi.org/10.1093/mnras/stab2891)
- Samus', N. N., Kazarovets, E. V., Durlevich, O. V., Kireeva, N. N., & Pastukhova, E. N. 2017, *Astronomy Reports*, 61, 80, doi: [10.1134/S1063772917010085](https://doi.org/10.1134/S1063772917010085)
- Santos, A. R. G., Godoy-Rivera, D., Mathur, S., et al. 2025, *A&A*, 697, A177, doi: [10.1051/0004-6361/202554030](https://doi.org/10.1051/0004-6361/202554030)
- Schleicher, D. R. G., Hidalgo, J. P., & Galli, D. 2023, *A&A*, 678, A204, doi: [10.1051/0004-6361/202346809](https://doi.org/10.1051/0004-6361/202346809)
- Schmitt, J. H. M. M., Czesla, S., Freund, S., Robrade, J., & Schneider, P. C. 2022, *A&A*, 661, A40, doi: [10.1051/0004-6361/202141132](https://doi.org/10.1051/0004-6361/202141132)
- Schöfer, P., Jeffers, S. V., Reiners, A., et al. 2019, *A&A*, 623, A44, doi: [10.1051/0004-6361/201834114](https://doi.org/10.1051/0004-6361/201834114)
- Schröder, C., Reiners, A., & Schmitt, J. H. M. M. 2009a, *A&A*, 493, 1099, doi: [10.1051/0004-6361:200810377](https://doi.org/10.1051/0004-6361:200810377)
- Schröder, C., Reiners, A., & Schmitt, J. H. M. M. 2009b, *A&A*, 493, 1099, doi: [10.1051/0004-6361:200810377](https://doi.org/10.1051/0004-6361:200810377)
- Sciortino, S., Damiani, F., Favata, F., & Micela, G. 1998, *A&A*, 332, 825
- See, V., Jardine, M., Vidotto, A. A., et al. 2016, *MNRAS*, 462, 4442, doi: [10.1093/mnras/stw2010](https://doi.org/10.1093/mnras/stw2010)
- Semenova, E., Bergemann, M., Deal, M., et al. 2020, *A&A*, 643, A164, doi: [10.1051/0004-6361/202038833](https://doi.org/10.1051/0004-6361/202038833)
- Sepulveda, A. G., Matrà, L., Kennedy, G. M., et al. 2019, *ApJ*, 881, 84, doi: [10.3847/1538-4357/ab2b98](https://doi.org/10.3847/1538-4357/ab2b98)
- Sestito, P., & Randich, S. 2005, *A&A*, 442, 615, doi: [10.1051/0004-6361:20053482](https://doi.org/10.1051/0004-6361:20053482)
- Sfeir, D. M., Lallement, R., Crifo, F., & Welsh, B. Y. 1999, *A&A*, 346, 785
- Shan, Y., Revilla, D., Skrzypinski, S. L., et al. 2024, *A&A*, 684, A9, doi: [10.1051/0004-6361/202346794](https://doi.org/10.1051/0004-6361/202346794)
- Sheret, I., Dent, W. R. F., & Wyatt, M. C. 2004, *MNRAS*, 348, 1282, doi: [10.1111/j.1365-2966.2004.07448.x](https://doi.org/10.1111/j.1365-2966.2004.07448.x)
- Sherry, W. H., Walter, F. M., Wolk, S. J., & Adams, N. R. 2008, *AJ*, 135, 1616, doi: [10.1088/0004-6256/135/4/1616](https://doi.org/10.1088/0004-6256/135/4/1616)
- Sibthorpe, B., Kennedy, G. M., Wyatt, M. C., et al. 2018, *MNRAS*, 475, 3046, doi: [10.1093/mnras/stx3188](https://doi.org/10.1093/mnras/stx3188)
- Siegler, N., Muzerolle, J., Young, E. T., et al. 2007, *ApJ*, 654, 580, doi: [10.1086/509042](https://doi.org/10.1086/509042)
- Sierchio, J. M., Rieke, G. H., Su, K. Y. L., et al. 2010, *ApJ*, 712, 1421, doi: [10.1088/0004-637X/712/2/1421](https://doi.org/10.1088/0004-637X/712/2/1421)
- Silaj, J., & Landstreet, J. D. 2014, *A&A*, 566, A132, doi: [10.1051/0004-6361/201321468](https://doi.org/10.1051/0004-6361/201321468)
- Silverstone, M. D., Meyer, M. R., Mamajek, E. E., et al. 2006, *ApJ*, 639, 1138, doi: [10.1086/499418](https://doi.org/10.1086/499418)
- Skrutskie, M. F., Cutri, R. M., Stiening, R., et al. 2006, *AJ*, 131, 1163, doi: [10.1086/498708](https://doi.org/10.1086/498708)
- Smith, B. J., Price, S. D., & Baker, R. I. 2004, *ApJS*, 154, 673, doi: [10.1086/423248](https://doi.org/10.1086/423248)
- Soderblom, D. R., Jones, B. F., Balachandran, S., et al. 1993a, *AJ*, 106, 1059, doi: [10.1086/116704](https://doi.org/10.1086/116704)
- Soderblom, D. R., & Mayor, M. 1993, *AJ*, 105, 226, doi: [10.1086/116422](https://doi.org/10.1086/116422)
- Soderblom, D. R., Stauffer, J. R., Hudon, J. D., & Jones, B. F. 1993b, *ApJS*, 85, 315, doi: [10.1086/191767](https://doi.org/10.1086/191767)
- Sousa, A. P., Bouvier, J., Alencar, S. H. P., et al. 2023, *A&A*, 670, A142, doi: [10.1051/0004-6361/202244720](https://doi.org/10.1051/0004-6361/202244720)
- Souto, D., Cunha, K., & Smith, V. V. 2021, *ApJ*, 917, 11, doi: [10.3847/1538-4357/abfdb5](https://doi.org/10.3847/1538-4357/abfdb5)
- Souza dos Santos, P. V., Porto de Mello, G. F., Costa-Bhering, E., et al. 2024, *MNRAS*, 532, 563, doi: [10.1093/mnras/stae1532](https://doi.org/10.1093/mnras/stae1532)

- Stassun, K. G., & Torres, G. 2016, *ApJL*, 831, L6, doi: [10.3847/2041-8205/831/1/L6](https://doi.org/10.3847/2041-8205/831/1/L6)
- Stassun, K. G., & Torres, G. 2018, *ApJ*, 862, 61, doi: [10.3847/1538-4357/aacafc](https://doi.org/10.3847/1538-4357/aacafc)
- Stassun, K. G., Oelkers, R. J., Paegert, M., et al. 2019, *AJ*, 158, 138, doi: [10.3847/1538-3881/ab3467](https://doi.org/10.3847/1538-3881/ab3467)
- Stauffer, J. R., Caillault, J. P., Gagne, M., Prosser, C. F., & Hartmann, L. W. 1994, *ApJS*, 91, 625, doi: [10.1086/191951](https://doi.org/10.1086/191951)
- Stauffer, J. R., & Hartmann, L. W. 1987, *ApJ*, 318, 337, doi: [10.1086/165371](https://doi.org/10.1086/165371)
- Stauffer, J. R., Hartmann, L. W., Prosser, C. F., et al. 1997, *ApJ*, 479, 776, doi: [10.1086/303930](https://doi.org/10.1086/303930)
- Stauffer, J. R., Schultz, G., & Kirkpatrick, J. D. 1998, *ApJL*, 499, L199, doi: [10.1086/311379](https://doi.org/10.1086/311379)
- Stauffer, J. R., Rebull, L. M., Carpenter, J., et al. 2005, *AJ*, 130, 1834, doi: [10.1086/444420](https://doi.org/10.1086/444420)
- Stauffer, J. R., Hartmann, L. W., Fazio, G. G., et al. 2007, *ApJS*, 172, 663, doi: [10.1086/518961](https://doi.org/10.1086/518961)
- Stauffer, J. R., Rebull, L. M., James, D., et al. 2010, *ApJ*, 719, 1859, doi: [10.1088/0004-637X/719/2/1859](https://doi.org/10.1088/0004-637X/719/2/1859)
- Steele, A., Hughes, A. M., Carpenter, J., et al. 2016, *ApJ*, 816, 27, doi: [10.3847/0004-637X/816/1/27](https://doi.org/10.3847/0004-637X/816/1/27)
- Steinmetz, M., Matijevic, G., Enke, H., et al. 2020, *AJ*, 160, 82, doi: [10.3847/1538-3881/ab9ab9](https://doi.org/10.3847/1538-3881/ab9ab9)
- Strassmeier, K., Washuettl, A., Granzer, T., Scheck, M., & Weber, M. 2000, *A&AS*, 142, 275, doi: [10.1051/aas:2000328](https://doi.org/10.1051/aas:2000328)
- Su, K. Y. L., Rieke, G. H., Stansberry, J. A., et al. 2006, *ApJ*, 653, 675, doi: [10.1086/508649](https://doi.org/10.1086/508649)
- Sullivan, D., Wilner, D. J., Matr a, L., et al. 2022, *AJ*, 164, 100, doi: [10.3847/1538-3881/ac80c5](https://doi.org/10.3847/1538-3881/ac80c5)
- Sung, H., Bessell, M. S., Lee, B.-W., & Lee, S.-G. 2002, *AJ*, 123, 290, doi: [10.1086/324729](https://doi.org/10.1086/324729)
- Susemihl, N., & Meyer, M. R. 2022, *A&A*, 657, A48, doi: [10.1051/0004-6361/202038582](https://doi.org/10.1051/0004-6361/202038582)
- Talon, S., & Charbonnel, C. 2005, *A&A*, 440, 981, doi: [10.1051/0004-6361:20053020](https://doi.org/10.1051/0004-6361:20053020)
- Tang, J., Bressan, A., Rosenfield, P., et al. 2014, *MNRAS*, 445, 4287, doi: [10.1093/mnras/stu2029](https://doi.org/10.1093/mnras/stu2029)
- Tang, S.-Y., Chen, W. P., Chiang, P. S., et al. 2018, *ApJ*, 862, 106, doi: [10.3847/1538-4357/aacb7a](https://doi.org/10.3847/1538-4357/aacb7a)
- Tang, S.-Y., Pang, X., Yuan, Z., et al. 2019, *ApJ*, 877, 12, doi: [10.3847/1538-4357/ab13b0](https://doi.org/10.3847/1538-4357/ab13b0)
- Tanner, A., Plavchan, P., Bryden, G., et al. 2020, *PASP*, 132, 084401, doi: [10.1088/1538-3873/ab895f](https://doi.org/10.1088/1538-3873/ab895f)
- Taylor, B. J. 2006, *AJ*, 132, 2453, doi: [10.1086/508610](https://doi.org/10.1086/508610)
- Testa, P., Saar, S. H., & Drake, J. J. 2015, *Philosophical Transactions of the Royal Society of London Series A*, 373, 20140259, doi: [10.1098/rsta.2014.0259](https://doi.org/10.1098/rsta.2014.0259)
- Thureau, N. D., Greaves, J. S., Matthews, B. C., et al. 2014, *MNRAS*, 445, 2558, doi: [10.1093/mnras/stu1864](https://doi.org/10.1093/mnras/stu1864)
- Tobin, T. L., Currie, T., Li, Y., et al. 2024, *AJ*, 167, 205, doi: [10.3847/1538-3881/ad3077](https://doi.org/10.3847/1538-3881/ad3077)
- Tokovinin, A. 2018, *ApJS*, 235, 6, doi: [10.3847/1538-4365/aaa1a5](https://doi.org/10.3847/1538-4365/aaa1a5)
- Tokovinin, A., Thomas, S., Sterzik, M., & Udry, S. 2006, *A&A*, 450, 681, doi: [10.1051/0004-6361:20054427](https://doi.org/10.1051/0004-6361:20054427)
- Torres, C. A. O., Quast, G. R., Melo, C. H. F., & Sterzik, M. F. 2008, in *Handbook of Star Forming Regions, Volume II*, ed. B. Reipurth, Vol. 5 (ASP Press, San Francisco, CA USA), 757, doi: [10.48550/arXiv.0808.3362](https://doi.org/10.48550/arXiv.0808.3362)
- Torres, G., Latham, D. W., & Quinn, S. N. 2021, *ApJ*, 921, 117, doi: [10.3847/1538-4357/ac1585](https://doi.org/10.3847/1538-4357/ac1585)
- Torres, G., & Ribas, I. 2002, *ApJ*, 567, 1140, doi: [10.1086/338587](https://doi.org/10.1086/338587)
- Torres, G., Schaefer, G. H., Monnier, J. D., et al. 2022, *ApJ*, 941, 8, doi: [10.3847/1538-4357/ac9d8d](https://doi.org/10.3847/1538-4357/ac9d8d)
- Torres, G., Schaefer, G. H., Stefanik, R. P., et al. 2024, *ApJ*, 971, 31, doi: [10.3847/1538-4357/ad54b2](https://doi.org/10.3847/1538-4357/ad54b2)
- Trilling, D. E., Stansberry, J. A., Stapelfeldt, K. R., et al. 2007, *ApJ*, 658, 1289, doi: [10.1086/511668](https://doi.org/10.1086/511668)
- Trilling, D. E., Bryden, G., Beichman, C. A., et al. 2008, *ApJ*, 674, 1086, doi: [10.1086/525514](https://doi.org/10.1086/525514)
- Tu, L., Johnstone, C. P., G udel, M., & Lammer, H. 2015, *A&A*, 577, L3, doi: [10.1051/0004-6361/201526146](https://doi.org/10.1051/0004-6361/201526146)
- Turon, C., Creze, M., Egret, D., et al. 1993, *Bulletin d'Information du Centre de Donnees Stellaires*, 43, 5
- Ujjwal, K., Kartha, S. S., Mathew, B., Manoj, P., & Narang, M. 2020, *AJ*, 159, 166, doi: [10.3847/1538-3881/ab76d6](https://doi.org/10.3847/1538-3881/ab76d6)
- Urban, L. E., Rieke, G., Su, K., & Trilling, D. E. 2012, *ApJ*, 750, 98, doi: [10.1088/0004-637X/750/2/98](https://doi.org/10.1088/0004-637X/750/2/98)
- Urban, S. E., Corbin, T. E., & Wycoff, G. L. 1998, *AJ*, 115, 2161, doi: [10.1086/300344](https://doi.org/10.1086/300344)
- van Altena, W. F., Lee, J. T., & Hoffleit, E. D. 1995, *The general catalogue of trigonometric [stellar] parallaxes* (Yale University Observatory, New Haven, CT USA)
- van Belle, G. T., von Braun, K., Ciardi, D. R., et al. 2021, *ApJ*, 922, 163, doi: [10.3847/1538-4357/ac1687](https://doi.org/10.3847/1538-4357/ac1687)
- van Leeuwen, F. 2007, *A&A*, 474, 653, doi: [10.1051/0004-6361:20078357](https://doi.org/10.1051/0004-6361:20078357)
- van Leeuwen, F., Evans, D. W., Grenon, M., et al. 1997, *A&A*, 323, L61
- Vaughan, A. H., & Preston, G. W. 1980, *PASP*, 92, 385, doi: [10.1086/130683](https://doi.org/10.1086/130683)
- Veras, D. 2021, in *Oxford Research Encyclopedia of Planetary Science* (IOP Publishing Ltd, Bristol, UK), 1, doi: [10.1093/acrefore/9780190647926.013.238](https://doi.org/10.1093/acrefore/9780190647926.013.238)

- Vican, L., Schneider, A., Bryden, G., et al. 2016, *ApJ*, 833, 263, doi: [10.3847/1538-4357/833/2/263](https://doi.org/10.3847/1538-4357/833/2/263)
- Voges, W., Boller, T., Englhauser, J., Freyberg, M., & Supper, R. 2001, in *Astronomical Society of the Pacific Conference Series*, Vol. 225, *Virtual Observatories of the Future*, ed. R. J. Brunner, S. G. Djorgovski, & A. S. Szalay, 234
- Voges, W., Aschenbach, B., Boller, T., et al. 1999, *A&A*, 349, 389, doi: [10.48550/arXiv.astro-ph/9909315](https://doi.org/10.48550/arXiv.astro-ph/9909315)
- Voges, W., Aschenbach, B., Boller, T., et al. 2000, *IAUC*, 7432, 3
- Walter, F. M., Vrba, F. J., Mathieu, R. D., Brown, A., & Myers, P. C. 1994, *AJ*, 107, 692, doi: [10.1086/116889](https://doi.org/10.1086/116889)
- Wang, J. J., Chen, L., Zhao, J. H., & Jiang, P. F. 1995, *A&AS*, 113, 419
- Wang, R., Luo, A. L., Chen, J.-J., et al. 2020, *ApJ*, 891, 23, doi: [10.3847/1538-4357/ab6dea](https://doi.org/10.3847/1538-4357/ab6dea)
- Wang, S., & Chen, X. 2019, *ApJ*, 877, 116, doi: [10.3847/1538-4357/ab1c61](https://doi.org/10.3847/1538-4357/ab1c61)
- Wang, S., Liu, J., Qiu, Y., et al. 2016, *ApJS*, 224, 40, doi: [10.3847/0067-0049/224/2/40](https://doi.org/10.3847/0067-0049/224/2/40)
- Weber, M. A., Schunker, H., Jouve, L., & Işık, E. 2023, *SSRv*, 219, 63, doi: [10.1007/s11214-023-01006-5](https://doi.org/10.1007/s11214-023-01006-5)
- Weiler, M., Carrasco, J. M., Fabricius, C., & Jordi, C. 2023, *A&A*, 671, A52, doi: [10.1051/0004-6361/202244764](https://doi.org/10.1051/0004-6361/202244764)
- Weis, E. W. 1993, *AJ*, 105, 1962, doi: [10.1086/116571](https://doi.org/10.1086/116571)
- Weisskopf, M. C., Brinkman, B., Canizares, C., et al. 2002, *PASP*, 114, 1, doi: [10.1086/338108](https://doi.org/10.1086/338108)
- Welsh, B. Y., & Shelton, R. L. 2009, *Ap&SS*, 323, 1, doi: [10.1007/s10509-009-0053-3](https://doi.org/10.1007/s10509-009-0053-3)
- White, J. A., Boley, A. C., MacGregor, M. A., Hughes, A. M., & Wilner, D. J. 2018, *MNRAS*, 474, 4500, doi: [10.1093/mnras/stx3098](https://doi.org/10.1093/mnras/stx3098)
- White, R. J., Gabor, J. M., & Hillenbrand, L. A. 2007, *AJ*, 133, 2524, doi: [10.1086/514336](https://doi.org/10.1086/514336)
- Williams, J. P., & Andrews, S. M. 2006, *ApJ*, 653, 1480, doi: [10.1086/508919](https://doi.org/10.1086/508919)
- Williams, J. P., Najita, J., Liu, M. C., et al. 2004, *ApJ*, 604, 414, doi: [10.1086/381721](https://doi.org/10.1086/381721)
- Wilner, D. J., MacGregor, M. A., Andrews, S. M., et al. 2018, *ApJ*, 855, 56, doi: [10.3847/1538-4357/aaacd7](https://doi.org/10.3847/1538-4357/aaacd7)
- Wilson, O. C. 1963, *ApJ*, 138, 832, doi: [10.1086/147689](https://doi.org/10.1086/147689)
- Winnick, I., Yana Galarza, J., Reggiani, H., et al. 2025, arXiv e-prints, arXiv:2508.16513, doi: [10.48550/arXiv.2508.16513](https://doi.org/10.48550/arXiv.2508.16513)
- Wood, M. L., Mann, A. W., Barber, M. G., et al. 2023, *AJ*, 165, 85, doi: [10.3847/1538-3881/aca8fc](https://doi.org/10.3847/1538-3881/aca8fc)
- Worley, C. E., & Douglass, G. G. 1997, *A&AS*, 125, 523, doi: [10.1051/aas:1997239](https://doi.org/10.1051/aas:1997239)
- Worthey, G., & Lee, H.-c. 2011, *ApJS*, 193, 1, doi: [10.1088/0067-0049/193/1/1](https://doi.org/10.1088/0067-0049/193/1/1)
- Wright, C. O., Egan, M. P., Kraemer, K. E., & Price, S. D. 2003, *AJ*, 125, 359, doi: [10.1086/345511](https://doi.org/10.1086/345511)
- Wright, E. L., Eisenhardt, P. R. M., Mainzer, A. K., et al. 2010, *AJ*, 140, 1868, doi: [10.1088/0004-6256/140/6/1868](https://doi.org/10.1088/0004-6256/140/6/1868)
- Wright, J. T., Marcy, G. W., Butler, R. P., & Vogt, S. S. 2004, *ApJS*, 152, 261, doi: [10.1086/386283](https://doi.org/10.1086/386283)
- Wyatt, M. C. 2021, in *ExoFrontiers; Big Questions in Exoplanetary Science*, ed. N. Madhusudhan (IOP Publishing Ltd, Bristol, UK), 15–1, doi: [10.1088/2514-3433/abfa8fch15](https://doi.org/10.1088/2514-3433/abfa8fch15)
- Wyatt, M. C., Smith, R., Su, K. Y. L., et al. 2007, *ApJ*, 663, 365, doi: [10.1086/518404](https://doi.org/10.1086/518404)
- Xiang, M., Ting, Y.-S., Rix, H.-W., et al. 2019, *ApJS*, 245, 34, doi: [10.3847/1538-4365/ab5364](https://doi.org/10.3847/1538-4365/ab5364)
- Yanny, B., Rockosi, C., Newberg, H. J., et al. 2009, *AJ*, 137, 4377, doi: [10.1088/0004-6256/137/5/4377](https://doi.org/10.1088/0004-6256/137/5/4377)
- Ye, L., Bi, S., Zhang, J., et al. 2024, *ApJS*, 271, 19, doi: [10.3847/1538-4365/ad1eee](https://doi.org/10.3847/1538-4365/ad1eee)
- Yelverton, B., Kennedy, G. M., & Su, K. Y. L. 2020, *MNRAS*, 495, 1943, doi: [10.1093/mnras/staa1316](https://doi.org/10.1093/mnras/staa1316)
- Yelverton, B., Kennedy, G. M., Su, K. Y. L., & Wyatt, M. C. 2019, *MNRAS*, 488, 3588, doi: [10.1093/mnras/stz1927](https://doi.org/10.1093/mnras/stz1927)
- Young, E. T., Lada, C. J., Teixeira, P., et al. 2004, *ApJS*, 154, 428, doi: [10.1086/422688](https://doi.org/10.1086/422688)
- Yu, H., Shao, Z., Diaferio, A., & Li, L. 2020, *ApJ*, 899, 144, doi: [10.3847/1538-4357/aba8f3](https://doi.org/10.3847/1538-4357/aba8f3)
- Zacharias, N., Finch, C. T., Girard, T. M., et al. 2013, *AJ*, 145, 44, doi: [10.1088/0004-6256/145/2/44](https://doi.org/10.1088/0004-6256/145/2/44)
- Zacharias, N., Urban, S. E., Zacharias, M. I., et al. 2004, *AJ*, 127, 3043, doi: [10.1086/386353](https://doi.org/10.1086/386353)
- Zerjal, M., Ireland, M. J., Crundall, T. D., Krumholz, M. R., & Rains, A. D. 2023, *MNRAS*, 519, 3992, doi: [10.1093/mnras/stac3693](https://doi.org/10.1093/mnras/stac3693)
- Zerjal, M., Ireland, M. J., Nordlander, T., et al. 2019, *MNRAS*, 484, 4591, doi: [10.1093/mnras/stz296](https://doi.org/10.1093/mnras/stz296)
- Zerjal, M., Rains, A. D., Ireland, M. J., et al. 2021, *MNRAS*, 503, 938, doi: [10.1093/mnras/stab513](https://doi.org/10.1093/mnras/stab513)
- Zhang, R., & Yuan, H. 2023, *ApJS*, 264, 14, doi: [10.3847/1538-4365/ac9dfa](https://doi.org/10.3847/1538-4365/ac9dfa)
- Zhang, W., Zhang, J., He, H., et al. 2022, *ApJS*, 263, 12, doi: [10.3847/1538-4365/ac9406](https://doi.org/10.3847/1538-4365/ac9406)
- Zhang, X., Green, G. M., & Rix, H.-W. 2023, *MNRAS*, 524, 1855, doi: [10.1093/mnras/stad1941](https://doi.org/10.1093/mnras/stad1941)
- Zhang, Y., Tang, S.-Y., Chen, W. P., Pang, X., & Liu, J. Z. 2020, *ApJ*, 889, 99, doi: [10.3847/1538-4357/ab63d4](https://doi.org/10.3847/1538-4357/ab63d4)
- Zhu, W., & Dong, S. 2021, *ARA&A*, 59, 291, doi: [10.1146/annurev-astro-112420-020055](https://doi.org/10.1146/annurev-astro-112420-020055)

- Zills, G., Criscuoli, S., Bertello, L., & Pevtsov, A. 2024, *Frontiers in Astronomy and Space Sciences*, 10, 1328364, doi: [10.3389/fspas.2023.1328364](https://doi.org/10.3389/fspas.2023.1328364)
- Zorec, J., & Royer, F. 2012, *A&A*, 537, A120, doi: [10.1051/0004-6361/201117691](https://doi.org/10.1051/0004-6361/201117691)
- Zucker, C., Saydjari, A. K., Speagle, J. S., et al. 2025, *ApJ*, 992, 39, doi: [10.3847/1538-4357/adf6e6](https://doi.org/10.3847/1538-4357/adf6e6)
- Zuckerman, B., Bessell, M. S., Song, I., & Kim, S. 2006, *ApJL*, 649, L115, doi: [10.1086/508060](https://doi.org/10.1086/508060)
- Zuckerman, B., Rhee, J. H., Song, I., & Bessell, M. S. 2011, *ApJ*, 732, 61, doi: [10.1088/0004-637X/732/2/61](https://doi.org/10.1088/0004-637X/732/2/61)
- Zuckerman, B., & Song, I. 2004, *ARA&A*, 42, 685, doi: [10.1146/annurev.astro.42.053102.134111](https://doi.org/10.1146/annurev.astro.42.053102.134111)
- Zuckerman, B., Song, I., Bessell, M. S., & Webb, R. A. 2001a, *ApJL*, 562, L87, doi: [10.1086/337968](https://doi.org/10.1086/337968)
- Zuckerman, B., Song, I., & Webb, R. A. 2001b, *ApJ*, 559, 388, doi: [10.1086/322305](https://doi.org/10.1086/322305)
- Zuckerman, B., Vican, L., Song, I., & Schneider, A. 2013, *ApJ*, 778, 5, doi: [10.1088/0004-637X/778/1/5](https://doi.org/10.1088/0004-637X/778/1/5)
- Zuckerman, B., Webb, R. A., Schwartz, M., & Becklin, E. E. 2001c, *ApJL*, 549, L233, doi: [10.1086/319155](https://doi.org/10.1086/319155)
- Zuo, F., Luo, A.-L., Du, B., et al. 2024, *ApJS*, 271, 4, doi: [10.3847/1538-4365/ad1eeb](https://doi.org/10.3847/1538-4365/ad1eeb)